

USING COMPUTER VISION PHOTOGRAMMETRY (AGISOFT PHOTOSCAN)  
TO RECORD AND ANALYZE UNDERWATER SHIPWRECK SITES

A Dissertation

by

KOTARO YAMAFUNE

Submitted to the Office of Graduate and Professional Studies of  
Texas A&M University  
in partial fulfillment of the requirements for the degree of

DOCTOR OF PHILOSOPHY

Chair of Committee,	Luis Filipe Viera de Castro
Committee Members,	Kevin J. Crisman
	Donny Hamilton
	Tim McLaughlin
Head of Department,	Cynthia Werner

May 2016

Major Subject: Anthropology

Copyright 2016 Kotaro Yamafune

## ABSTRACT

In 2010, a new off-the-shelf software for Computer Vision Photogrammetry, Agisoft PhotoScan, became available to nautical archeologists, and this technology has since become a popular method for recording underwater shipwreck sites. Today (2015), there are still active discussions regarding the accuracy and usage of Computer Vision Photogrammetry in the discipline of nautical archaeology. The author believes that creating a 1:1 scale constrained photogrammetric model of a submerged shipwreck site is not difficult as long as archaeologists first establish a local coordinate system of the site. After creation of a 1:1 scale constrained photogrammetric model, any measurements of the site can be obtained from the created 3D model and its digital data. This means that archaeologists never need to revisit the archaeological site to take additional measurements. Thus, Computer Vision Photogrammetry can substantially reduce archaeologists' working time in water, and maximize quantity and quality of the data acquired.

Furthermore, the author believes that the acquired photogrammetric data can be utilized in traditional ship reconstruction and other general studies of shipwrecks. With this idea, the author composed a new methodology that fuses Computer Vision Photogrammetry and other digital tools into traditional research methods of nautical archaeology. Using this method, archaeologists can create 3D models that accurately represent submerged cultural heritage sites, and these can be used as representative archaeological data. These types of representative data include (but are not limited to)

site plans, technical artifact or timber drawings, shipwreck section profiles, georeferenced archaeological information databases, site-monitoring systems, digital hull fragment models and many other types of usable and practical 3D models. In this dissertation, the author explains his methodology and related new ideas.

## DEDICATION

To my father and mother, who always trust and encourage me.

Without their support, I could not finish this research.

I hereby present this dissertation to my loving parents to be apprised that they are the  
best father and mother in the world.

## ACKNOWLEDGEMENTS

I would like to thank my committee chair, Dr. Luis Filipe Viera de Castro, who always supported my efforts. Without him, I would have never finished this research. I would also like to recognize the support and important contributions of my committee members, Dr. Kevin J. Crisman, Dr. Donny Hamilton and Dr. Tim McLaughlin.

I would like to acknowledge my friends Dr. Rodrigo Torres and Ms. Samila Ferreira. As teammates in the J. Richard Steffy Ship Reconstruction Laboratory, we spent long days and memorable moments together; we were best colleagues, best friends, and they became my family in College Station. They always helped me with my research and my life in America.

I also want to give my gratitude to all of my friends in the Nautical Archaeology Program, who always delivered to me new ideas, knowledge, insights, and smiles; especially to Lindsey Thomas and Dave Ruff, who revised my dissertation and helped me with my English all the time without any complaints.

In the end, I give my utmost gratitude to my parents, Shigeki Yamafune and Nobuko Yamafune, who have always loved and encouraged me these past 31 years. They are the most loving parents, yet I hope they know that they are the most loved parents as well.

## TABLE OF CONTENTS

		Page
ABSTRACT .....		ii
DEDICATION .....		iv
ACKNOWLEDGEMENTS .....		v
TABLE OF CONTENTS .....		vi
LIST OF FIGURES .....		ix
LIST OF TABLES .....		xvi
 CHAPTER		
I	INTRODUCTION .....	1
	Introduction: Objective of This Dissertation .....	1
	Current Status of Study .....	4
	Methodology .....	7
II	DATA COLLECTION .....	8
	Photography .....	8
	Underwater Coded Targets .....	20
	Recommended Sizes for Coded Targets (Based on Focal Length and Distance).....	23
	Recommended Flight Plan with Coded Targets .....	27
	Local Coordinate Network .....	28
	Methodology for Testing Different Local Coordinate Systems.....	31
	Trilateration (Direct Survey Method) .....	32
	Enclosure .....	35
	Scale Bars.....	37
	Total Station .....	38
	Comparison of the Different Methods.....	40
	Conclusion: Recommended Survey Method .....	42
	Data Collection and Database .....	44
	Data Collection .....	45

CHAPTER	Page
Database .....	48
III DATA PROCESSING.....	51
Computer Vision Photogrammetry (Agisoft PhotoScan) .....	51
Align Photos.....	53
Build Dense Cloud .....	57
Build Mesh .....	62
Build Texture .....	67
Photogrammetric Model of the <i>Saveiro</i> Wooden Ship Model .....	74
Modeling a Sail (Mesh Replacement Techniques).....	79
Video Frame Photogrammetry .....	82
Underwater Video Frame Photogrammetry Using GoPro .....	89
Georeferenced Orthophotos .....	94
GIS Based Spatial Data Archive .....	97
2D Site Plan and Timber Catalog Templates .....	100
Erasing Instead of Tracing Method .....	101
Timber Drawing Templates (with Automated Masking).....	106
Section Profiles of Shipwreck Sites .....	113
Exporting Photogrammetric Models to Autodesk Maya.....	116
Creating CT Scan Cameras in Maya .....	119
Conclusion: Section Profiles .....	124
IV DATA ANALYSIS .....	125
Data Analysis: Legacy of J. Richard Steffy .....	125
Hull Line Reconstruction .....	125
Mold-and-Batten Model Fairing .....	131
Testing Author’s Hull Line Reconstruction .....	133
Archival Research and Shipwreck Analysis .....	138
Hull Analysis.....	139
Interactive Fragment Model.....	140
Site Analysis.....	149
Photogrammetry Based Site Monitoring.....	150
3D Reconstructions .....	153
NURBS Modeling and Polygon Modeling .....	154
V PUBLIC OUTREACH & PUBLICATION .....	159
Visual Tour Animation .....	159

CHAPTER	Page
Interactive Virtual Museum.....	164
Publications .....	167
VI CONCLUSION .....	170
Conclusions .....	170
Digital <i>in situ</i> Preservation.....	171
Computer Vision Photogrammetry as a Tool against Treasure Hunters .....	172
Legacy Photogrammetry .....	173
To Conclude: Leaving Data for Future Generations .....	175
REFERENCES .....	178



## LIST OF FIGURES

FIGURE	Page
1-1 The workflow of the proposed methodology .....	2
2-1 Difference of coverage areas based on focal lengths .....	9
2-2 Difference of coverage areas based on sensor sizes.....	10
2-3 Photogrammetric models of the Gnalíć shipwreck site (based on photos with/without strobe lights) .....	18
2-4 Recommended underwater camera equipment .....	19
2-5 Sparse points cloud of the Gnalíć shipwreck site on 18 July 2014 in PhotoScan .....	21
2-6 Underwater coded targets and their additional weights .....	22
2-7 Photo of coded targets shown in a minimum recommended size .....	26
2-8 Photo of coded targets shown in a maximum recommended size .....	26
2-9 Recommended flight path for photogrammetric recording .....	28
2-10 Local coordinate network of the Gnalíć shipwreck site from 2014 field season (in 3H Site Recorder) .....	30
2-11 <i>Saveiro</i> wooden ship model (1:10 size) for photogrammetry .....	32
2-12 The local coordinate network of datum points (control network) around the <i>saveiro</i> wooden model (Top view: horizontal plane) .....	33
2-13 The local coordinate network of reference points and control points around the <i>saveiro</i> wooden model (Top view: horizontal plane) .....	34
2-14 The local coordinate network of reference points and control points around the <i>saveiro</i> wooden model (Front view: vertical plane).....	34
2-15 Examples of rope lengths for enclosure method (using the Pythagorean Theorem) .....	36

FIGURE	Page
2-16 Distances between the four corners of the <i>saveiro</i> wooden model for the enclosure method .....	36
2-17 Seven 10 cm scale bars created on the <i>saveiro</i> photogrammetric model for the scale bar method .....	38
2-18 Coordinates of the control points and reference points on the <i>saveiro</i> wooden model by total station that were plotted in Rhinoceros 3D CAD software .....	39
2-19 The photogrammetric model of the <i>saveiro</i> wooden ship model and the measured distances between reference points for the comparison .....	40
2-20 Example of an underwater sketch by an archaeologist .....	45
2-21 A working scene of archaeologists on the Gnalić shipwreck .....	46
2-22 An artifact from the Gnalić shipwreck site being chemically treated.....	47
2-23 Artifacts raised from the Gnalić shipwreck site were recorded and stored in an organized manner .....	48
2-24 Photo database of the Gnalić artifacts .....	49
2-25 Digital database of the Gnalić project 2014 field season .....	49
3-1 A photogrammetric model of two cubes .....	52
3-2 Align Photos process with Key Point Limit: 40,000 (default) setting .....	54
3-3 Align Photos process with Key Point Limit: 80,000 setting .....	55
3-4 Align Photos process with Tie Point Limits: 1000 (default) setting .....	56
3-5 Align Photos process with Tie Point Limits: 2000 setting .....	56
3-6 Accuracy: High setting on Build Dense Cloud process .....	57
3-7 Accuracy: Medium setting on Build Dense Cloud process .....	58
3-8 Accuracy: Low setting on Build Dense Cloud process .....	58

FIGURE	Page
3-9 Accuracy: Lowest setting on Build Dense Cloud process .....	59
3-10 Build Dense Cloud process with Depth filtering: Aggressive setting.....	60
3-11 Build Dense Cloud process with Depth filtering: Mild setting .....	60
3-12 Build Dense Cloud process with Depth filtering: Moderate setting .....	61
3-13 Build Dense Cloud process with Depth filtering: Disabled setting .....	61
3-14 Build Mesh process with Surface Type: Arbitrary setting .....	62
3-15 Build Mesh process with Surface Type: Height Field setting .....	63
3-16 Build Mesh process with Surface Count: High setting .....	64
3-17 Build Mesh process with Surface Count: Medium setting .....	64
3-18 Build Mesh process with Surface Count: Low setting .....	65
3-19 Build Mesh process with Interpolation: Disabled setting .....	66
3-20 Build Mesh process with Interpolation: Enabled setting .....	66
3-21 Build Mesh process with Interpolation: Extrapolated setting .....	67
3-22 Build Texture process with Mapping mode: Generic setting .....	69
3-23 Build Texture process with Mapping mode: Orthophoto setting .....	69
3-24 Build Texture process with Mapping mode: Adaptive orthophoto setting .....	70
3-25 Build Texture process with Mapping mode: Spherical setting .....	70
3-26 Build Texture process with Blending mode: Mosaic setting .....	72
3-27 Build Texture process with Blending mode: Average setting .....	72
3-28 Build Texture process with Blending mode: Max Intensity setting .....	73
3-29 Build Texture process with Blending mode: Min Intensity setting .....	73

FIGURE	Page
3-30 Dense Points Cloud of the <i>saveiro</i> wooden ship model .....	75
3-31 An example of photos of the <i>saveiro</i> wooden model that were disabled for Build Dense Cloud process .....	75
3-32 Dense Point Cloud of the <i>Saveiro</i> Wooden Ship Model After 247 Oblique Angle Photos Were Disabled (Processed with 364 Photos) .....	76
3-33 Finished photogrammetric model of the <i>saveiro</i> wooden ship model that is intended to be used for visualization purposes .....	78
3-34 Finished photogrammetric model of the <i>saveiro</i> wooden ship model that is intended for use as a source of archaeological data .....	79
3-35 Photogrammetric model of a Chinese junk model with unsuccessfully reconstructed sail .....	80
3-36 Sail of a Chinese junk model reconstructed in Autodesk Maya modeling/animation software .....	81
3-37 Photogrammetric model of a Chinese junk with edited sail after re-importing to PhotoScan from Maya .....	82
3-38 Manual extraction of still frames using Adobe Premiere Pro CS6 .....	83
3-39 Automate extraction of still frames using Adobe Photoshop CS6 .....	84
3-40 Process for removing blurred images in PhotoScan .....	86
3-41 Video Frame Photogrammetry of the Gnalić shipwreck site .....	88
3-42 Computer Vision Photogrammetry of the Gnalić shipwreck site .....	88
3-43 The original GoPro video footage before the color and distortion correction .....	91
3-44 GoPro video footage after the color and distortion correction .....	91
3-45 Photogrammetric model based on video footage with color and distortion corrections applied in Photoshop .....	93

FIGURE	Page
3-46 Photogrammetric Model Based on Video Footage Without the Color and Distortion Corrections .....	93
3-47 Composed orthophotos of the Gnalić shipwreck site from the 2014 field season .....	96
3-48 Image of the visualized projection planes of orthophotos .....	97
3-49 The Gnalić shipwreck site in ArcGIS software .....	99
3-50 2D site plan of the Gnalić shipwreck based on the 2014 field season .....	100
3-51 Orthophoto of the Gnalić shipwreck site from 2014 field season .....	104
3-52 Sketch-like conversion of the orthophoto of the Gnalić site .....	104
3-53 Proposed 2D site plan created with the erasing method .....	106
3-54 An example of conventional timber drawing (from <i>Cais do Sodre</i> shipwreck) .....	107
3-55 An example of a timber drawing template .....	108
3-56 Computer Vision Photogrammetry with masked photos .....	111
3-57 Artifact drawing of a port tiller block found in Red River wreck site based on exported orthophotos .....	113
3-58 2D site plan of the Gnalić shipwreck from 2013 field season with positions of the transversal sections .....	115
3-59 Transversal section profiles of the Gnalić shipwreck site from 2013 and 2014 combined photogrammetric models .....	116
3-60 Imported <i>saveiro</i> 's photogrammetric model in Maya .....	119
3-61 Extracting a section profiles from the photogrammetric model of the <i>saveiro</i> wooden model in Maya .....	122
3-62 Approximate positions of extracted section profiles on the <i>saveiro</i> wooden model .....	123

FIGURE	Page
3-63 Section profiles of the <i>saveiro</i> photogrammetric model .....	123
4-1 Illustration of water displacement calculation based on hull lines.....	126
4-2 Illustration of the block coefficient .....	126
4-3 Illustration of the prismatic coefficient .....	127
4-4 Reconstruction of the hull lines of the <i>Cais do Sodré</i> shipwreck .....	127
4-5 The process of reconstructing section lines based on the <i>saveiro</i> photogrammetric model .....	129
4-6 The reconstructed twelve master frames of the <i>saveiro</i> wooden ship model .....	129
4-7 Plotted section lines of the <i>saveiro</i> wooden ship model .....	130
4-8 Mold-and-Batten Model reconstruction by J. R. Steffy .....	131
4-9 Mold-and-Batten Model Fairing in Rhinoceros 3D CAD software .....	133
4-10 A traced and scaled sketch of a <i>saveiro</i> 's molds by Dr. Castro .....	135
4-11 The process of designing pre-made master frames of the <i>saveiro</i> wooden ship model .....	136
4-12 Comparison of the reconstructed hull lines based on photogrammetric data and the original design of the <i>saveiro</i> wooden ship model .....	137
4-13 An image of the hull of the Pepper Wreck being reconstructed in Maya based on Dr. Castro's lines drawing .....	142
4-14 A 3D reconstruction of the Pepper Wreck based on historical and archaeological data .....	142
4-15 Illustration of 3D model deformation .....	144
4-16 Photogrammetric model of the Gnalić shipwreck structures <i>in situ</i> overlaid with the skeleton tool in Maya .....	145
4-17 Deformation of the Gnalić shipwreck site in Maya .....	146

FIGURE	Page
4-18 Photogrammetric model of the Gnalić shipwreck site and reconstructed 3D Ship Model in Position .....	146
4-19 Flattened Gnalić shipwreck site juxtaposed with hypothetical reconstructed ship model .....	147
4-20 The Gnalić shipwreck site brought back to the hypothetical original shape using the Interactive Fragment Model .....	147
4-21 Storage pattern of the barrels on Interactive Fragment Model of the Gnalić shipwreck site .....	148
4-22 A reconstructed set of hull lines based on shipwrights' treatises .....	149
4-23 Visualizing the progression of the Gnalić 2014 excavation using CloudCompare .....	152
4-24 A 3D model of a ship's hull as an example of NURBS modeling .....	155
4-25 3D reconstruction of a boiler from the shipwreck of the <i>Westfield</i> steamship created by Justin Parkoff .....	155
4-26 3D model of Stella 1 shipwreck as an example of Polygon modeling .....	157
4-27 Hypothetical reconstruction of an early 17 <sup>th</sup> -century rigging arrangement of a Portuguese East Indiaman as an example of Polygon modeling .....	157
5-1 An example of simple Key Frame Animation .....	160
5-2 Key Frame Animation of transparency of the materials .....	161
5-3 A created flying camera in Maya .....	162
5-4 Converting still images to an animation using Image Sequence import in Adobe Premiere Pro CS6 .....	163
5-5 Photogrammetric model of the Gnalić shipwreck site in Sketchfab .....	166
6-1 Legacy Photogrammetry of the <i>Batavia</i> shipwreck .....	174
6-2 Section profile extraction of <i>Batavia</i> shipwreck .....	175

## LIST OF TABLES

TABLE	Page
2-1 Major camera types that have available underwater housings .....	11
2-2 Approximate coverage area of one photo by a camera with an APS-C sensor (23.5 mm x 15.6 mm) .....	13
2-3 Approximate coverage area of one photo by a camera with a full-frame sensor (35.9 mm x 24 mm) .....	13
2-4 Approximate frequency of photo taking to keep ideal overlapping by a camera with an APS-C Sensor (23.5 mm x 15.6 mm) .....	14
2-5 Approximate frequency of photo taking to keep ideal overlapping by a camera with a full-frame sensor (35.9 mm x 24 mm) .....	14
2-6 Recommended total number of photos to cover a required area by a camera with a APS-C sensor (23.5 mm x 15.6 mm) .....	15
2-7 Recommended total number of photos to cover a required area by a camera with a full-frame sensor (35.9mm x 24mm).....	16
2-8 Coded targets recognition by a camera with 11 mm focal length (DSLR camera with APS-C sensor size) .....	24
2-9 Coded targets recognition by a camera with 18 mm focal length (DSLR camera with APS-C sensor size) .....	24
2-10 Coded targets recognition by a camera with 24mm focal length (DSLR camera with APS-C sensor size) .....	25
2-11 Local coordinates of reference points based on DSM .....	34
2-12 Coordinates of the reference points measured by total station .....	39
2-13 A distances between reference points to compare different surveying methods to fix distortions and scales of the <i>saveiro</i> wooden ship model's photogrammetric model .....	41



# CHAPTER I

## INTRODUCTION

### **Introduction: Objective of This Dissertation**

In recent years, applications of Computer Vision Photogrammetry have become popular in nautical archaeology. This technology has been repeatedly tested in archaeological surveys and excavations, both in dry and submerged environments, yet there are still active discussions about the efficiency and accuracy of photogrammetry models. With a team from the Nautical Archaeology Program in the Anthropology and analyze underwater shipwreck sites with off-the-shelf software. The methodology utilized a technique called Computer Vision Photogrammetry (Fig. 1-1). As a modification of traditional photogrammetry, Computer Vision Photogrammetry does not require the traditional two-camera equipment set-up. Instead, it uses sets of independent images with a certain amount of overlap (Agisoft LLC, 2014). This methodology produces reliable archaeological data based on 1:1 scale-constrained photogrammetry models. Examples of data that can be produced include 2D site plans, artifact and timber drawings, section profiles of shipwreck sites and reconstructed hull lines, georeferenced archaeological information databases, point based site-monitoring systems, digital format fragment models for hull analysis, and various styles of 3D models of shipwrecks, all in an easily shared format.

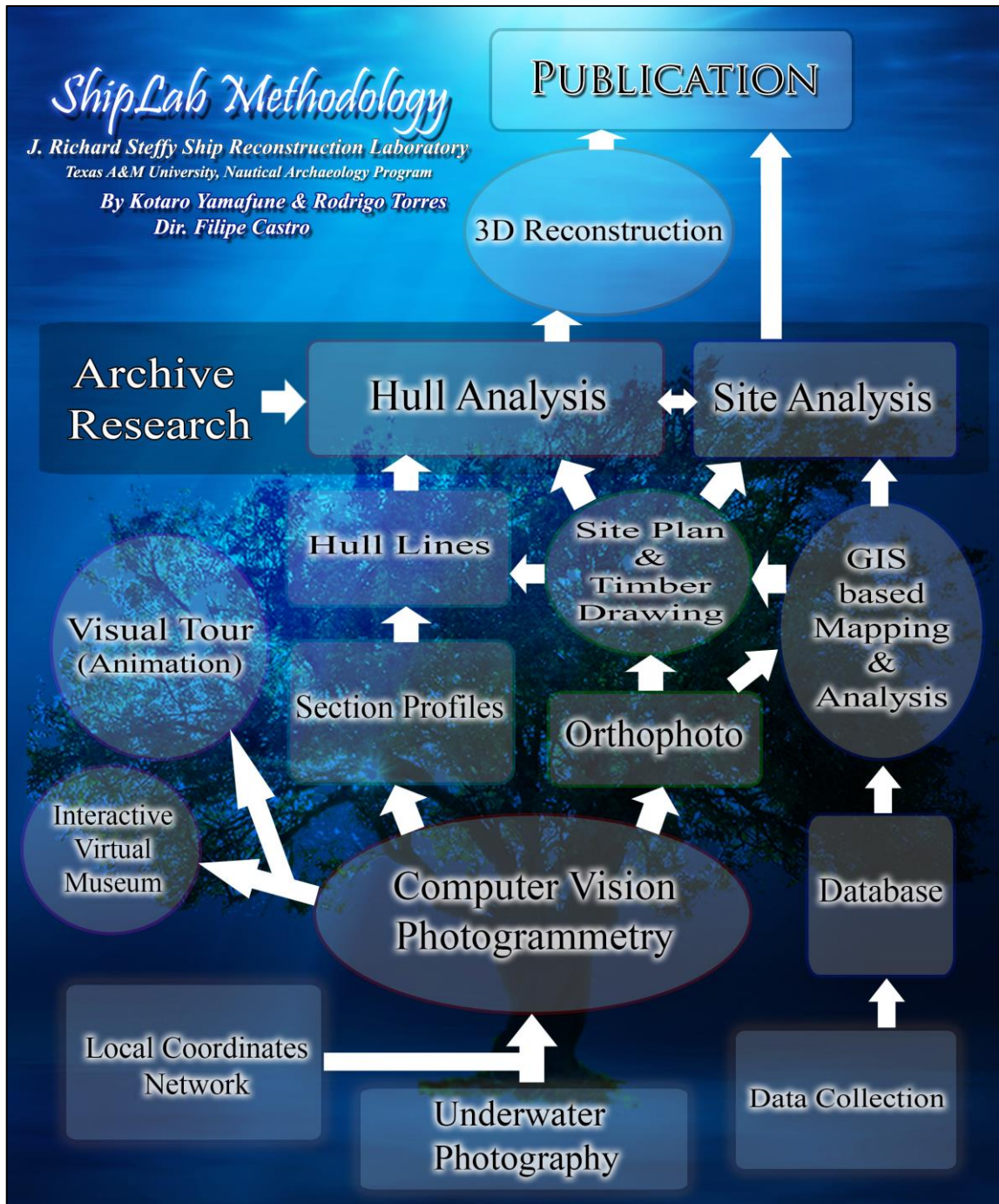


Figure 1-1. The workflow of the proposed methodology. This methodology follows the conventional research methods of nautical archaeology developed by J. Richard Steffy, the first director of the Ship Reconstruction Laboratory (ShipLab) at Texas A&M University, and was developed by the author and his colleagues in the ShipLab. For those reasons, the author named this methodology the "ShipLab methodology". (Image: Yamafune)

This dissertation follows the methodological workflow developed by the author and his colleagues, Dr. Rodrigo Torres and Dr. Luis Filipe Viera de Castro, and proposes a methodology to fuse new technologies with conventional nautical archaeology research methods. This dissertation is composed of six chapters, with Chapter I introducing the topic. Chapter II reviews techniques and methods employed to collect data used to produce accurate 3D photogrammetric models and to capture other important archaeological information to understand the shipwreck site. Chapter III discusses methods used to process data in order to create accurate 1:1 scale-constrained photogrammetric models, and to produce organized databases, accurate 2D site plans and artifact drawings, section profiles of shipwreck sites, and georeferenced high resolution photo mosaics. Chapter IV presents a method for analyzing shipwreck sites using generated output to better understand the ship; this chapter is similar to conventional research applied by nautical archaeologists, but it includes additional new methods proposed to facilitate archaeological research. These proposed analysis methods are the Interactive Fragment Model for hull analysis, and a cloud-based site monitoring method for site analysis. Chapter V discusses methods for sharing research outcomes with the general public, and Chapter VI concludes the dissertation by reviewing potential uses of the proposed methodology.

The workflow proposed in this dissertation was designed to combine Computer Vision Photogrammetry and traditional archaeological excavation methods. Although photogrammetric models are primarily used for visualization purposes, the author proposes that they can be used as sources of accurate archaeological data, and support

traditional archaeological work. The major advantage of Computer Vision Photogrammetry in underwater excavations is that it simplifies the data acquisition procedure, thus reducing the recording time. The underwater recording process is reduced to the establishment of a basic reference grid, and the acquisition of high quality photos with a certain amount of overlap. Photogrammetry minimizes the underwater recording time and maximizes the quality of the data acquired. Furthermore, this process produces extremely versatile digital datasets, which can be migrated and converted into many formats, then stored, organized and processed in order to analyze site formation processes and reconstruct the archaeological remains. Application in the field of the methods proposed in this dissertation will save time, save money, and produce accurate, reproducible, and sharable datasets for analyzed wreck sites.

### **Current Status of Study**

Archaeologists destroy the sites they excavate, which makes recording and publishing two serious responsibilities. From its development in the 19th century, photography has been one of the archaeologist's best companions. Photogrammetry – the art and science of deriving accurate 3D metric and descriptive object information from multiple images (Al-Ruzouq, 2012) – was originally developed as a technology to provide topographic information for map making (Burtch, 2008; Van Damme, 2015; Konecny, 2003). During the 20th century it slowly became a useful tool for archaeologists, but it was not until the 1960s that it was used underwater, when Dr. George Bass experimented with photogrammetry for the recording of the Byzantine

shipwreck Yassiada 2 (Drap, 2012). Dr. Bass used one camera mounted along a rail to shoot pairs of photogrammetric images, and later mounted two synchronized cameras on the University of Pennsylvania submarine *Ashera* (Bass and Van Doorninck, 1971; Bass and Rosencrantz, 1972; Rosencrantz, 1975). Starting in the early 1960s as a discipline informed by scientific principles, nautical archaeology developed quickly, and underwater photography was used as a basic tool from the beginning (Baker and Green, 1976; Green, 2004). Nautical archaeology aims to reconstruct ship shapes and structures, which are more often than not complex surfaces, defined by complex curves, sometimes conceived using combinations of simple curves whose reconstruction is relevant for understanding the history of technology, science, and thought.

Underwater archaeology is often constrained by depth, current, temperature, and visibility, and demands continuous economy of the archaeologist's time underwater. These factors have fueled a constant search for increased speed and accuracy. The development of computers in the 1980s created opportunities for the development of iterative trigonometric software to triangulate tridimensional points; such software could be applied to underwater photography (Cancian *et al.*, 2002; Drap, 2012). In the beginning of the 21st century, surveying methods using photography underwent rapid development, and photogrammetry to calculate coordinates of assigned points using an accurately calibrated camera made its appearance in underwater archaeology (Green, Matthews, and Turanli, 2002). Off-the-shelf software using digital images, such as PhotoModeler, was tested and discussed its accuracy in comparison with triangulation

software such as Site Surveyor (Green, Matthews, and Turanli, 2002; Holt 2003; Green and Gainsford 2003).

In the last five years, a new software package using Computer Vision Photogrammetry (also known as multi-image photogrammetry, or close-range photogrammetry) became available to archaeologists (Skarlatos and Rova, 2010; Doneus *et al.*, 2011; Drap, 2012; Diamanti, Georgopoulos, and Vlachaki, 2011; Zhukvsky, Kuznetsov, and Olkhovsky, 2013; Henderson, Pizarro, Johnson-Roberson, and Mahon, 2013; McCarthy and Benjamin, 2014). Under the commercial designation PhotoScan, this package does not require calibration of the cameras.

Using Computer Vision Photogrammetry, PhotoScan creates meshes, or geometry of 3D models, using pixel information from digital images, producing data files similar to those obtained from tridimensional laser scanners. The author sought to use this software in combination with other digital tools to record and reconstruct ship shapes and structures, as well as to produce animations, drawings, and orthogonal projections aiming at divulging and explaining the projects as they unfold.

The main goal of this methodology is to extract archaeological information from tridimensional models. Once accurate 1:1 scale tridimensional models are created, archaeologists can extract data from the digital models without having to revisit the actual sites. Care was taken to refine the data acquisition methodology in order to expand its application to non-intrusive and rescue archaeology projects.

## **Methodology**

In this dissertation the author will discuss methodology for acquiring data, processing data, and analyzing data. The core of the recording method is Computer Vision Photogrammetry; the goal of this methodology is to understand and reconstruct the ship during its operational career. The author originally designed the methodology as a guideline for archaeologists to record and analyze underwater shipwreck sites. The dissertation also discusses different methods used to collect data and to evaluate the accuracy of acquired data. In the main discussion, Chapter IV, the author presents methods for reconstructing the original ships based on data extracted from Computer Vision photogrammetric models.

This proposed methodology is not blinding flash of an original idea; instead, it is a combination of conventional archaeological recording and research methods with newly available technologies. In other words, archaeologists still need the same information to understand shipwreck sites; however, this methodology provides the required information faster and more accurately. Consequently, nautical archaeologists can proceed and complete their excavations and research more efficiently using this proposed methodology, while concurrently preserving tridimensional data of underwater shipwreck sites for subsequent generations of researchers.

## CHAPTER II

### DATA COLLECTION

#### **Photography**

The first step in creating accurate tridimensional models from Computer Vision photogrammetry is to take good photos. Choosing the right camera and accessory equipment is essential to ensure that clear and properly colored images are captured. Although there is a range of acceptable solutions from which archaeologists can choose, the best results depend heavily on the equipment. (Zhukovsky, Kuznetsov, and Olkhovsky, 2013) discussed constraints in underwater photography, which include optical distortion and optical noise.

Optical distortion is generated when light passes through media of different densities, such as water and then the air in the underwater camera housing. Refraction causes distortion in images; it also narrows the coverage area of a single photo (Gietler, 2009). To minimize optical distortion, the best possible solution is a hemispheric dome-port (Zhukovsky, Kuznetsov, and Olkhovsky, 2013). The hemispherical shape of the dome allows light to enter the lens through the underwater housing perpendicularly; therefore, it can minimize the refraction caused by the different densities of the water and air.

Optical noise can be minimized by the use of wider-angle lenses (focal length of 11mm – 18mm). Cameras with wider-angle lenses can get closer to the subject while keeping a wider coverage area. Simply put, an 11 mm focal length lens can capture twice



the area of a 22 mm focal length lens (Fig. 2-1). In other words, a camera with an 11 mm lens can be used at half the distance from the object as the same camera with a 22 mm lens, while covering the same area. This is an important factor in capturing crisp images for successful photogrammetry because underwater visibility introduces limitations for underwater photography and photogrammetry. Using a wide-angle lens minimizes the capture of optical noise, while still covering a large area, thus minimizing the number of photos required for effective Computer Vision Photogrammetry.



Figure 2-1. Difference of coverage areas based on focal lengths (From outside: 11 mm, 16 mm, 18 mm, 24 mm, 35 mm). (Image: Yamafune)

Another factor that affects the size of the coverage area and quality of the images is the sensor size of the camera (Crisp, 2013). Larger sensors can collect more pixel data (light information) and can cover a wider area in the same way as wider-angle lenses.

Technically speaking, underwater photogrammetry can be done by any type of camera that can be operated at the desired depth in water; nonetheless, more professional, or expensive, cameras tend to have larger sensor sizes and more precise exposure-control over the photos (Fig. 2-2). This is one of the main reasons that Digital Single Lens Reflex cameras (DSLRs) are recommended for underwater photography and photogrammetry.

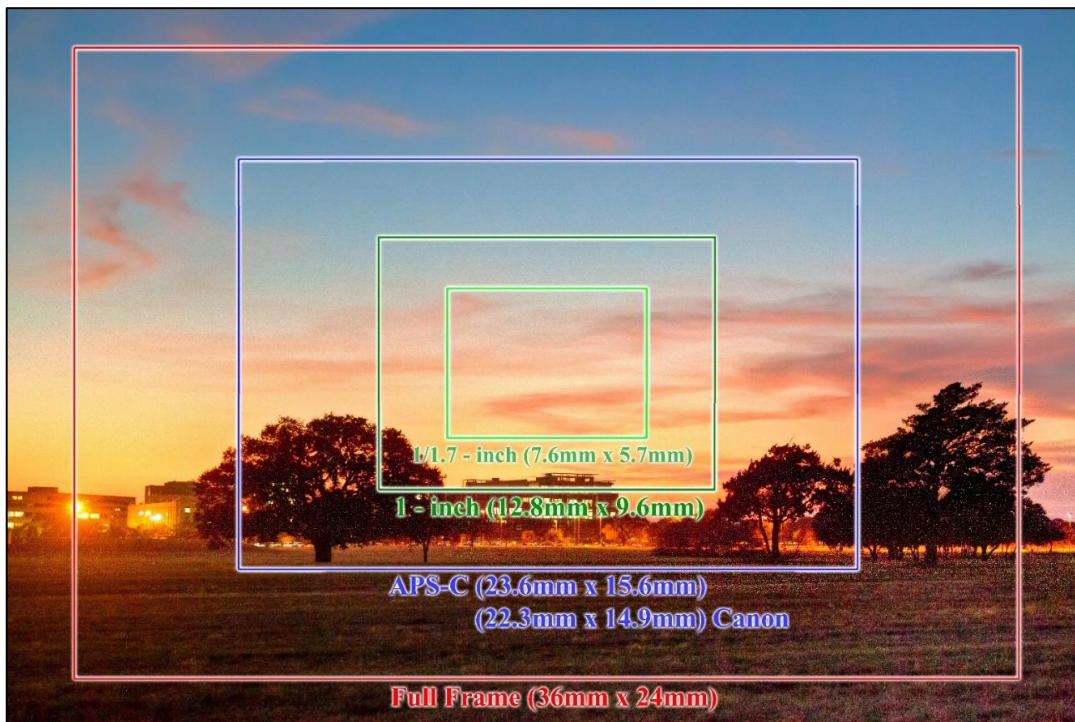


Figure 2-2. Difference of coverage areas based on sensor sizes (From outside: Full Frame (Professional DSLRs), APS-C (Advanced Amateur DSLRs), 1-inch (Higher-End Compacts), and 1/1.7-inch (Compact Cameras)). (Image: Yamafune)

Most manufactured DSLRs are categorized as either professional level or advanced-amateur level. As a result, DSLRs are more expensive than compact cameras. Another benefit of DSLRs is that they have greater options for lens types and accessory equipment, including underwater camera housings and strobe lights. Most manufactured compact cameras tend to come equipped with fixed-lenses which are not interchangeable, and the minimum focal length of those fixed lens are, in most cases, around 24 mm. Thus, DSLR cameras with larger sensor sizes and wider lens options are recommended for use in underwater photogrammetry.

Table 2-1 displays recently manufactured camera models of Canon, Nikon, and Sony, and their approximate retail sales price as indicated by their official company web pages (as of August 2015). The models in the table were selected based on availability of compatible underwater housings; in other words, only camera types that have available underwater housings manufactured by well-known companies (as of August 2015) were listed on Table 2-1. The underwater housing companies selected by the author were Ikelite, Equinox Underwater Housings, Nauticam, Sea and Sea, and Aquatica.

**Table 2-1. Major camera types that have available underwater housings**

	Full Frame (36 x 24mm)	APS-C (22.3 x 14.9mm) Canon (23.6 x 15.6mm) Others	1-in (13.8 x 8.8mm)	1/1.7-in (7.60 x 5.50mm)
Canon	1DX (\$5,999.00)	7D Mark II (\$1799.00)	G7 X (\$699.99)	G16 (\$499.99)
	5D mark III (\$3,099.00)	6Da (\$1,499.00)		S120 (\$449.99)

**Table 2-1 Continued**

	6D (\$1,799.00)	70D (\$1,199.00)		S110 (\$299.99)
	5DSR (\$3,899.00)	60D (\$899.99)		
	5DS (\$3,699.00)	Rebel T5i (\$849.00)		
		Rebel SL1 (\$699.99)		
		Rebel T3i (\$599.99)		
		Rebel T5 (\$549.99)		
		Rebel T3 (\$449.99)		
		Rebel T6s (\$1,199.00)		
		*Rebel T6i (\$899.00)		
Nikon	D4 (\$5,999.95)	D7100 (\$999.95)		P7800 (\$549.95)
	D4S (\$5,999.95)	D7000 (\$999.95)		P340 (\$349.95)
	D810 (\$2,999.95)	D5300 (\$699.95)		
	D750 (\$2,299.95)	D5200 (\$549.95)		
	D610 (\$1,499.95)	D3300 (\$449.95)		
	D810 (\$3,799.95)	D3200 (\$449.95)		
		D5500 (\$899.95)		
Sony	A7R (\$2,099.00)	A6000 (\$549.00)	RX100 III (\$799.99)	
	A99 (\$1,999.00)	A5000 (\$399.00)	RX 100 (\$499.99)	

Tables 2-2 and 2-3 indicate coverage areas of one photo by each sensor size, based on different focal lengths, lens types, and distance from the object. In short, these two tables show sizes of coverage areas based on equipment and circumstance. For instance, when an advanced amateur camera with APS-C sensor size equipped 16 mm focal length lens was used from 1.5 m away from the subject, a photo image can cover 2.20 m horizontally, and 1.47 m vertically.

**Table 2-2.** *Approximate coverage area of one photo by a camera with an APS – C sensor (23.5 mm x 15.6 mm)*

<b>Length Subject Distance</b>	<b>Focal</b>	<b>11 mm HAV: 93.78</b>	<b>16 mm HAV: 72.59</b>	<b>18 mm HAV: 66.27</b>	<b>24 mm HAV: 52.17</b>	<b>35 mm HVA: 37.12</b>
0.5 m		1.07 x 0.71 m	0.73 x 0.49 m	0.65 x 0.43 m	0.49 x 0.33 m	0.34 x 0.22 m
1.0 m		2.14 x 1.42 m	1.47 x 0.98 m	1.31 x 0.87 m	0.98 x 0.65 m	0.64 x 0.45 m
1.5 m		3.20 x 2.13 m	2.20 x 1.46 m	1.96 x 1.30 m	1.47 x 0.98 m	1.01 x 0.67 m
2.0 m		4.27 x 2.84 m	2.94 x 1.95 m	2.61 x 1.73 m	1.96 x 1.30 m	1.34 x 0.89 m
2.5 m		5.34 x 3.55 m	3.64 x 2.44 m	3.26 x 2.17 m	2.45 x 1.63 m	1.68 x 1.11 m
3.0 m		6.41 x 4.69 m	4.41 x 2.93 m	3.92 x 2.60 m	2.94 x 1.95 m	2.01 x 1.34 m

**Table 2-3.** *Approximate coverage area of one photo by a camera with a full-frame sensor (35.9 mm x 24 mm)*

<b>Length Subject Distance</b>	<b>Focal</b>	<b>11 mm HAV: 117.00</b>	<b>16 mm HAV: 96.57</b>	<b>18 mm HAV: 89.84</b>	<b>24 mm HAV: 73.59</b>	<b>35 mm HVA: 54.30</b>
0.5 m		1.63 x 1.09 m	1.12 x 0.75 m	1.00 x 0.67 m	0.75 x 0.50 m	0.51 x 0.34 m
1.0 m		3.26 x 2.18 m	2.24 x 1.50 m	1.99 x 1.33 m	1.50 x 1.00 m	1.03 x 0.69 m
1.5 m		4.90 x 3.27 m	3.37 x 2.25 m	2.99 x 2.00 m	2.24 x 1.50 m	1.54 x 1.03 m
2.0 m		6.53 x 4.36 m	4.49 x 3.00 m	3.99 x 2.67 m	2.99 x 2.00 m	2.05 x 1.37 m
2.5 m		8.16 x 5.45 m	5.61 x 3.75 m	4.99 x 3.33 m	3.74 x 2.50 m	2.56 x 1.71 m
3.0 m		9.79 x 6.55 m	6.73 x 4.50 m	5.98 x 4.00 m	4.49 x 3.00 m	3.08 x 2.06 m

The creators of Agisoft PhotoScan recommend that two consecutive photos have an 80% overlapping area with the forward image, and a 60% overlapping area with the adjacent image for successful photogrammetry coverage (Agisoft LLC, 2014). This 80% overlap results in each specific location appearing in at least four separate photographs for successful photogrammetry coverage. Based on this recommendation, the values of Tables 2-4 and 2-5 display the progression of camera positions from the previous photo location to the following one. For instance, when a camera has a full-frame sensor size with a 24 mm focal length lens, and photos are taken 3.0 m away from the subject, photos are recommended to be taken every 60 cm forward, with 180 cm side overlap.

**Table 2-4.** *Approximate frequency of photo taking to keep ideal overlapping by a camera with an APS-C sensor (23.5 mm x 15.6 mm)*

<b>Focal</b> <b>Length</b> <b>Subject Distance</b>	<b>11 mm</b> HAV: 93.78	<b>16 mm</b> HAV: 72.59	<b>18 mm</b> HAV: 66.27	<b>24 mm</b> HAV: 52.17	<b>35 mm</b> HVA: 37.12
<b>0.5 m</b>	Forward: 14 cm Side: 43 cm	Forward: 10 cm Side: 29 cm	Forward: 9 cm Side: 26 cm	Forward: 7 cm Side: 20 cm	Forward: 4 cm Side: 14 cm
<b>1.0 m</b>	Forward: 28 cm Side: 86 cm	Forward: 19 cm Side: 59 cm	Forward: 17 cm Side: 52 cm	Forward: 13 cm Side: 39 cm	Forward: 9 cm Side: 36 cm
<b>1.5 m</b>	Forward: 43 cm Side: 128 cm	Forward: 29 cm Side: 88 cm	Forward: 26 cm Side: 78 cm	Forward: 20 cm Side: 59 cm	Forward: 13 cm Side: 40 cm
<b>2.0 m</b>	Forward: 57 cm Side: 171 cm	Forward: 39 cm Side: 118 cm	Forward: 35 cm Side: 104 cm	Forward: 26 cm Side: 78 cm	Forward: 18 cm Side: 54 cm
<b>2.5 m</b>	Forward: 71 cm Side: 214 cm	Forward: 49 cm Side: 146 cm	Forward: 43 cm Side: 130 cm	Forward: 33 cm Side: 98 cm	Forward: 22 cm Side: 67 cm
<b>3.0 m</b>	Forward: 94 cm Side: 256 cm	Forward: 59 cm Side: 176 cm	Forward: 52 cm Side: 157 cm	Forward: 39 cm Side: 118 cm	Forward: 27 cm Side: 80 cm

**Table 2-5.** *Approximate frequency of photo taking to keep ideal overlapping by a camera with a full-frame sensor (35.9 mm x 24 mm)*

<b>Focal</b> <b>Length</b> <b>Subject Distance</b>	<b>11 mm</b> HAV: 117.00	<b>16 mm</b> HAV: 96.57	<b>18 mm</b> HAV: 89.84	<b>24 mm</b> HAV: 73.59	<b>35 mm</b> HVA: 54.30
<b>0.5 m</b>	Forward: 22 cm Side: 65 cm	Forward: 15 cm Side: 45 cm	Forward: 13 cm Side: 40 cm	Forward: 10 cm Side: 30 cm	Forward: 7 cm Side: 20 cm

**Table 2-5 Continued**

<b>1.0 m</b>	Forward: 43 cm Side: 130 cm	Forward: 30 cm Side: 90 cm	Forward: 27 cm Side: 80 cm	Forward: 20 cm Side: 60 cm	Forward: 14 cm Side: 41 cm
<b>1.5 m</b>	Forward: 65 cm Side: 196 cm	Forward: 45 cm Side: 135 cm	Forward: 40 cm Side: 120 cm	Forward: 30 cm Side: 90 cm	Forward: 21 cm Side: 62 cm
<b>2.0 m</b>	Forward: 87 cm Side: 261 cm	Forward: 60 cm Side: 180 cm	Forward: 53 cm Side: 160 cm	Forward: 40 cm Side: 120 cm	Forward: 27 cm Side: 82 cm
<b>2.5 m</b>	Forward: 109 cm Side: 326 cm	Forward: 75 cm Side: 224 cm	Forward: 67 cm Side: 200 cm	Forward: 50 cm Side: 150 cm	Forward: 34 cm Side: 102 cm
<b>3.0 m</b>	Forward: 131 cm Side: 392 cm	Forward: 90 cm Side: 269 cm	Forward: 80 cm Side: 239 cm	Forward: 60 cm Side: 180 cm	Forward: 41 cm Side: 123 cm

Lastly, Tables 2-6 and 2-7 show the total recommended number of photos required to provide proper image overlap (80% forward and 60% side). For example, when a camera with an APS-C sensor equipped with an 11 mm focal length lens is employed at 1.0 m distance to cover a 5 m x 5 m area, 50 photos are required to cover the entire area with the recommended overlap.

**Table 2-6. Recommended total number of photos to cover a required area by a camera with a APS-C sensor**

<b>Focal</b> <b>Length</b> <b>Subject Distance</b>	<b>11 mm</b> HAV: 93.78	<b>16 mm</b> HAV: 72.59	<b>18 mm</b> HAV: 66.27	<b>24 mm</b> HAV: 52.17	<b>35 mm</b> HVA: 37.12
<b>0.5 m</b>	10 m <sup>2</sup> : 1680 5 m <sup>2</sup> : 442 3 m <sup>2</sup> : 160	10 m <sup>2</sup> : 3430 5 m <sup>2</sup> : 882 3 m <sup>2</sup> : 308	10 m <sup>2</sup> : 4290 5 m <sup>2</sup> : 1080 3 m <sup>2</sup> : 384	10 m <sup>2</sup> : 7191 5 m <sup>2</sup> : 1820 3 m <sup>2</sup> : 656	10 m <sup>2</sup> : 17856 5 m <sup>2</sup> : 4551 3 m <sup>2</sup> : 1606
<b>1.0 m</b>	10 m <sup>2</sup> : 442 5 m <sup>2</sup> : 112 3 m <sup>2</sup> : 36	10 m <sup>2</sup> : 918 5 m <sup>2</sup> : 225 3 m <sup>2</sup> : 84	10 m <sup>2</sup> : 1140 5 m <sup>2</sup> : 308 3 m <sup>2</sup> : 112	10 m <sup>2</sup> : 2025 5 m <sup>2</sup> : 518 3 m <sup>2</sup> : 189	10 m <sup>2</sup> : 4252 5 m <sup>2</sup> : 1080 3 m <sup>2</sup> : 416
<b>1.5 m</b>	10 m <sup>2</sup> : 198 5 m <sup>2</sup> : 50 3 m <sup>2</sup> : 15	10 m <sup>2</sup> : 396 5 m <sup>2</sup> : 112 3 m <sup>2</sup> : 36	10 m <sup>2</sup> : 519 5 m <sup>2</sup> : 126 3 m <sup>2</sup> : 50	10 m <sup>2</sup> : 882 5 m <sup>2</sup> : 216 3 m <sup>2</sup> : 84	10 m <sup>2</sup> : 1950 5 m <sup>2</sup> : 481 3 m <sup>2</sup> : 168
<b>2.0 m</b>	10 m <sup>2</sup> : 113 5 m <sup>2</sup> : 28 3 m <sup>2</sup> : 12	10 m <sup>2</sup> : 216 5 m <sup>2</sup> : 55 3 m <sup>2</sup> : 24	10 m <sup>2</sup> : 297 5 m <sup>2</sup> : 78 3 m <sup>2</sup> : 28	10 m <sup>2</sup> : 518 5 m <sup>2</sup> : 126 3 m <sup>2</sup> : 50	10 m <sup>2</sup> : 1081 5 m <sup>2</sup> : 260 3 m <sup>2</sup> : 105
<b>2.5 m</b>	10 m <sup>2</sup> : 79 5 m <sup>2</sup> : 15 3 m <sup>2</sup> : 6	10 m <sup>2</sup> : 152 5 m <sup>2</sup> : 36 3 m <sup>2</sup> : 15	10 m <sup>2</sup> : 198 5 m <sup>2</sup> : 50 3 m <sup>2</sup> : 15	10 m <sup>2</sup> : 319 5 m <sup>2</sup> : 84 3 m <sup>2</sup> : 32	10 m <sup>2</sup> : 704 5 m <sup>2</sup> : 168 3 m <sup>2</sup> : 60
<b>3.0 m</b>	10m <sup>2</sup> : 46 5m <sup>2</sup> : 12 3m <sup>2</sup> : 4	10 m <sup>2</sup> : 105 5 m <sup>2</sup> : 28 3 m <sup>2</sup> : 12	10 m <sup>2</sup> : 126 5 m <sup>2</sup> : 32 3 m <sup>2</sup> : 12	10 m <sup>2</sup> : 216 5 m <sup>2</sup> : 55 3 m <sup>2</sup> : 24	10 m <sup>2</sup> : 468 5 m <sup>2</sup> : 119 3 m <sup>2</sup> : 50

**Table 2-7. Recommended total number of photos to cover a required area by a camera with a full-frame sensor (35.9mm x 24mm)**

<b>Focal</b> <b>Length</b> <b>Subject Distance</b>	<b>11 mm</b> HAV: 117.00	<b>16 mm</b> HAV: 96.57	<b>18 mm</b> HAV: 89.84	<b>24 mm</b> HAV: 73.59	<b>35 mm</b> HVA: 54.30
<b>0.5 m</b>	10 m <sup>2</sup> : 704 5 m <sup>2</sup> : 189 3 m <sup>2</sup> : 72	10 m <sup>2</sup> : 1495 5 m <sup>2</sup> : 384 3 m <sup>2</sup> : 144	10 m <sup>2</sup> : 1950 5 m <sup>2</sup> : 481 3 m <sup>2</sup> : 168	10 m <sup>2</sup> : 3332 5 m <sup>2</sup> : 864 3 m <sup>2</sup> : 308	10 m <sup>2</sup> : 7191 5 m <sup>2</sup> : 1820 3 m <sup>2</sup> : 656
<b>1.0 m</b>	10 m <sup>2</sup> : 198 5 m <sup>2</sup> : 50 3 m <sup>2</sup> : 15	10 m <sup>2</sup> : 384 5 m <sup>2</sup> : 105 3 m <sup>2</sup> : 32	10 m <sup>2</sup> : 468 5 m <sup>2</sup> : 119 3 m <sup>2</sup> : 50	10 m <sup>2</sup> : 864 5 m <sup>2</sup> : 207 3 m <sup>2</sup> : 78	10 m <sup>2</sup> : 1750 5 m <sup>2</sup> : 442 3 m <sup>2</sup> : 160
<b>1.5 m</b>	10 m <sup>2</sup> : 84 5 m <sup>2</sup> : 24 3 m <sup>2</sup> : 9	10 m <sup>2</sup> : 168 5 m <sup>2</sup> : 50 3 m <sup>2</sup> : 15	10 m <sup>2</sup> : 207 5 m <sup>2</sup> : 55 3 m <sup>2</sup> : 18	10 m <sup>2</sup> : 384 5 m <sup>2</sup> : 105 3 m <sup>2</sup> : 32	10 m <sup>2</sup> : 782 5 m <sup>2</sup> : 198 3 m <sup>2</sup> : 78
<b>2.0 m</b>	10 m <sup>2</sup> : 50 5 m <sup>2</sup> : 12 3 m <sup>2</sup> : 4	10 m <sup>2</sup> : 105 5 m <sup>2</sup> : 28 3 m <sup>2</sup> : 9	10 m <sup>2</sup> : 119 5 m <sup>2</sup> : 32 3 m <sup>2</sup> : 12	10 m <sup>2</sup> : 207 5 m <sup>2</sup> : 55 3 m <sup>2</sup> : 18	10 m <sup>2</sup> : 455 5 m <sup>2</sup> : 119 3 m <sup>2</sup> : 45
<b>2.5 m</b>	10 m <sup>2</sup> : 32 5 m <sup>2</sup> : 9 3 m <sup>2</sup> : 4	10 m <sup>2</sup> : 60 5 m <sup>2</sup> : 15 3 m <sup>2</sup> : 4	10 m <sup>2</sup> : 78 5 m <sup>2</sup> : 18 3 m <sup>2</sup> : 6	10 m <sup>2</sup> : 144 5 m <sup>2</sup> : 32 3 m <sup>2</sup> : 12	10 m <sup>2</sup> : 308 5 m <sup>2</sup> : 78 3 m <sup>2</sup> : 28
<b>3.0 m</b>	10 m <sup>2</sup> : 24 5 m <sup>2</sup> : 4 3 m <sup>2</sup> : 4	10 m <sup>2</sup> : 50 5 m <sup>2</sup> : 12 3 m <sup>2</sup> : 4	10 m <sup>2</sup> : 55 5 m <sup>2</sup> : 15 3 m <sup>2</sup> : 4	10 m <sup>2</sup> : 105 5 m <sup>2</sup> : 28 3 m <sup>2</sup> : 9	10 m <sup>2</sup> : 207 5 m <sup>2</sup> : 55 3 m <sup>2</sup> : 18

The tables above can be used as guidelines when choosing cameras and lenses based on the unique conditions and requirements of a given archaeological site, and the characteristics under which a camera is expected to be used during its lifetime.

Archaeologists must choose cameras and related equipment based on cost, available lenses, accessories, and water-visibility of the archaeological sites to be recorded. The indicated total number of photos must be considered in order to allow a good choice of computing power and required storage capacity of the project's computer.

Under-exposure environments are another relevant problem in underwater photography; photos taken under water tend to be underexposed and have a marked shift to the blue side of the color spectrum. Hence, lower lighting environments call for the use of strobe lights to ensure proper exposure and solve the blue coloration problem (Fig. 2-3). Artificial light also solves the light-column problem caused by shadows



projected from the water surface in shallow water. Two strobe lights with long articulated arms create the best and most flexible equipment arrangement for Computer Vision Photogrammetry (Fig. 2-4). PhotoScan and other Computer Vision Photogrammetry software recognize pixel information to develop the depth in point clouds. Shadows cast by strobe lights must be avoided because they change position from image to image, and do not reveal a stable color for the materials of the objects being recorded.

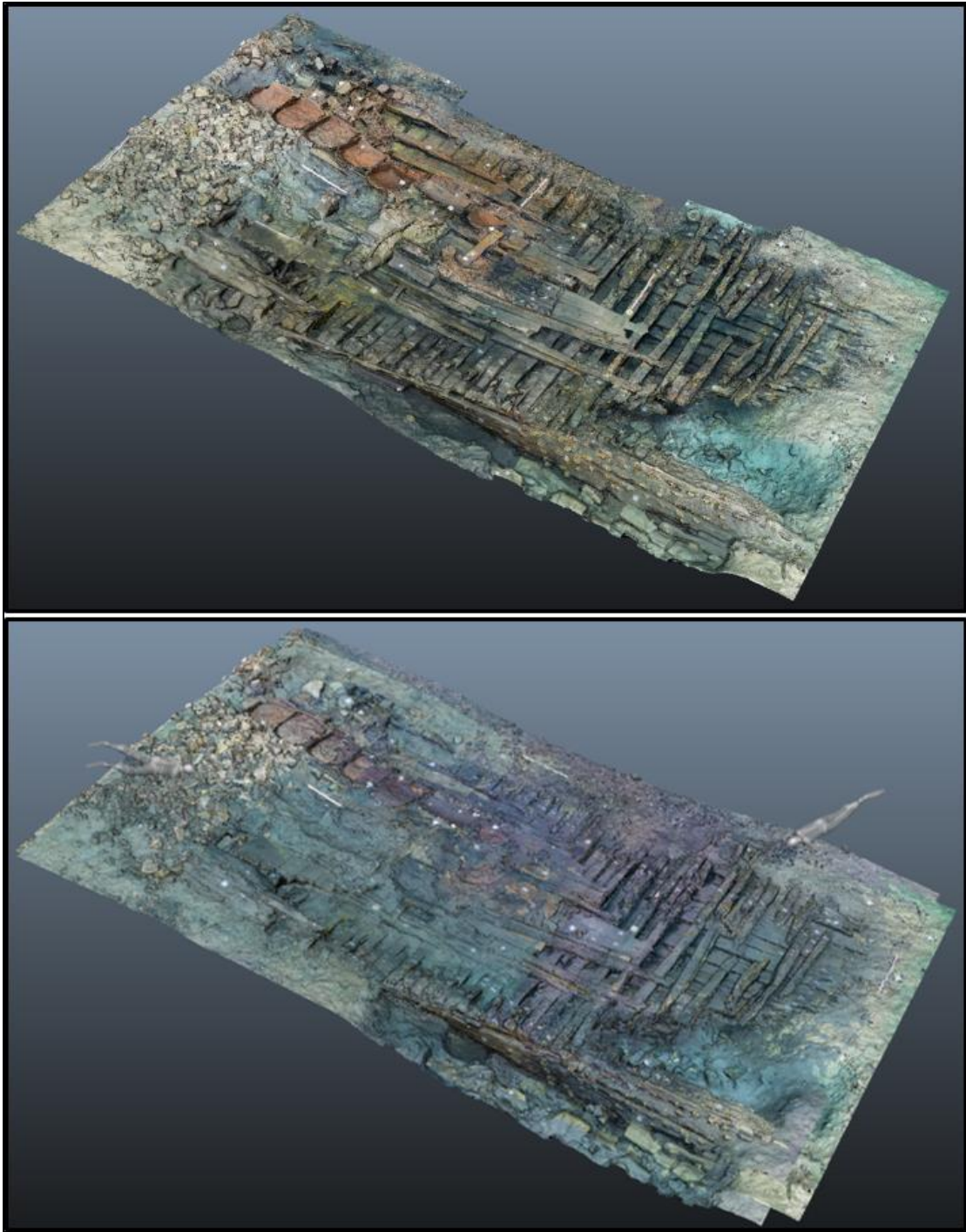


*Figure 2-3.* Photogrammetric models of the Gnalić shipwreck site (based on photos with/without strobe lights). The top model is based on photos taken with strobe lights (photos taken between August 4th and 13th 2014), and the bottom photogrammetric model is based on photos taken without strobe lights (photos taken on July 18th 2014). As can be seen, the left model has more original colors of materials than that the right model. (Image: Yamafune)

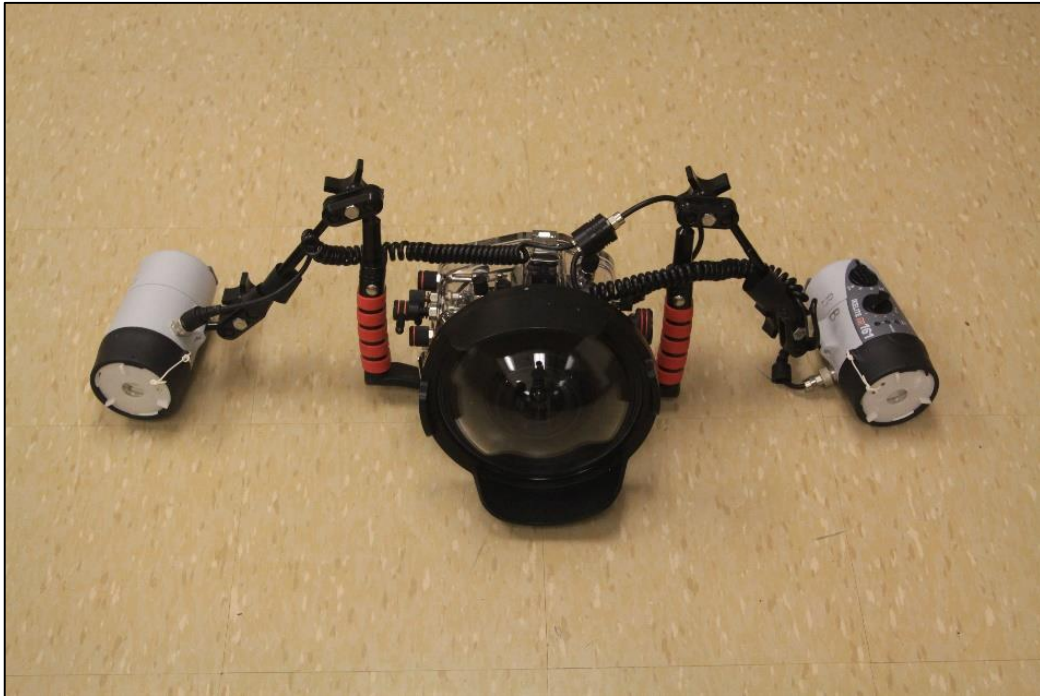


*Figure 2-4.* Recommended underwater camera equipment. The housing is equipped with two strobe lights and an eight-inch hemispheric dome port. (Photo: Yamafune)

Care must be taken to manage the capacity and duration of strobe light batteries. This is typically a difficult problem to resolve because the number of pictures required is always high; batches of 1,000 photos per dive may be necessary to ensure the proper coverage of a given site. If the battery of a strobe light is exhausted during a photogrammetry dive, the colors in the photos before and after the battery failure will vary, and the PhotoScan Align Photos function will be seriously compromised. Again, using DSLR cameras in conjunction with a strobe presents an added advantage, as their wider coverage reduces the total number of pictures required.

## **Underwater Coded Targets**

There is another practice related to underwater photography that increases the accuracy of Computer Vision Photogrammetry. As noted above, the proposed methodology in this dissertation uses Agisoft PhotoScan Professional Edition for Computer Vision Photogrammetry. PhotoScan has four main steps for the photogrammetric modeling: Align Photos, Build Dense Cloud (a point cloud), Build Mesh (in which the Mesh is the surface of the model made up of polygons overlaid over the point cloud), and Build Texture. The result can be improved using a number of relatively simple procedures. One of these is the use of coded targets, an array of simple, unique images that PhotoScan uses to help identify the area being recorded.

PhotoScan provides a collection of coded targets in PDF format, which can be printed at chosen sizes. Following a series of trials carried out at the Texas A&M Ship Reconstruction Laboratory (ShipLab) and in a nearby swimming pool in early 2014, the author found that targets with a center circle radii of between 5 and 10 mm worked best underwater. These values were selected for a camera with an APS-C sensor size, with an 11 mm lens, shooting at a distance of 1.5 m. The results of this laboratory testing were field-tested during the summer of 2014 when the author employed coded targets with a 7.5 mm center circle radius at the Gnalić Project in Croatia. The benefits of using coded targets to help the software align the photos were tremendous. On 18 July 2014, the author placed 36 coded targets on the Gnalić shipwreck site prior to the photo-shooting session. That session required 1653 photos, which covered a 16 m x 12 m area. In the subsequent Align Photos process, the total number of successfully aligned photos

amounted to 100%, meaning that all 1,653 photos were successfully aligned (Fig. 2-5). When the author tried the function Align Photos using same images and settings, but without recognizing the coded targets, the total number of successfully aligned photos dropped to 804 (49% alignment).

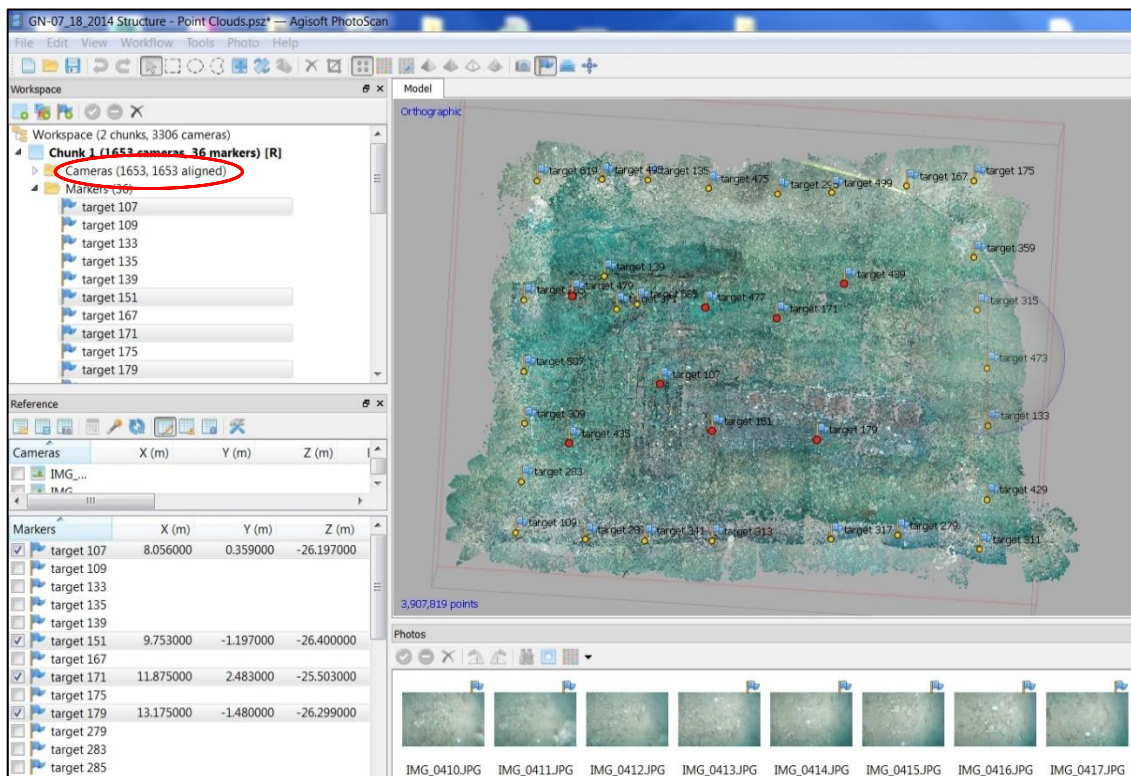
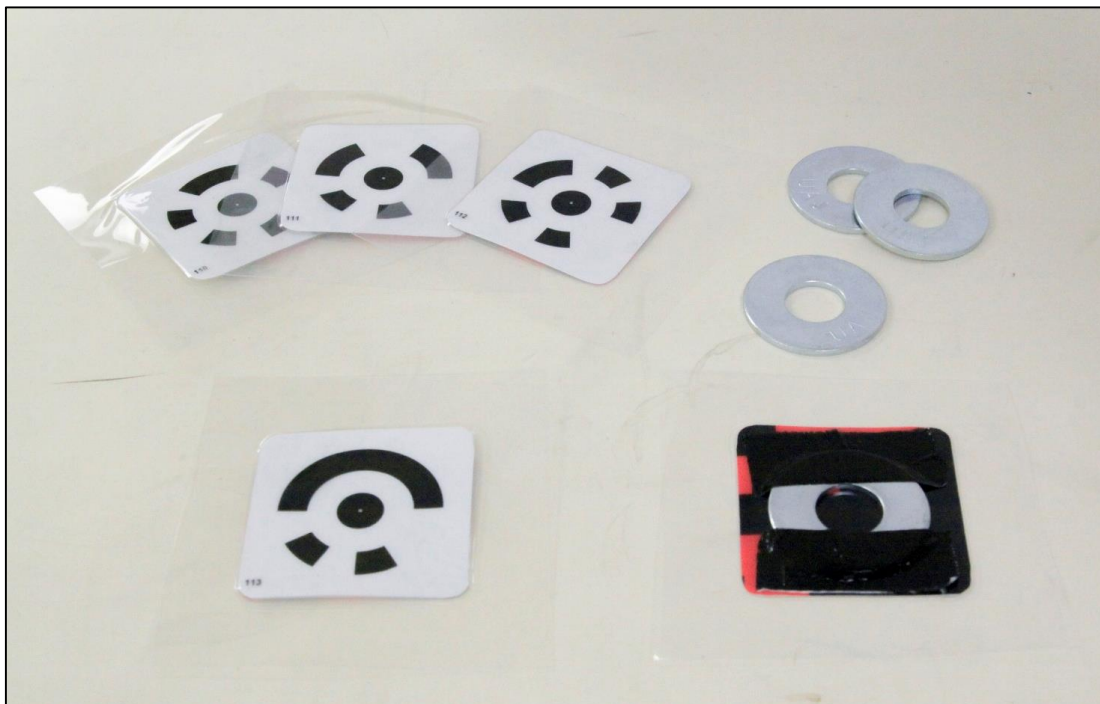


Figure 2-5. Sparse point clouds of the Gnalčić shipwreck site on 18 July 2014 in PhotoScan. Number in the red circle indicates that 1,653 photos are aligned from 1,653 uploaded photos. The yellow and red dots on the point cloud model are coded target locations. Targets with red dots (selected targets) were also used as reference points, which have known coordinates. (Image: Yamafune)

Because coded targets were designed for use on terrestrial sites, using them in water requires some special care. Before leaving for Croatia, the author prepared 80

coded targets for the Gnalić 2014 field season by waterproofing them with a thermal plastic lamination, as described below. Some of the targets were fixed to the shipwreck structure during the entire two months of the excavation; the pristine condition of those targets at the end of the excavation validated the waterproofing technique for underwater target durability (Fig. 2-6).



*Figure 2-6. Underwater coded targets and their additional weights (zinc washers). (Photo: Yamafune)*

The targets were printed on Mylar (plastic paper) to take advantage of the transparency of the material. An important point to keep in mind is that targets must be printed using a laser printer; the toner of laser printers does not dissolve in water. The

printed coded targets were then cut into individual pieces and glued on white plastic boards. For the final step, the coded targets were laminated for additional durability and to create additional margins around the targets to allow the use of nails to fix the targets to the structure. For targets that needed to be moved to provide daily coverage, zinc washers were attached with duct tape to provide sufficient weight.

PhotoScan can also automatically detect coded targets in any photo. Using this function, coded targets are advantageous and can be used as reference points by recording known coordinates that are measured *in situ*, which are then input into the photogrammetry process in order to create 1:1 exact scaled photogrammetric models.

#### *Recommended Sizes for Coded Targets (Based on Focal Length and Distance)*

The print size of coded targets must be chosen based on camera choice and anticipated focal length. To test successful recognition, the author prepared different sizes of coded targets: center point diameter of 2.5 mm, 5.0 mm, 7.5 mm, 10.0 mm, 15.0 mm, and 20.0 mm. Twenty of each size of coded target were fixed on a wall, and photos were taken at different distances from the wall: 0.5 m, 1.0 m, 1.5 m, 2.0 m, and 3.0 m. The author used a Nikon D7100, an advanced amateur-level camera with APS-C sensor size. This examination was repeated using three different focal lengths: 11 mm, 18 mm, and 24 mm. Then all the photos were imported to PhotoScan, and automate marker detection was applied on those photos (with detection tolerance of 50). Tables below display the results (Table 2-8, 2-9, and 2-10).

**Table 2-8.** Coded targets recognition by a camera with 11 mm focal length (DSLR camera with APS-C sensor size)

CTs Distance	0.5 m	1.0 m	1.5 m	2.0 m	3.0 m
Center Point Radius					
CTs 2.5 mm	100%	× (95%)	× (0%)	× (0%)	× (0%)
CTs 5.0 mm	100%	100%	100%	× (95%)	× (5%)
CTs 7.5 mm	100%	100%	100%	100%	100%
CTs 10.0 mm	100%	100%	100%	100%	100%
CTs 15.0 mm	× (0%)	100%	100%	100%	100%
CTs 20.0 mm	× (0%)	× (70%)	100%	100%	100%
CTs 25.0 mm	× (0%)	× (0%)	100%	100%	100%

**Table 2-9.** Coded targets recognition by a camera with 18 mm focal length (DSLR camera with APS-C sensor size)

CTs Distance	0.5 m	1.0 m	1.5 m	2.0 m	3.0 m
Center Point Radius					
CTs 2.5 mm	100%	100%	100%	× (0%)	× (0%)
CTs 5.0 mm	100%	100%	100%	100%	100%
CTs 7.5 mm	100%	100%	100%	100%	100%
CTs 10.0 mm	× (0%)	× (90%)	100%	100%	100%
CTs 15.0 mm	× (0%)	× (0%)	100%	100%	100%
CTs 20.0 mm	× (0%)	× (0%)	× (65%)	100%	100%
CTs 25.0 mm	× (0%)	× (0%)	× (0%)	× (15%)	100%



**Table 2-10. Coded targets recognition by a camera with 24mm focal length (DSLR camera with APS-C sensor size)**

CTs Distance	0.5 m	1.0 m	1.5 m	2.0 m	3.0 m
Center Point Radius					
CTs 2.5 mm	100%	100%	100%	× (90%)	× (0%)
CTs 5.0 mm	× (45%)	100%	100%	100%	100%
CTs 7.5 mm	× (0%)	100%	100%	100%	100%
CTs 10.0 mm	× (0%)	× (0%)	100%	100%	100%
CTs 15.0 mm	× (0%)	× (0%)	× (0%)	100%	100%
CTs 20.0 mm	× (0%)	× (0%)	× (0%)	× (0%)	100%
CTs 25.0 mm	× (0%)	× (0%)	× (0%)	× (0%)	× (35%)

These results suggest that a coded target will be recognized successfully when the diameter of its outer circle is shown between 80 pixels and 300 pixels in a photo (Fig. 2-7 and 2-8). This success range for target size should be confirmed for a specific camera at a specific focal length by taking a photo of a coded target to check if its outer circle has a pixel diameter between 80 pixels and 300 pixels.

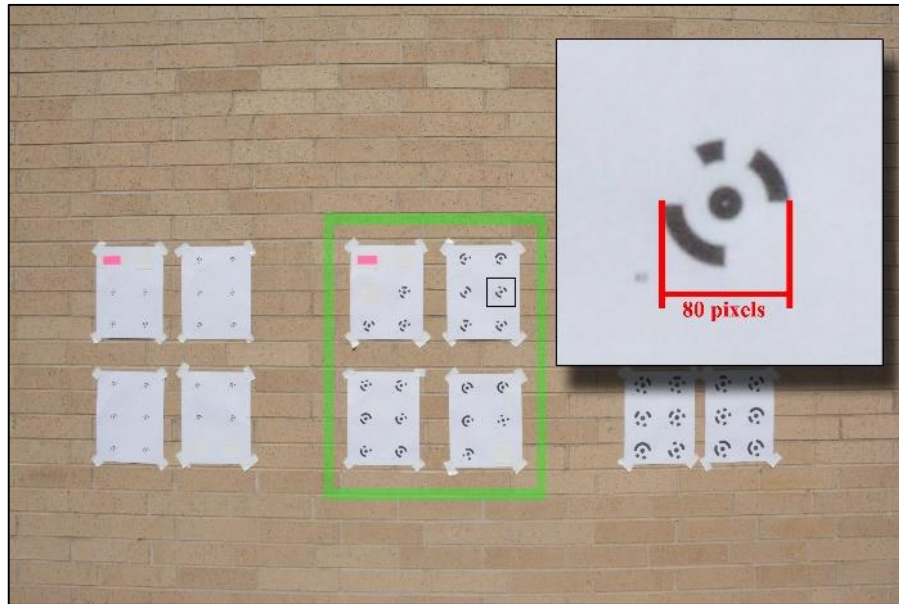


Figure 2-7. Photo of coded targets shown in a minimum recommended size. Photo was taken by a camera with APS-C sensor (with 18 mm Focal Length and 2 m away from the CTs) (6000 x 4000 pixels / 300dpi). The series of targets in the center (7.5 mm center point radius) have 80 pixels at the outer circle. 80pixel diameter is a recommended minimum size for coded targets. (Photo: Yamafune)



Figure 2-8. Photo of coded targets shown in a maximum recommended size. Photo was taken by a camera with APS-C sensor (with 18 mm Focal Length and 2.0 m away from the CTs) (6000 x 4000 pixels / 300dpi). The targets (20.0 mm center point radius) have 300 pixels at the outer circle. 300 pixel diameter is a recommended maximum size for coded targets. (Photo: Yamafune)

### *Recommended Flight Path with Coded Targets*

As discussed above, photo alignment is the most important factor for successful photogrammetric modeling. In order to maximize the probability of creating successful photo alignment, the author developed a flight path with coded targets for photo shooting. Technically speaking, higher numbers of coded targets increase the accuracy of photo alignment; however, an excessive number of coded targets on shipwreck structures and artifacts may detract from the aesthetic appearance of the site, and may also cover important diagnostic features. To avoid placing coded targets directly on the wreck structure, the author recommends a flight path that places coded targets around a shipwreck structure to increase the accuracy of photo alignment (Fig. 2-9). Furthermore, the best results have been achieved by capturing surrounding coded targets first to Lock the site. Then, photographs are taken perpendicularly to capture a top view of the site with appropriate overlap. After complete photo shooting in both transversal and longitudinal paths, additional photographs must be taken with the camera tilted to capture vertical surfaces of rich tridimensional structures. Actual flight path of archaeological sites can vary depending on multiple factors; therefore, meticulous planning of a flight path is an important part of successful photogrammetric recording.

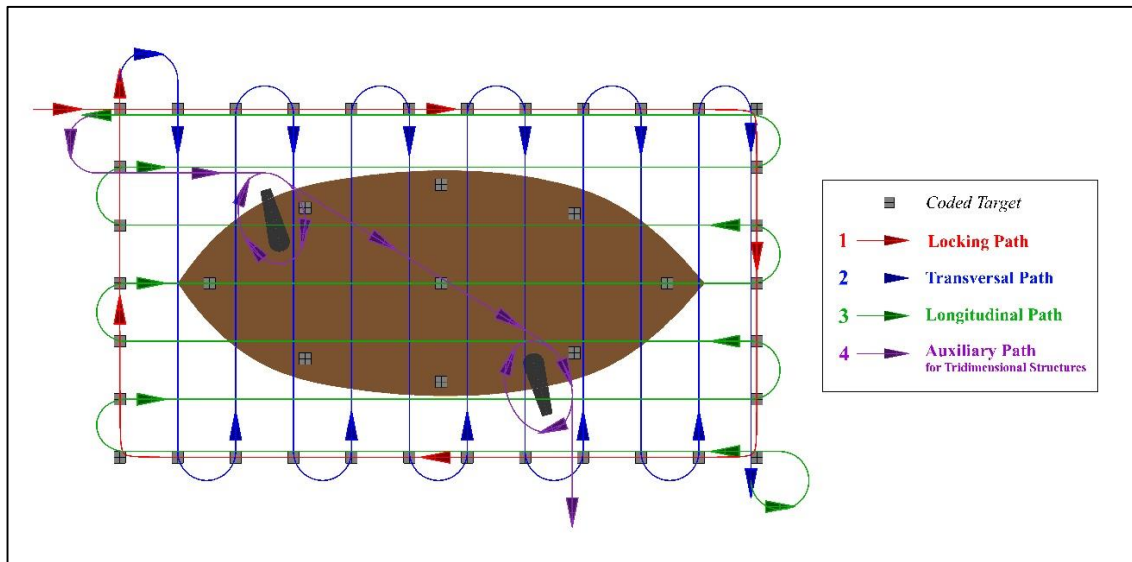


Figure 2-9. Recommended flight path for photogrammetric recording. (Image: Yamafune)

## Local Coordinate Network

Tying the site plan to a set of local coordinates is a key factor of this workflow process. There are two reasons that creating a local set of coordinates is important: to correct scale and distortion of the photogrammetric models and to geographically reference the site plan.

One of the advantages of Computer Vision Photogrammetry is that it does not require precise calibration of the camera. Although calibration is recommended, the software primarily uses pixel information to reconstruct a site, which means that the construction of the point clouds does not require manual calibration. Moreover, the software reads metadata from the camera and lens and minimizes the errors. Distortions are inevitable, however, and this factor alone argues for the necessity of establishing a set of precisely positioned datum points.

The second reason to establish a number of datum points is that unless tied to a system of coordinates, models float in unspecified tridimensional fields. To fix the models in the correct position, local coordinates have to be included on the models. Without this, it is impossible to export the computer graphics files to mapping software with the correct position. Georeferenced information facilitates a straightforward workflow when models and orthophotos (high resolution photomosaics) are exported. The processing and rendering capacity of the PhotoScan software is limited by both software and hardware configurations. This constrains the maximum polygon count for the mesh (which makes up the surface of the model), and the maximum number and resolution of UV mapped textures ('UV' is a XY coordinates for texture), which are composed photomosaic on surfaces of mesh. Large data sets can be divided into smaller Chunks (PhotoScan's term), which are separately processed. These Chunks can be imported into other modeling and mapping software applications and merged without decimation (the reducing of the polygon count). When models and orthophotos are georeferenced, the merging process is automatic, and exported files are opened in their correct positions in other software. A set of local coordinates is paramount to ensure an accurate manipulation of models or orthophotos.

During the Gnalić 2014 field season, the author and ShipLab team created a control network using eight datum points solidly fixed to the site bedrock and shored with sand bags. These eight points were positioned using *3H Site Recorder*, a mapping software that uses statistical adjustment of trilateration, also known as Direct Survey Method (DSM). Depths of all points were taken with a depth gauge in rapid sequence to

avoid the effect of tide. Several measurements were taken and averaged (Fig. 2-10). The accuracy of DSM has been discussed and judged reliable by multiple sources (Atkinson *et al.*, 1988; Rule, 1989; Green *et al.*, 2002; Holt, 2003; Green and Gainsford, 2003). As Holt (2003) pointed out, the acquisition of direct measurements and manipulation of the software are very simple, but can generate errors when handled by novice divers alone. Holt (2003) recommends the use of experienced divers in this phase.

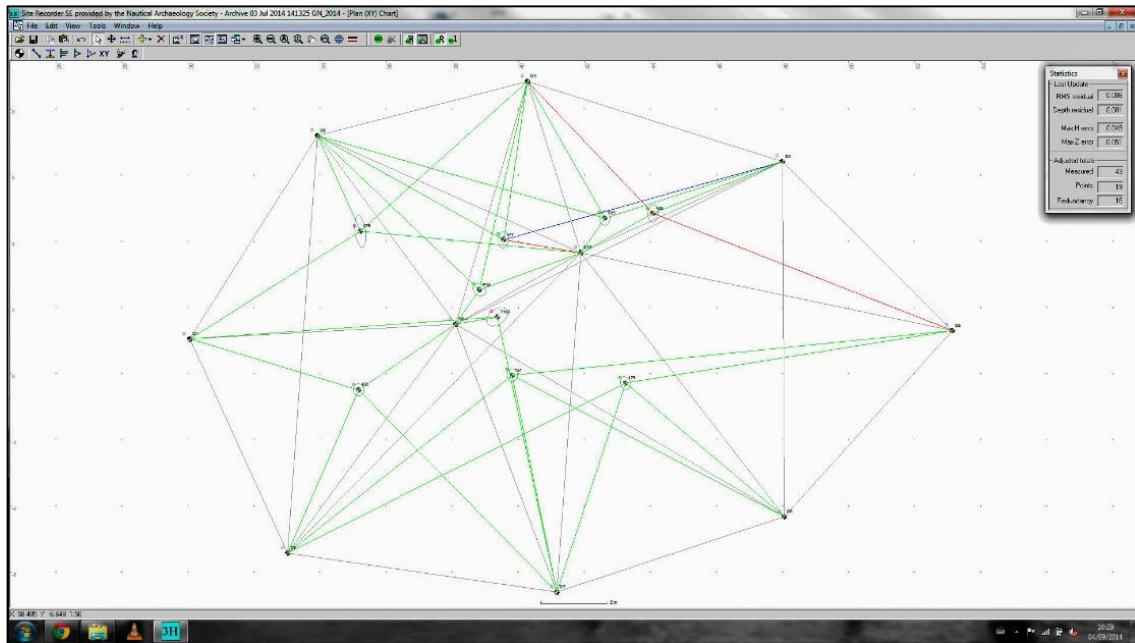


Figure 2-10. Local coordinate network of the Gnalčić shipwreck site from 2014 field season (in 3H Site Recorder). (Image: Reprinted with permission from Torres, 2014a)

While several articles have discussed the accuracy of survey methods using trilateration (DSM), PhotoScan allows the input of measurements in a different way. PhotoScan uses scale bars, or known distance, instead of importing local coordinates

collected using DSM. At actual archaeological sites, establishing control points and local coordinates may take a week or two. This may not be suitable for a short-term survey project. This chapter discusses four different methods to fix distortions and scale of photogrammetric models. To test accuracy, local coordinates or known distances that were established using the four different methods were applied to a photogrammetric model. Then, the dimensions of the fixed models were compared with the control measurements to check relative accuracies.

#### *Methodology for Testing Different Local Coordinate Systems*

Measuring methods that will be discussed and compared in this chapter are: trilateration(DSM) using 3H Site Recorder, creating an enclosure using rope that is cut to known distances, scale bars that are placed on the site, and coordinates taken by total station. To compare and examine the accuracy of these four methods, local coordinates and known distances of these four methods were applied to a photogrammetric model, and each different method was compared to control measurements. The control measurements were taken directly from the wooden model. For this test, the author used a 1/10 scale wooden model of a *saveiro*, a 20<sup>th</sup>-century Brazilian coastal sailing boat. In order to simulate an archaeological shipwreck site, the wooden model was laid down on its starboard side, and its floor timbers were pulled slightly out so that its starboard futtocks lay on the bottom (Fig. 2-11). An historical and structural description of the original *saveiro* ship shall be discussed in Chapter VI.

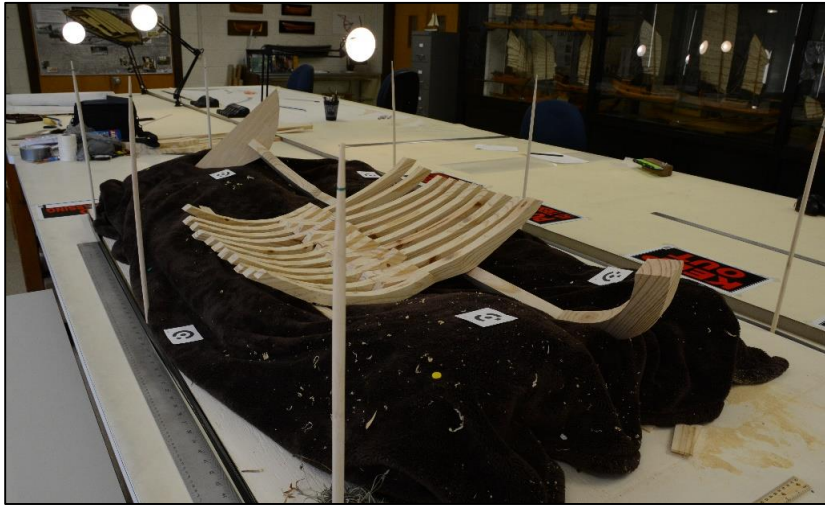


Figure 2-11. *Saveiro* wooden ship model (1:10 size) for photogrammetry. This model was used for testing different survey methods that correct distortions and scales of a created photogrammetric model. (Photo: Yamafune)

### *Trilateration (Direct Survey Method)*

The first method to discuss is trilateration, also known as Direct Survey Method (DSM). Trilateration (DSM) has been repeatedly used in underwater archaeological recordings. For this DSM, the author used 3H Site Recorder (Demo Version). In order to acquire coordinates of reference points, a control network first had to be established. The author placed eight control points around the wooden model, set all the control points to a congruent height (40 cm from the ground), and set this height as the surface of the water, or depth of 0 cm. To establish the positions of the control points, or a control network, 19 measurements were taken (Fig. 2-12). The tolerance established for errors was set at 0.3 cm; therefore, all distance errors bigger than 0.3 cm were shown in red (shorter) and blue (longer). Only one distance (CP5 – CP7) showed a + 0.39 cm statistical error after the adjustment of the control points.



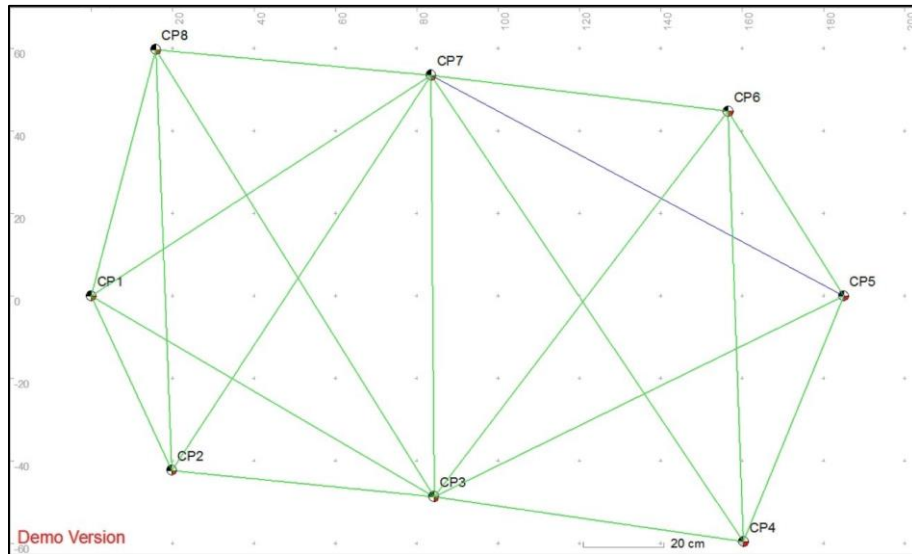


Figure 2-12. The local coordinate network of datum points (control network) around the *saveiro* wooden model (Top view: horizontal plane). (Image: Yamafune)

After the control network, or positions of datum points, was established, 11 reference points were placed on the model. A total of 44 measurements were taken from the control points; each reference point was measured from the nearest four control points (Fig. 2-13 and 2-14). Two measurements indicated over 0.3 cm error; however, both errors were less 0.5 cm, which is within an acceptable range of error. After the local coordinate network of the *saveiro* model was established, XYZ coordinates of the reference points were extracted (Table 2-9). Then, these coordinates were plotted on the photogrammetric *saveiro* model.

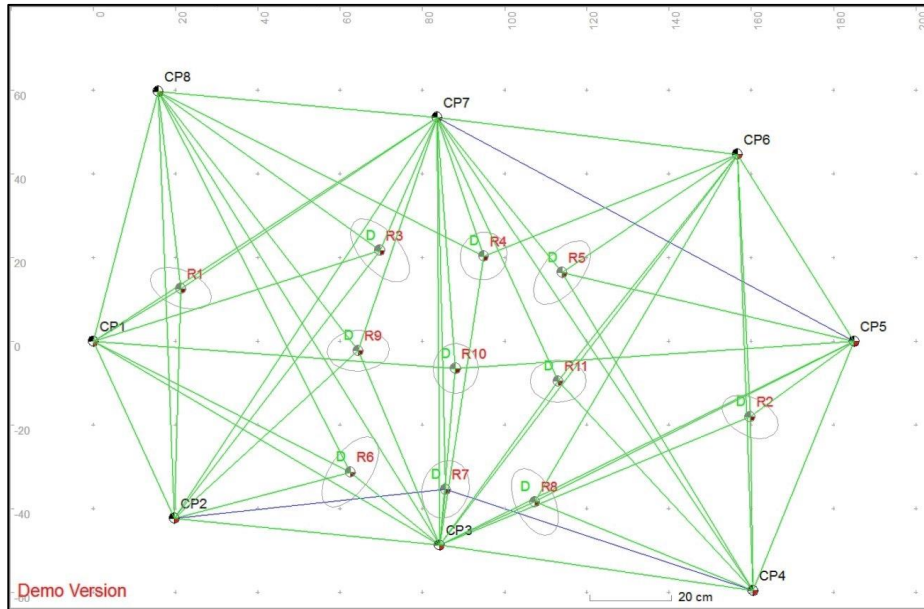


Figure 2-13. The local coordinate network of reference points and control points around the *saveiro* wooden model (Top view: horizontal plane). (Image: Yamafune)

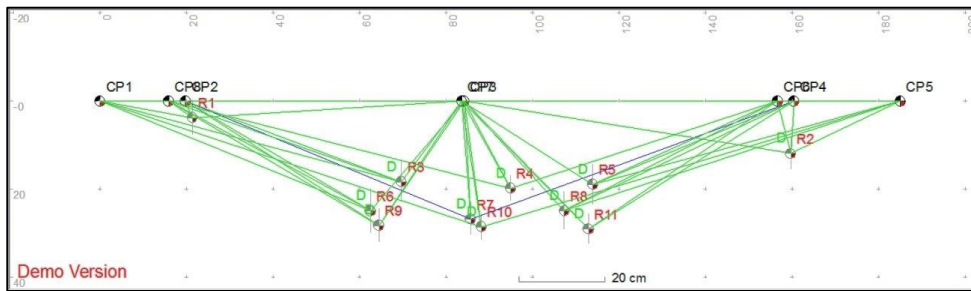


Figure 2-14. The local coordinate network of reference points and control points around the *saveiro* wooden model (Front view: vertical plane). (Image: Yamafune)

**Table 2-11.** Local coordinates of reference points based on DSM. (in 3H Site Recorder)

Reference Points	X coordinate (cm): (Easting)	Y coordinate (cm): (Northing)	Z coordinate (cm): (Altitude)
<b>R1</b>	21.286	12.682	-3.755
<b>R2</b>	159.698	-18.054	-11.948
<b>R3</b>	69.658	21.771	-18.348
<b>R4</b>	94.853	20.398	-19.842

**Table 2-11** Continued

<b>R5</b>	113.955	16.491	-18.990
<b>R6</b>	62.489	-31.233	-24.989
<b>R7</b>	85.599	-35.372	-26.887
<b>R8</b>	107.292	-38.358	-24.991
<b>R9</b>	64.402	-2.273	-28.310
<b>R10</b>	88.080	-6.521	-28.613
<b>R11</b>	112.957	-9.543	-29.085

*Enclosure*

The next method to be examined was designated the enclosure method. This method is based on the idea of enclosing an archaeological site using ropes (using measuring tapes as ropes is recommended) that are cut in predetermined, controlled lengths; therefore, the distances between the four corners will be known without having to take a series of tape measurements. Using the known distances that surround a site, distortions and scales of a photogrammetric model can be fixed. The relative coordinates of the four corners of any given site can be calculated using simple trigonometric equations or existing tools in CAD software. Additionally, using the Pythagorean Theorem, the angles of the four corners of a rectangular area can be exactly set at 90 degrees (Fig. 2-15). To test the accuracy of the enclosure method, the author used the four corners of the base of the *saveiro* wooden model. These were measured: 101.2 cm at the stern, 101.5 cm at the bow, 182.8 cm at the starboard side, and 182.6 cm at the port side. The angle of each corner was measured at 90 degrees. The four distances were entered on the photogrammetric model (Fig. 2-16).

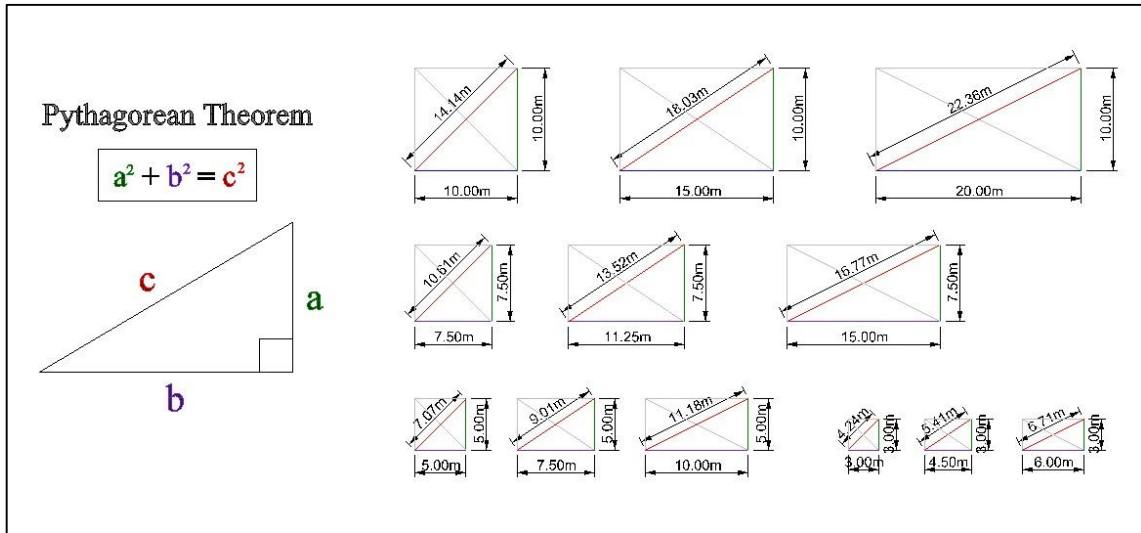


Figure 2-15. Examples of rope lengths for enclosure method. Using the Pythagorean Theorem, the angles of the corners can be controlled as 90 degrees. (Image: Yamafune)

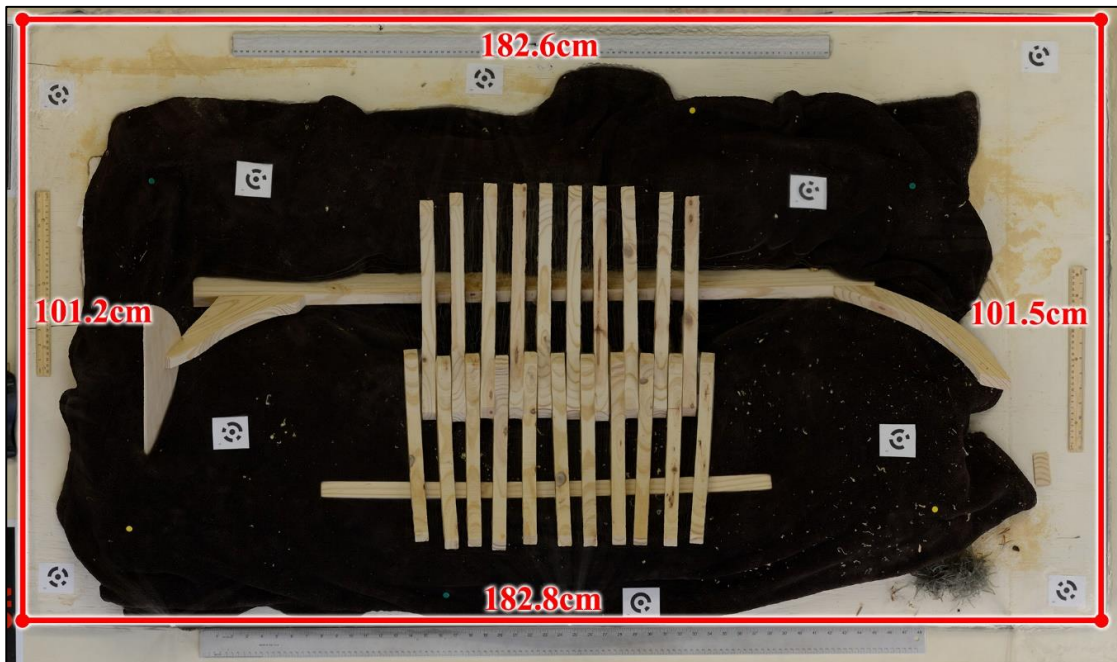


Figure 2-16. Distances between the four corners of the *savairo* wooden model for the enclosure method. (Image: Yamafune)

### *Scale Bars*

Scale bars are often used when pictures of archaeological sites are taken. These scale bars can be extremely useful in Computer Vision Photogrammetry. Scale bars give accurate scale information in archaeological photography, and when a site is being mapped using Computer Vision Photogrammetry, they can be used to check measurements after other methods, such as DSM, were used to correct distortion and scale of a created photogrammetric model. However, distortions and dimensions can be fixed by using only scale bars, a feature that allows archaeologists to skip the time consuming and sometimes inaccurate DSM system. This may be one of the simplest methods used to record a site. To test the accuracy of this method, four scale bars were placed on the four sides of the *saveiro* model. In this particular case, considering the size of the model the four scale bars available were unnecessarily long. Therefore, seven 10 cm scale bars with markers were created on the existing scale bars. These smaller 10 cm bars were entered as fixed distances in the photogrammetric model (Fig. 2-17).

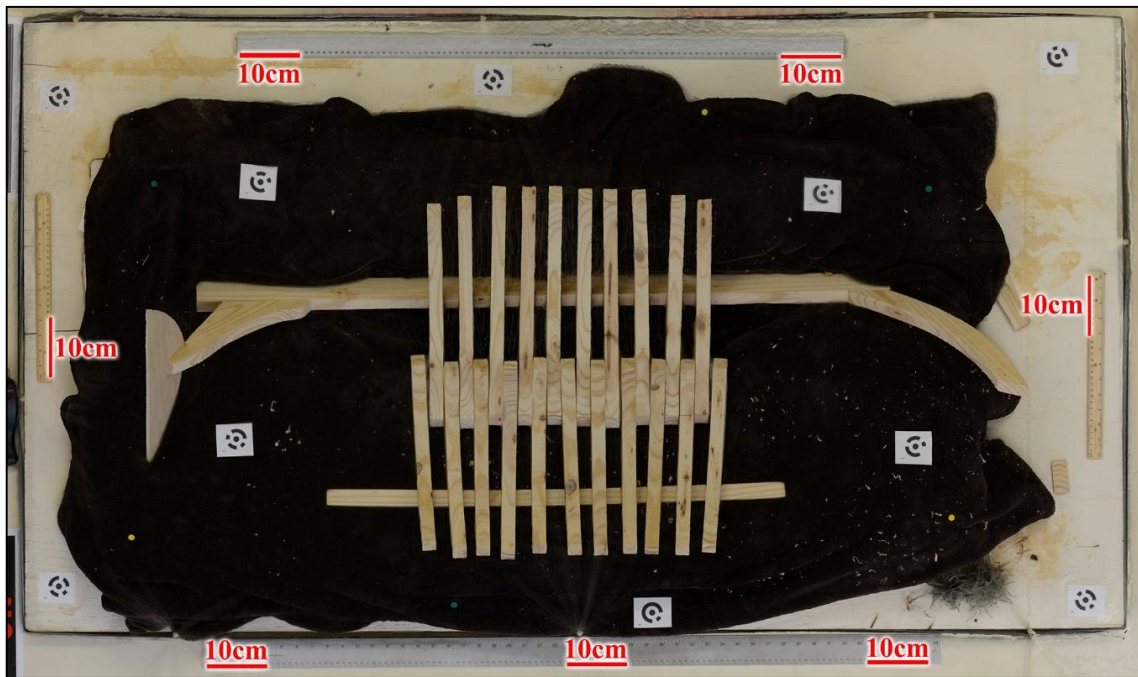


Figure 2-17. Seven 10 cm scale bars created on the *saveiro* photogrammetric model for the scale bar method (Image: Yamafune)

### *Total Station*

On terrestrial archaeological sites, total stations are used as an effective and easy way to acquire local coordinates; total stations cannot, however, be used in underwater environments. Nonetheless, not all shipwreck sites are submerged, and total stations are a widely used recording method known for accuracy. To compare the accuracy of the different methods described above, the coordinates of the *saveiro* model were also collected with a total station. A series of coordinates of control points and reference points were taken with a total station, and these points were plotted in Rhinoceros 3D-CAD modeling software. Then all the points were re-oriented to match the coordinate system previously established, which has Control point 1 as the origin of the coordinate

system. Control point 1 (CP1) was attributed coordinates X=0, Y=0, Z=0, and control point 5 (CP5) was placed on the X-axis, or the easting line (Fig. 2-18). Coordinates of the reference points measured by the total station were shown in Table 2-12.

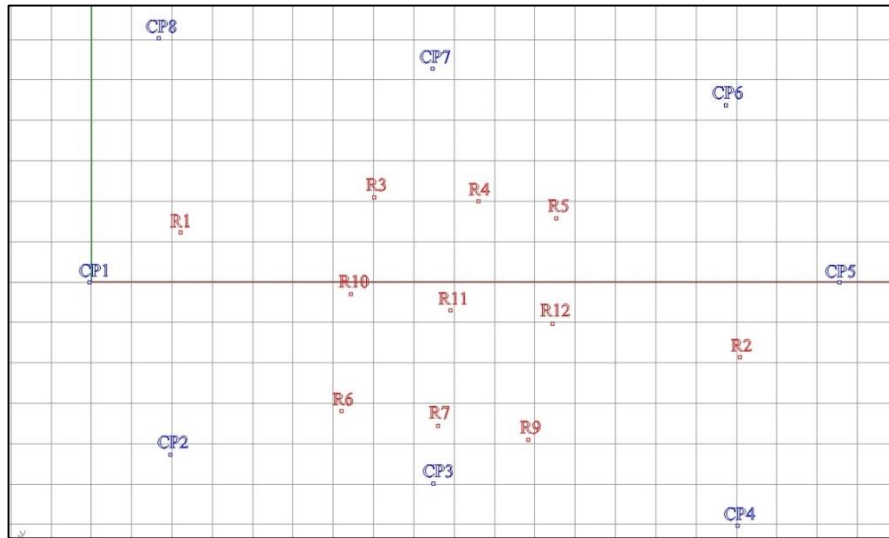


Figure 2-18. Coordinates of the control points and reference points on the *saveiro* wooden model by total station that were plotted in Rhinoceros 3D CAD software. (Image: Yamafune)

**Table 2-12.** *Coordinates of the reference points measured by total station*

Reference Points	X Coordinates (cm): (Easting)	Y Coordinates (cm): (Northing)	Z Coordinates (cm): (Altitude)
<b>R1</b>	22.17	12.30	-5.10
<b>R2</b>	160.92	-18.67	-12.20
<b>R3</b>	70.24	21.00	-18.80
<b>R4</b>	95.97	19.94	-20.60
<b>R5</b>	115.41	15.65	-19.10
<b>R6</b>	62.11	-32.00	-25.20
<b>R7</b>	85.94	-35.52	-26.80
<b>R8</b>	108.43	-39.13	-24.90
<b>R9</b>	64.38	-2.91	-28.70
<b>R10</b>	85.94	-35.52	-26.80
<b>R11</b>	114.30	-10.30	-29.40

### *Comparison of the Different Methods*

To test the accuracy of the survey methods mentioned above, the measurements from all photogrammetric models of the *saveiro* were compared within a single set of control measurements. The control measurements were taken directly from the wooden model; 21 selected distances between reference points were taken for this purpose (Fig. 2-19). The control measurements were compared to the measurements obtained by the other methods, and corrected as indicated above (Table 2-13).

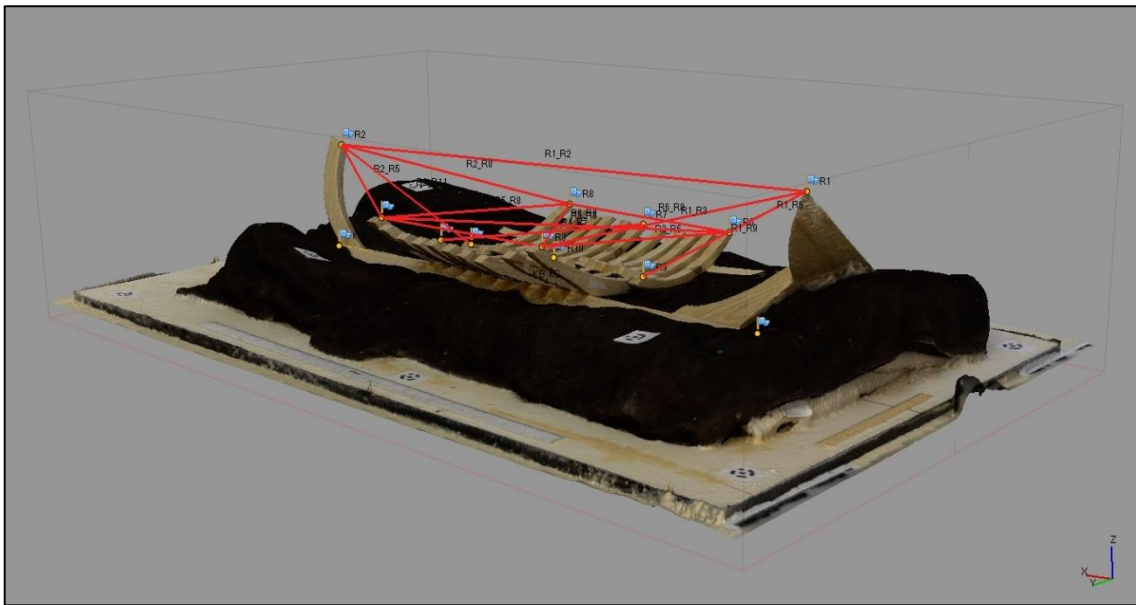


*Figure 2-19.* The photogrammetric model of the *saveiro* wooden ship model and the measured distances between reference points for the comparison. (Image: Yamafune)



**Table 2-13.** Distances between reference points to compare different surveying methods to fix distortions and scales of the saveiro wooden ship models photogrammetric model

	<b>Control (cm)</b>	<b>Trilateration (DSM) (cm)</b>	<b>Enclosure (cm)</b>	<b>Scale Bars (cm)</b>	<b>Total Station (cm)</b>
<b>R1 – R2</b>	<b>142.5</b>	142.0	142.5	142.2	142.3
<b>R1 – R3</b>	<b>51.2</b>	51.3	51.1	51.0	50.7
<b>R1 – R9</b>	<b>51.1</b>	51.8	51.0	50.9	50.7
<b>R1 – R6</b>	<b>63.4</b>	63.9	63.4	63.2	62.9
<b>R2 – R5</b>	<b>57.6</b>	57.8	57.5	57.4	57.4
<b>R2 – R11</b>	<b>50.4</b>	50.5	50.4	50.3	50.4
<b>R2 – R8</b>	<b>57.0</b>	57.7	57.5	57.4	57.7
<b>R3 – R5</b>	<b>44.9</b>	44.6	45.2	45.1	45.5
<b>R6 – R8</b>	<b>46.6</b>	45.4	46.7	46.6	46.9
<b>R3 – R6</b>	<b>54.2</b>	53.9	54.4	54.3	54.0
<b>R5 – R8</b>	<b>55.3</b>	55.6	55.5	55.3	55.5
<b>R4 – R7</b>	<b>57.0</b>	57.0	57.2	57.1	56.7
<b>R3 – R8</b>	<b>71.3</b>	71.2	71.4	71.2	71.5
<b>R6 – R5</b>	<b>71.0</b>	70.4	71.8	71.7	71.7
<b>Length of Keel</b>	<b>115.2</b>	115.0	115.4	115.2	115.2
<b>Average Error</b>		0.39	0.20	0.19	0.33

The results suggest that trilateration (DSM) is not the most accurate method to correct scale in a photogrammetric model. The measurements taken from the photogrammetric model with trilateration (DSM) coordinates display an average error of 0.39 cm, although the 3H Site Recorder software used in the trilateration (DSM) method indicated that the measurements between control points and reference points had errors of less than 0.3 cm. The second least accurate method in our experiment was the total station, but its 0.33 cm average error can be explained by the scale of the *saveiro* model. Total stations are designed to measure large distances and are less accurate when the measurements are this small. One must keep in mind that the nature of the total station suggests that this 0.3 cm error remains the same when the size of the site to be recorded

increases, making its accuracy better as the site size increases. The more accurate results obtained were through the enclosure method and the use of scale bars; the enclosure displayed an average error of 0.2 cm, and the scale bars allowed an average error of 0.19 cm.

*Conclusion: Recommended Survey Method*

The results of the experiments discussed in this section show that the enclosure method and the scale bars method provided better results in fixing scales from Computer Vision Photogrammetry surveys. The main disadvantage of trilateration (DSM) is that it requires many measurements. For instance, the *saveiro* model required 19 measurements to establish the control point network and 44 measurements to calculate the coordinates of reference points. On the other hand, the enclosure method only required four measurements (six measurements if you use the Pythagorean Theorem) plus the depths of the corners of the area. The scale bar method does not require any measurements. However, it is important to note that the enclosure and the scale bars methods cannot establish a local coordinates system. This is a disadvantage when compared to the traditional trilateration (DSM) method; the enclosure and scale bars can fix distortion and scale of photogrammetric models, but they need a complementary method to establish local coordinates. Other surveying methods will be proposed in the following sections of this dissertation that take advantage of the accuracy and simplicity of the enclosure and scale bars methods while simultaneously allowing the archaeologist to acquire a local system of coordinates.

These surveying methods require only three steps. The first step is to create a 1:1 scale photogrammetric model using both enclosure and scale bars. The second step is to place the model in a 3D field using one of the corners as a datum point ( $X=0, Y=0, Z=0$ ) and calculating the remaining corners using the measurements from the enclosure method. To add the depth of the site and correct the enclosure – if it turns out not to be an exact square or rectangle – simple trigonometry or CAD software can be used for minor adjustments. The third and final step is to extract the coordinates of the reference points marked inside the enclosure and over the structure to be recorded. Coded targets may help expedite this process, another reason to employ coded targets during the first photo-shooting session for the photogrammetry model. In the end, this method establishes a local coordinate system using a 1:1 scale photogrammetric model of the site.

This base model can be created at the beginning of the field season—it is simple and accurate. Based on site experience, the establishment of a local coordinate system using trilateration (DSM) may take five to ten days with a shipwreck that is larger than 20 m. The methodology presented in this section takes only two to three days to establish a local coordinate system and also produce the first photogrammetric model of the site.

Nonetheless, the author still consider that Direct Survey Methods is very reliable survey methods in terms of establishing the XYZ local coordinate systems.

Henceforward, careful planning for choice of survey methods (based on available budgets, time, and personnel) is strongly recommended before the field season.

## **Data Collection and Database**

The author shall only briefly discuss data collection and database management in this dissertation; however, it must be noted that data collection and database management are the most important tasks during field projects. Newly developed technologies and ideas certainly can help to accelerate archaeological field projects, yet they cannot replace many necessary conventional tasks performed by archaeologists and other scholars. The author has learned several computer drafting and modeling software suites to facilitate archaeological work; however, full exploitation of software capabilities requires shipbuilding knowledge and archaeological training in addition to software proficiency. For instance, if young nautical archaeologists want to learn Rhinoceros 3D CAD design software to employ on ship reconstruction, they must first know how to draw hull lines by hand. Today various computer programs automate processes that archaeologists have long done by hand, and computers can perform mathematical calculations of reconstructed ships, such as water displacement and coefficients. However, a fundamental understanding of the applicable facets of nautical archaeology, based on the history of shipbuilding and a ship's historical context, is paramount to successful application of software to a specific excavation.

It cannot be overemphasized that data collection is a first step and most important task in field projects. Without good data collection in the field, the workflow being discussed in this dissertation is useless.

### Data Collection

Data collection as discussed in this methodology is conventional data collection by hand. Even when archaeologists can create an accurate 1:1 scale photogrammetric model and extract any desired measurements from the created model, these are just measurements. To truly understand the shipbuilding techniques employed during construction of the ship, sketches made by trained archaeologists are critical (Fig. 2-20). Archaeological training is crucial in the selection of hull areas of interest and specific components to be recorded; a profound knowledge of shipbuilding is invaluable in the field as well as during reconstruction in the laboratory.

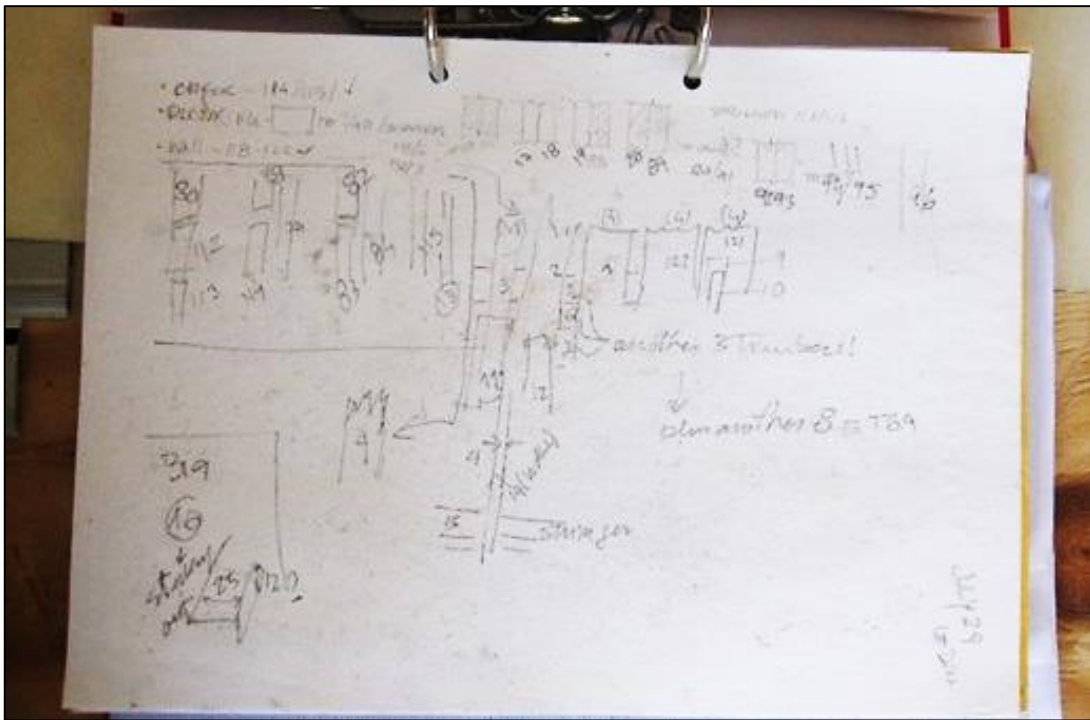


Figure 2-20. Example of an underwater sketch by an archaeologist. (Photo: Reprinted with permission from Castro, 2014a)

Two prerequisite tasks in fieldwork site preparation are digging and subsequently cleaning the archaeological site (Fig. 2-21). A basic concept in the discipline of archaeology is that excavation results in the destruction of archaeological sites (with precise recording). Nonetheless, careful excavation supervised by trained archaeologists can minimize unnecessary damage to shipwreck sites. Additionally, good recording, including Computer Vision Photogrammetry, requires good cleaning; in other words, the results obtained in recording are largely dependent on traditional methods of excavation and cleaning archaeological sites; both tasks require experience and training.



*Figure 2-21.* A working scene of archaeologists on the Gnalić shipwreck. An archaeologist on the right is recording provenience of an artifact while others are excavating and cleaning the wooden structure. (Photo: Reprinted with permission from Pandozi, 2014)

At all shipwreck sites, archaeologists find various artifacts during excavation. When artifacts are removed from the site during the project, it is important to record the provenience of all artifacts and to take photos. Artifacts brought to a project's base or a laboratory for conservation must be stored and recorded properly under the supervision of conservation specialists (Fig. 2-22 and 2-23). When there is no space, funding, or plans for proper conservation, it is unwise (and often illegal) to remove artifacts from the archaeological site. Preservation of artifacts *in situ*, while not ideal, is preferable to the artifact compromise and destruction that will be caused by removal and failure to conserve. Each artifact provides potentially valuable information; the excavating archaeologist has a duty to maximize the information obtained from each artifact while minimizing destruction and loss.



Figure 2-22. An artifact from the Gnalíć shipwreck site being chemically treated by Chris Dostal and Katarina Batur, conservation specialists, in the temporary laboratory of the Gnalíć Project. (Photo: Reprinted with permission from Govorčin, 2014)



*Figure 2-23.* Artifacts raised from the Gnalić shipwreck site were recorded and stored in an organized manner by archaeologists and conservators (Carla Pereira). (Photo: Reprinted with permission from Batur, 2014a)

### *Database*

Information about artifacts from shipwreck sites and the associated photos must be organized properly so that project information can be easily retrieved in the future. Moreover, all underwater sketches and diaries of archaeologists and divers who participate in a project should be scanned or photographed every day and stored in the database. Traditionally, nautical archaeologists have preferred a paper-based database. The author strongly recommends the use of a database in digital format, which can easily be duplicated, transferred, and shared, and theoretically can last forever. For example, during three seasons of the Gnalić project, recovered artifacts were recorded and photographed properly, and the data stored in a digital database (Fig. 2-24 and 2-25). The second primary reason to use a digital database is that archaeologists can link data to



GIS-based mapping software to create a geo-referenced database, making spatial analysis of artifacts and ship structure possible. The author will explain GIS-based mapping and database in Chapter III.

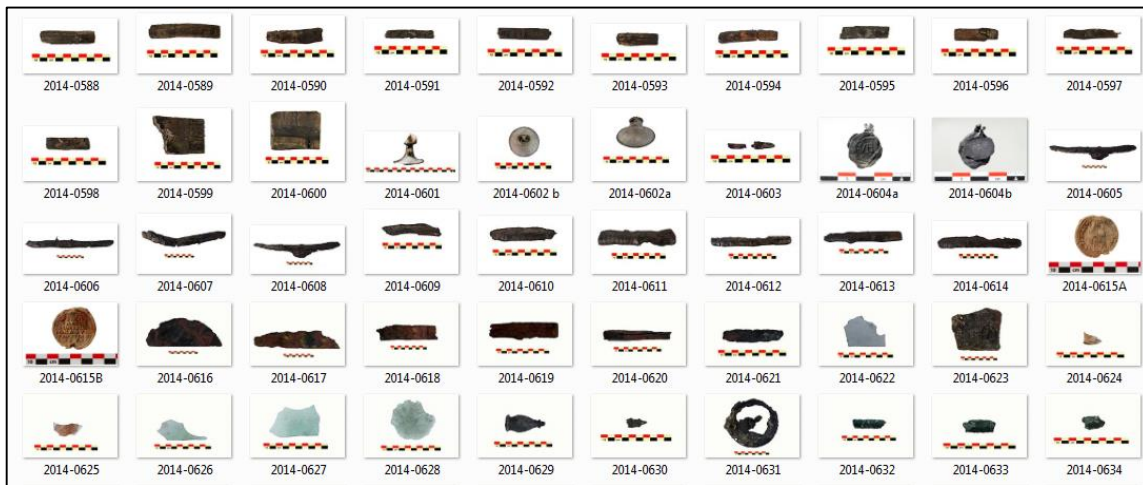


Figure 2-24. Photo database of the Gnalčić artifacts. All raised artifacts were photographed and organized in digital database. (Image: Reprinted with permission from Batur, 2014b)

Inventory number	Artifact type	Material	Position	Category	Dimensions							Designations	State of preservation	Description	Typology designation (Lazar, Willmott, 2006)	Observation	Date Recovered
					Length (cm) / Width of Goblet base (cm)	Width (cm)	Height/ Thickness (cm)	Diameter (cm)	Weight (kg)	Width at end of the stave (cm)	Length from end of stave to chime (cm)						
2014-0001	Bevel	Glass	surface find	Cargo	8.0	1.7	0.3						D	Foot of the bevel, which was probably	B10		2014-06-23
2014-0002	Window glass	Glass	surface find	Cargo	9.3	9.3	0.1						C	Window glass without rim			2014-06-23
2014-0003	Wood with nail concretions	Wood	surface find	Hull	14.4	10.3	8.8						X	Unidentifiable wood fragment with			2014-06-23
2014-0004	Wood with nail concretions	Wood	surface find	Hull	21.5	7.3	6.8						X	Unidentifiable wood fragment with			2014-06-23
2014-0005	Unidentifiable metal artifact	Metal	surface find	Cargo	8.4	1.8	0.2						E	Rem of metal object, possibly metal vessel			2014-06-23
2014-0006	Window glass	Glass	surface find	Cargo	4.8	3.2	0.3						E	Window glass with rim			2014-06-23
2014-0007	Window glass	Glass	surface find	Cargo	9.9	7.3	0.1						D	Window glass without rim			2014-06-26
2014-0008	Barrel stave	Wood	C20.1	Cargo	23.2	8	1.6			7.8	1.8		D	Barrel stave, preserved one end, Unidentifiable wood fragment with			2014-06-26
2014-0009	Wood with nail concretions	Wood	B15	Hull	5.4	3.7	2.6						X	Unidentifiable wood fragment with			2014-06-30
2014-0010	Piece of ceramic	Ceramics	A20	Cargo	3.3	3.3	0.9						E	Unlabeled ceramic fragment			2014-06-30
2014-0011	Wood with nail concretions	Wood	B15	Hull	4.0	3.4	2.3						X	Unidentifiable wood fragment with			2014-06-30
2014-0012	Window glass	Glass	C18.4 / C20.3	Cargo	13.0	9.8	1.0						C	Three pieces of window glass without rim		Armed barrel 11 and barrel 11	2014-07-01
2014-0013	Window glass	Glass	C18.4 / C20.3	Cargo	7.2	6.9	0.1						C	Window glass without rim, Armed barrel 11 and barrel 11		Armed barrel 11 and barrel 11	2014-07-01
2014-0014	Window glass	Glass	C18.4 / C20.3	Cargo	11.0	10.3	0.1						C	Window glass without rim, possibly Armed barrel 11 and barrel 11		Armed barrel 11 and barrel 11	2014-07-01
2014-0015	Window glass	Glass	CC18.4 / C20.3	Cargo	10.5	10.0	0.05						C	Window glass without rim, Armed barrel 11 and barrel 11		Armed barrel 11 and barrel 11	2014-07-01
2014-0016	Window glass	Glass	C18.4 / C20.3	Cargo	9.6	6.2	0.2						C	Window glass without rim		Armed barrel 11 and barrel 11	2014-07-01
2014-0017	Mirror glass (rounded)	Glass	C18.4 / C20.3	Cargo			0.2	8.9					A	Rounded mirror, Armed barrel 11		Armed barrel 11 and barrel 11	2014-07-01
2014-0018	Window glass	Glass	C18.4 / C20.3	Cargo	15.0	0.6	0.2						E	Window glass rim, Armed barrel 11		Armed barrel 11 and barrel 11	2014-07-01
2014-0019	Window glass	Glass	C18.4 / C20.3	Cargo	11.0	1.9	0.2						E	Window glass with rim, Armed barrel 11		Armed barrel 11 and barrel 11	2014-07-01

Figure 2-25. Digital database of the Gnalčić Project 2014 field season. All raised artifacts were measured and briefly analyzed by conservators and archaeologists. Applicable information were entered into the digital database in an organized manner. (Image: Reprinted with permission from Batur, 2014c)

It must be noted that database development is one of the most important tasks in archaeological projects; future accessibility of the collected data depends completely on the database. This may be the most difficult task in an archaeological field project. Often inexperienced archaeologists and attending divers do not recognize the importance of data organization. Project directors must emphasize the importance of this task and assign dedicated attending archaeologists and students to managing data organization and storage. Without good organization, important information may be lost forever.

In summary, manual data collection and the subsequent development of a well-organized database in digital format are the most important steps in any archaeological project; without accomplishing these two tasks, the methodology outlined in this dissertation is useless.

## CHAPTER III

### DATA PROCESSING

#### **Computer Vision Photogrammetry (Agisoft PhotoScan)**

The author was in charge of photogrammetric modeling of the Gnalić shipwreck during the 2014 field season, and this chapter is a reflection on that experience. During the excavation, several photogrammetric models of the Gnalić shipwreck site were created using Agisoft PhotoScan (professional edition). (in 2015) Photoscan professional edition costs \$3,499 for a stand-alone license and \$549 for an educational license. Photoscan was first released in the middle of 2010 as a mapping software based on aerial photography, but was soon appropriated by other disciplines, including architecture, the motion picture industry, and terrestrial and underwater archaeology. To reconstruct tridimensional structures of a given scenario or landscape, PhotoScan uses an algorithm that was developed in a discipline called Computer Vision. Computer Vision is a sub-discipline of computer science that was designed to help robotic devices to understand surrounding structures (Van Damme, 2015; Huang 1996; Szelski, 2010). Computer Vision algorithms find common features among images of a given target, taken from different angles, and process those images to derive depths of the structures mapped (Van Damme, 2015; Szelski, 2010). In the author's opinion based on working with multiple software suites, off-the-shelf PhotoScan software is more accurate and user-friendly than other available photogrammetry software. The workflow of PhotoScan has four basic steps: Align Photos, Build Dense Cloud, Build Mesh, and Build Texture. This

workflow is simple, but each step must be executed properly. The author has developed a number of additional tasks with associated sub-settings of basic workflow processes of PhotoScan to optimize the results of these processes. Unfortunately, the user manual of PhotoScan does not address the factors and influences of each sub-setting. In order to fully understand the meanings and functions of these sub-settings to optimize output results, the author conducted an experiment in which he produced photogrammetric models of two cubes with different surface patterns. Those photogrammetric models were processed using different sub-settings (Fig. 3-1). Although the user manual of PhotoScan does not fully explain the nuances of sub-settings, Photoscan programmers and professional users argue differences and advantages of various sub-settings to optimize PhotoScan output on Agisofts forum pages (Agisoft Online Forum, 2015). The starting point for some of the specific sub-settings tested was selected by review of those forum pages. In all cases, the settings provided below were developed from testing, rather than from accepting forum discussions at face value.

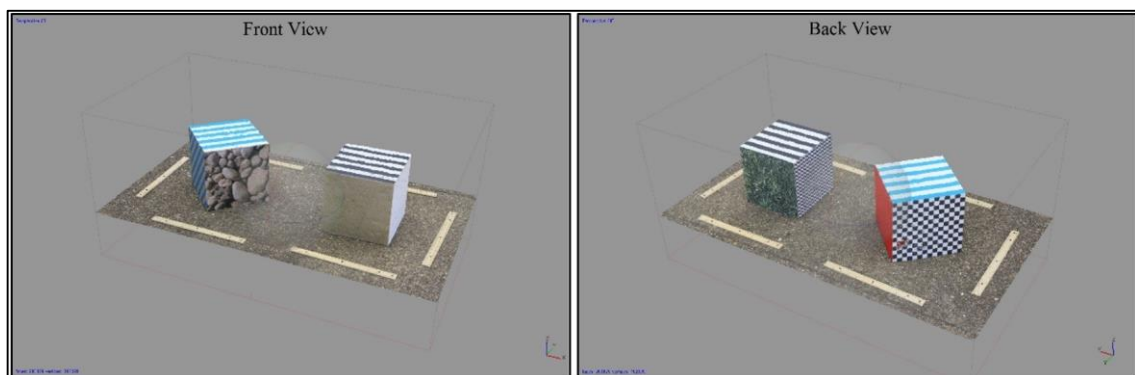


*Figure 3-1.* A Photogrammetric model of two cubes. Each face of each cube has a different patterned texture image. (Image: Yamafune)

### *Align Photos*

After uploading photos into the program, the first step of photogrammetric modeling is Align Photos. One of the forum discussions (Alignment Experiments by [handle name] Marcel) discusses Align Photos settings (Marcel, 2015). Align Photos has three different Accuracy settings: High, Medium, and Low. High Accuracy uses full resolution images, Medium uses 50% resolution, and Low uses 25% resolution. The next sub-setting is Pair Pre Selection; this sub-setting allows PhotoScan to perform a quick pre-scan before it begins full common feature detection in photo. This quick pre-scan can detect two photos that share similar views. Based on this pre-scan, PhotoScan can skip the whole image point detections to align each single photos. Instead, it only scans two pre-selected images each time to locate camera position. As a result, employing Pair Pre Selection reduces processing time. Pair Pre Selection has Generic and Disabled options. To activate pre selection, Generic must be selected.

The next Align Photos setting of interest is Key Point Limit. This setting specifies how many pixels PhotoScan uses from each photo to detect common features in images. The default setting of Key Point Limit is 40,000 (for reference, a typical 36 Megapixel photo has approximately 240,000 pixels, and a 21 Megapixel photo has approximately 180,000 pixels). One Agisoft forum discussion stated that selecting a higher number for Key Point Limit will increase the processing time until the value reaches 240,000, supporting full processing of photos having 36 Megapixels (240,000 pixels). However, the forum also noted that if the setting chosen for Key Point Limit is more than 40,000, there will be no improvement in the quality of Dense Clouds in

subsequent processing. Thus if accuracy is the primary concern, projection error can be minimized to 0.3 pixel by increasing Key Point Limit to 120,000 (although an average projection error with Key Point Limit set to 40,000 is 0.7 pixels--already less than 1 pixel) (Marcel, 2015). The author tested the Align Photos process with Key Point Limit: 40,000 (default) and Key Points Limit: 80,000 (Fig. 3-2 and 3-3). No significant difference was noted in the development of the created sparse points.

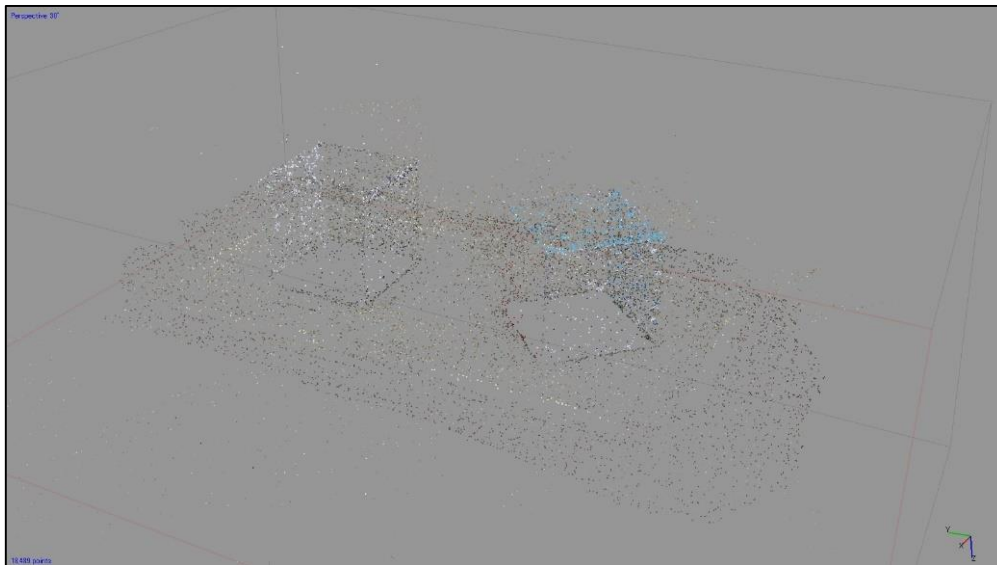


*Figure 3-2.* Align Photos process with Key Point Limit: 40,000 (default) setting. Total number of created sparse points was 18,489. (Image: Yamafune)

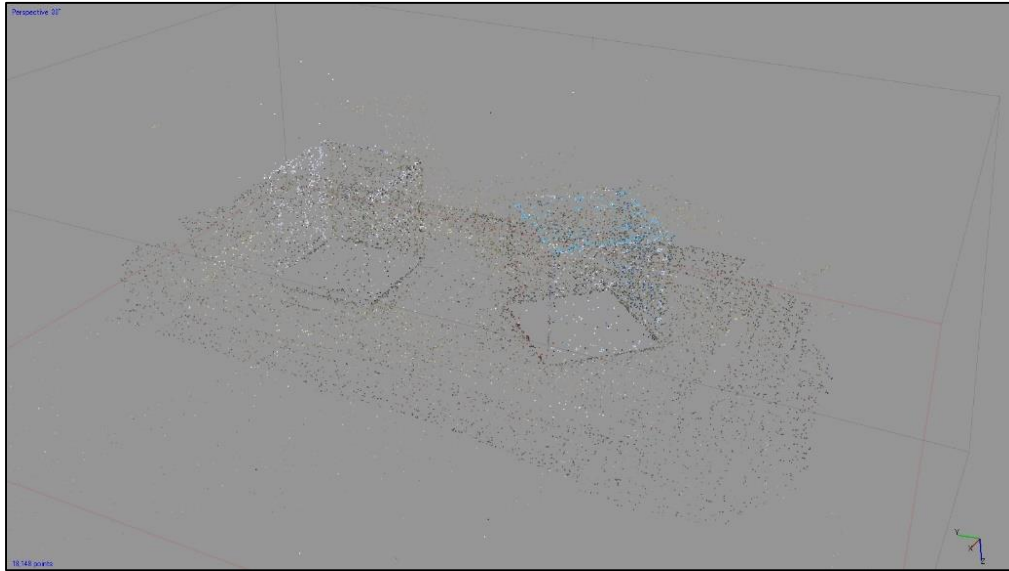


*Figure 3-3.* Align Photos process with Key Point Limit: 80,000 setting. Total number of created sparse points was 18,148. (Image: Yamafune)

The last sub-setting of the Align Photos stage is Tie Point Limit, which specifies how many detected common points are actually used to calculate the depth of the scene. For instance, when 40,000 Key Point Limit and 1,000 Tie Point Limit are applied, 40,000 points of each image are used to detect common points to match images, and then the 1,000 highest quality common points from each image are used to calculate camera positions and to create sparse point clouds. Decreasing the Tie points setting decreases the processing time of photo alignment (Pasumansky, 2015). During the Align Photos stage the author used a setting of Tie Point Limits: 1,000 (default) and Tie Point Limit 2,000; doubling the number of tie point limits more than doubled the number of created sparse points, but at a cost of a significantly longer processing time (Fig. 3-4 and 3-5). Judging from the results, the Tie Point Limits value directly affects the total number of sparse points. The author elected not to perform experiments on the Quality sub-setting

at this stage of processing because successful photo alignment largely depends on photo-shooting, not Quality sub-settings.

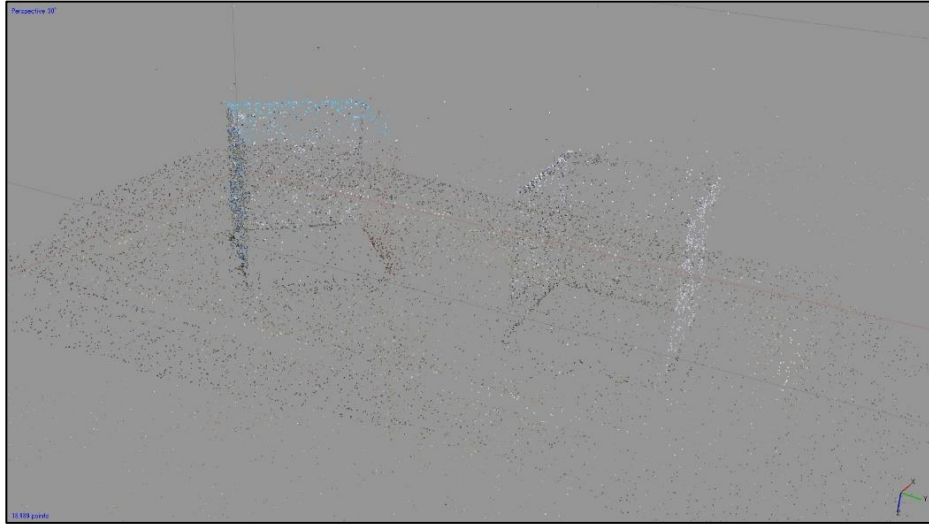


*Figure 3-4.* Align Photos process with Tie Point Limits: 1000 (default) setting. Total number of created sparse points was 18,489. (Image: Yamafune)

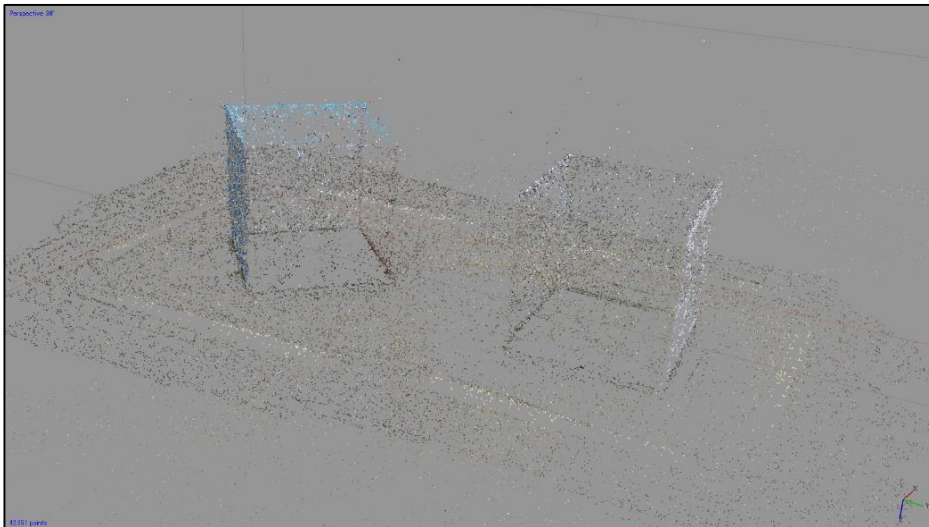


*Figure 3-5.* Align Photos process with Tie Point Limits: 2000 setting. Total number of created sparse points was 42,651. (Image: Yamafune)



### *Build Dense Cloud*

Once photos are aligned, the next step is Build Dense Cloud. This process has five quality settings: Ultra High, High, Medium, Low, and Lowest. Ultra High quality uses full size image resolution, High uses 50% of the original scale, Medium uses 25%, Low uses 12.5%, and Lowest uses 6.75%. These percentages directly affect the total number of points in the dense cloud (Marcel, 2014) (Fig. 3-6, 3-7, 3-8, and 3-9). For this test, the author intentionally skipped a trial of the Ultra High sub-setting because once the computer began processing, it provided an estimated processing time of more than two weeks. Thus, this setting is not practical for typical archaeological projects, which are usually conducted without the services of a super computer.

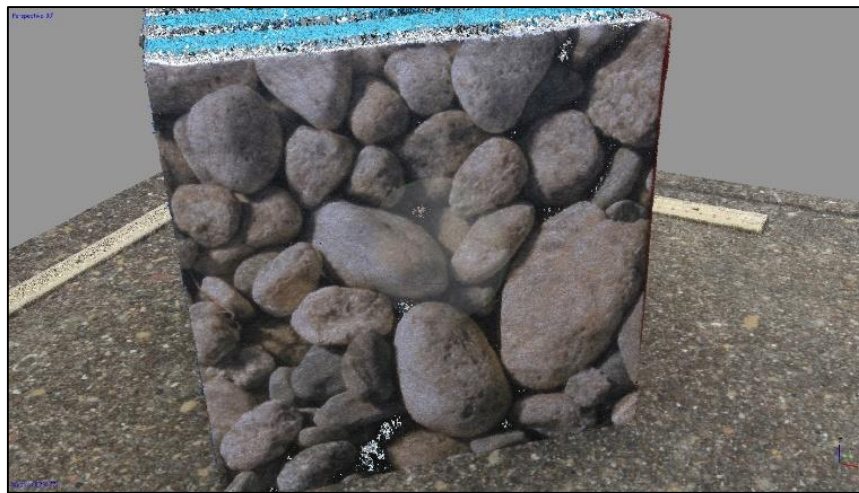


*Figure 3-6.* Accuracy: High setting on Build Dense Cloud process. Total number of the points is 38,283,371. (Image: Yamafune)



*Figure 3-7.* Accuracy: Medium setting on Build Dense Cloud process. Total number of the points is 9,979,748. (Image: Yamafune)



*Figure 3-8.* Accuracy: Low setting on Build Dense Cloud process. Total number of the points is 2,573,953. (Image: Yamafune)



Figure 3-9. Accuracy: Lowest setting on Build Dense Cloud process. Total number of the points is 644,590. (Image: Yamafune)

Another sub-setting is Depth Filtering. This filter has four selectable options: Disabled, Mild, Moderate, and Aggressive. The Aggressive option means that if the object is monotone, PhotoScan will recognize it as void space and will not create points within that space (Fig. 3-10). Selecting the Mild option prompts the program to recognize monotone areas as objects, and to create points within those spaces (Fig. 3-11). For example, the Aggressive depth filter does not recognize the surface of a white board as an object, and it creates a hole in its photogrammetric model; on the other hand, the Mild setting may recognize blue sky as a blue object, and thus create point clouds in what would otherwise be void space. Therefore, Mild works well on a monotone surface, and Aggressive works well with images that contain actual void spaces. Moderate filtering works between the previous two filtering options (Fig. 3-12). Disabled mode does not recognize depth; in other words, if an object has a monotone colored surface, PhotoScan does not regard it as a surface and creates void spaces (Fig. 3-13). In

summary, each depth filtering selection has advantages and disadvantages, therefore the Depth Filtering setting must be chosen based on photography conditions.

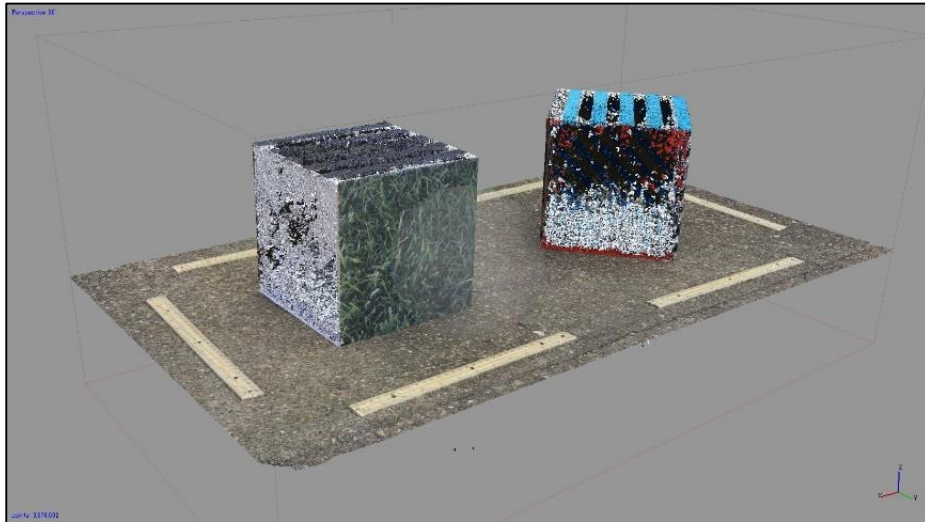


Figure 3-10. Build Dense Cloud process with Depth filtering: Aggressive setting. (Image: Yamafune)

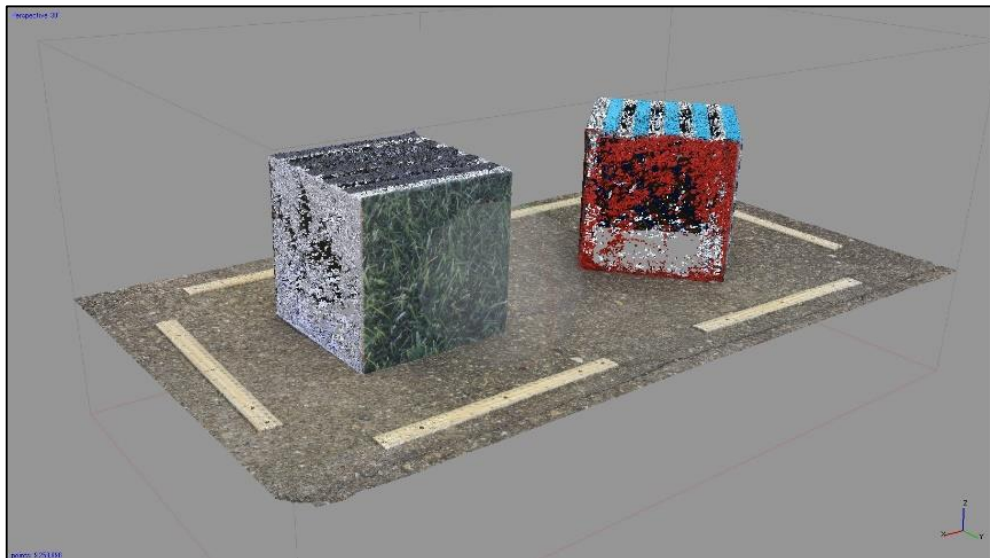


Figure 3-11. Build Dense Cloud process with Depth filtering: Mild setting. (Image: Yamafune)

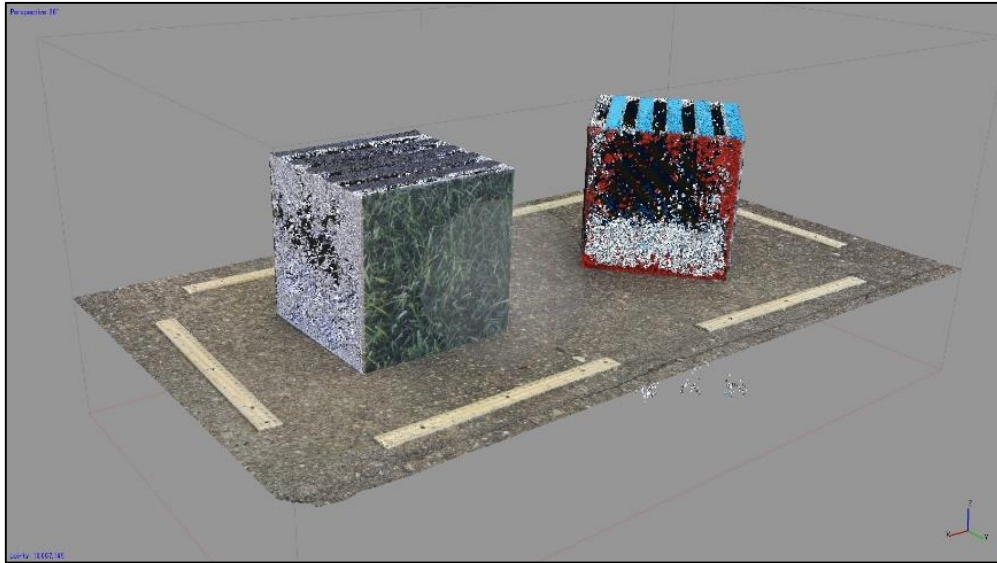


Figure 3-12. Build Dense Cloud process with Depth filtering: Moderate setting. (Image: Yamafune)

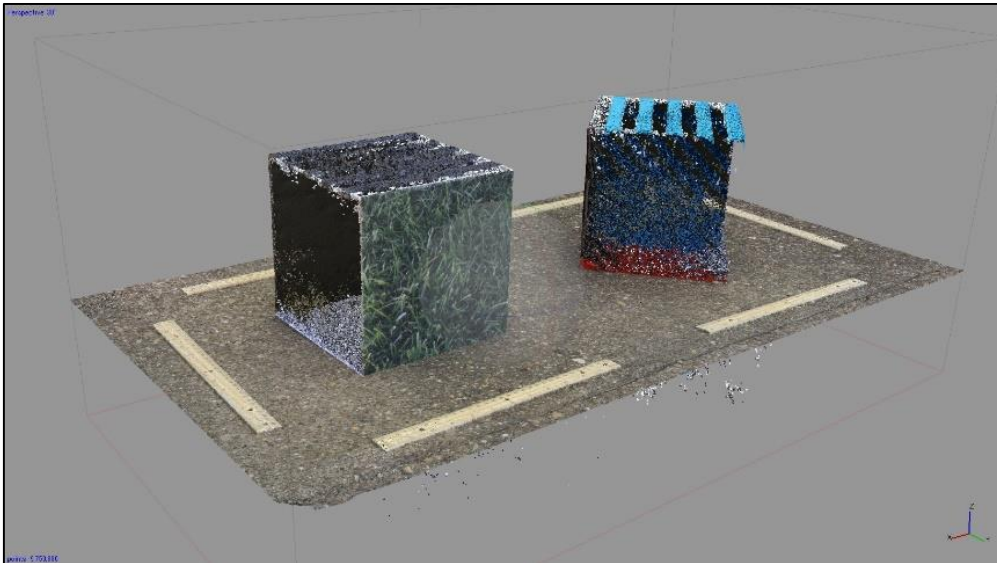
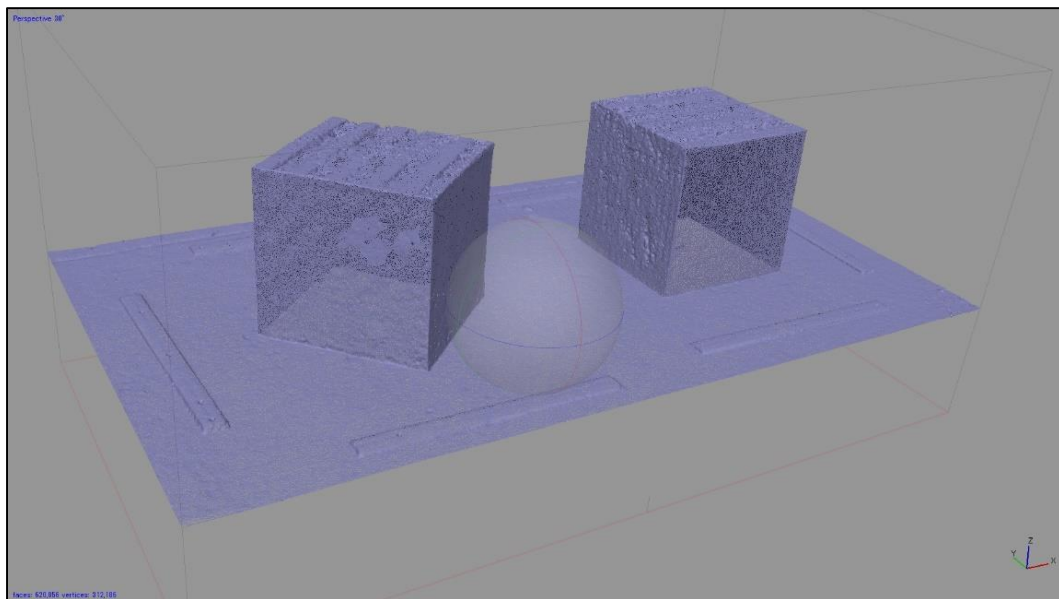


Figure 3-13. Build Dense Cloud process with Depth filtering: Disabled setting. (Image: Yamafune)

### *Build Mesh*

The next process is Build Mesh (mesh is the geometry of the created model based on the point cloud). Sub-settings for this process are Surface Type, Source Data, Face Count, Interpolation, and Point Classes. Surface Type has options Height Field and Arbitrary; when the subject of photogrammetric modeling is a flat structure, such as a level field (ex. aerial photography), Height Field is sufficient; however, if an object has 3D structure, Arbitrary must be selected (Fig. 3-14 and 3-15). From Source data, either Sparse Cloud or Dense Cloud may be chosen. In general, Dense Cloud is preferable since it generates more minute details.



*Figure 3-14.* Build Mesh process with Surface Type: Arbitrary setting. (Image: Yamafune)

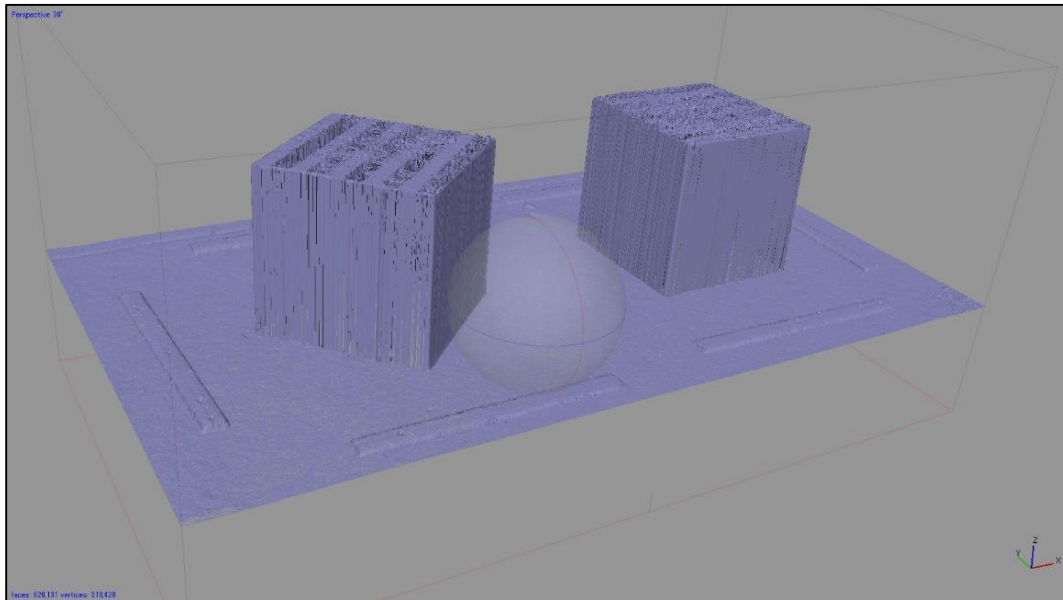


*Figure 3-15. Build Mesh process with Surface Type: Height Field setting. (Image: Yamafune)*

The Face Count (Face Count means total number of the created surface of mesh) sub-setting has High, Medium, and Low options; High creates faces, or surface of meshes, that are made of  $1/5$  of the number of points in the Dense point cloud, Medium creates  $1/15$  of the point cloud ( $1/3$  of the High setting), and Low creates  $1/45$  of the point cloud ( $1/9$  of the High setting) (Fig. 3-16, 3-17 and 3-18).

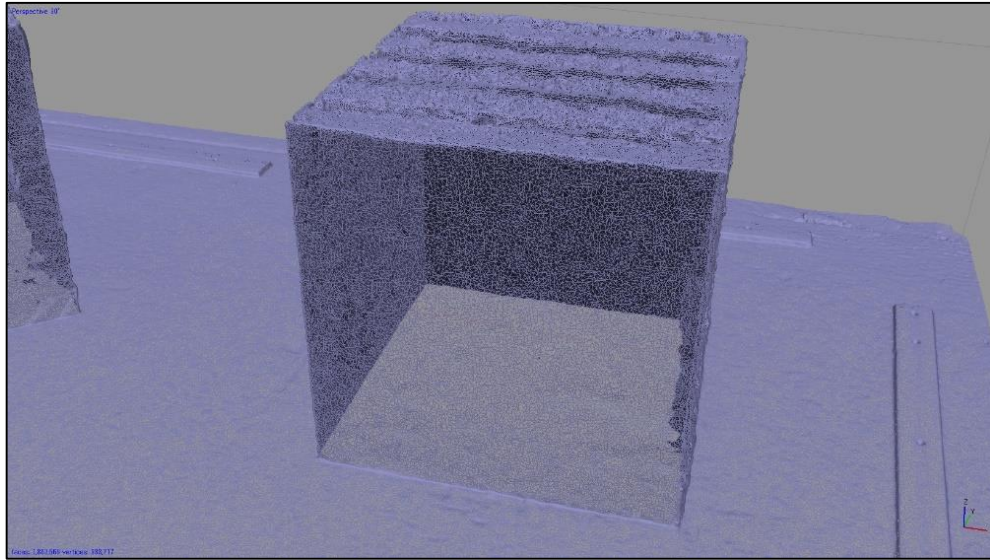


Figure 3-16. Build Mesh process with Surface Count: High setting. Total face count is 1,862,579. (Image: Yamafune)

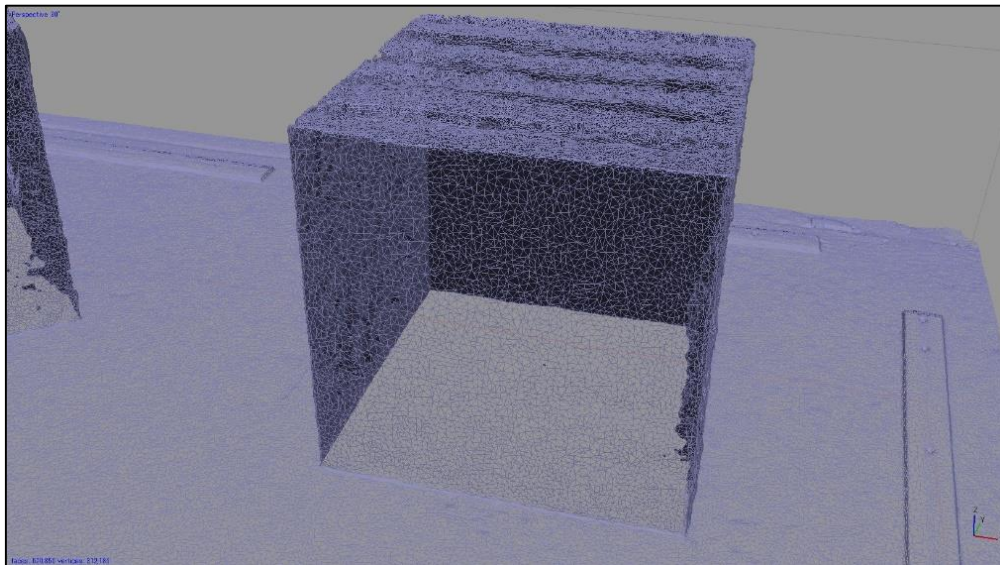
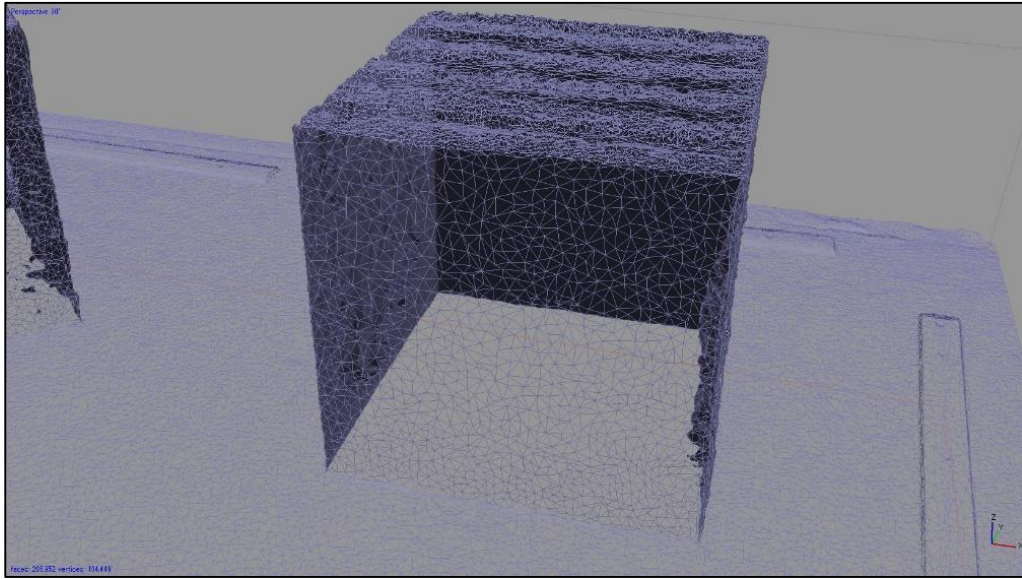


Figure 3-17. Build Mesh process with Surface Count: Medium setting. Total face count is 620,856. (Image: Yamafune)





*Figure 3-18.* Build Mesh process with Surface Count: Low setting. Total face count is 206,952. (Image: Yamafune)

Another sub-setting is Interpolation. This sub-setting has three options: Disabled, Enabled (default), and Extrapolated. Disabled accurately reconstructs meshes based on point clouds (Fig. 3-19). Alternatively, Enabled measures a certain diameter from each point and creates meshes as if the separated points were located within the diameter; in short, it automatically fills small holes (Fig. 3-20). Extrapolated creates meshes between separate points and aggressively fills holes, including large holes (Fig. 3-21). Consequently, if the purpose of a photogrammetry project is to acquire accurate archaeological data, the Disabled Interpolation setting is preferred. On the other hand, when visualization is the main goal of the photogrammetric modeling, Enabled is the better choice.

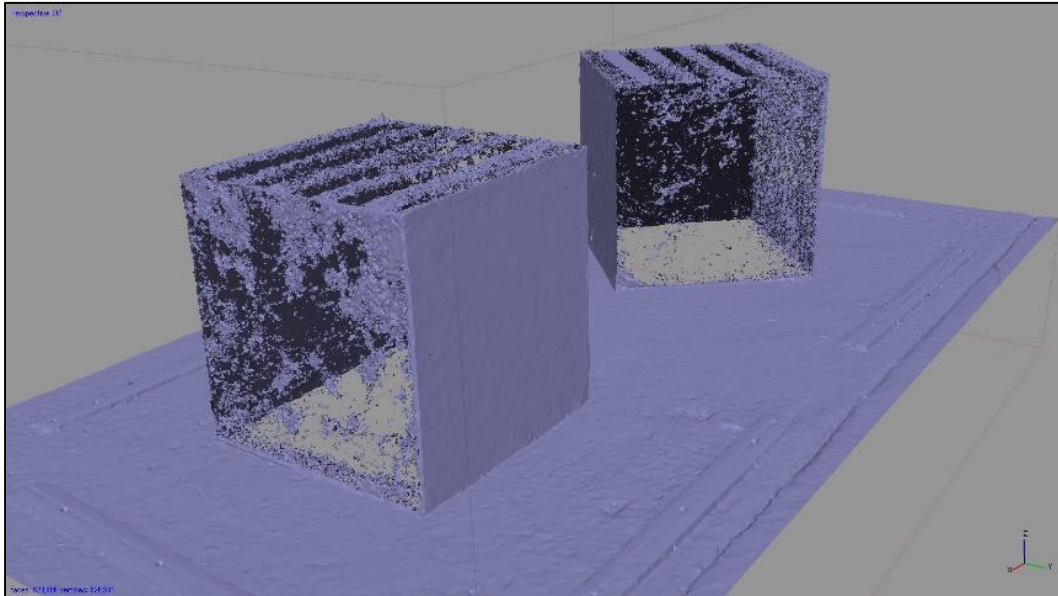


Figure 3-19. Build Mesh process with Interpolation: Disabled setting. (Image: Yamafune)

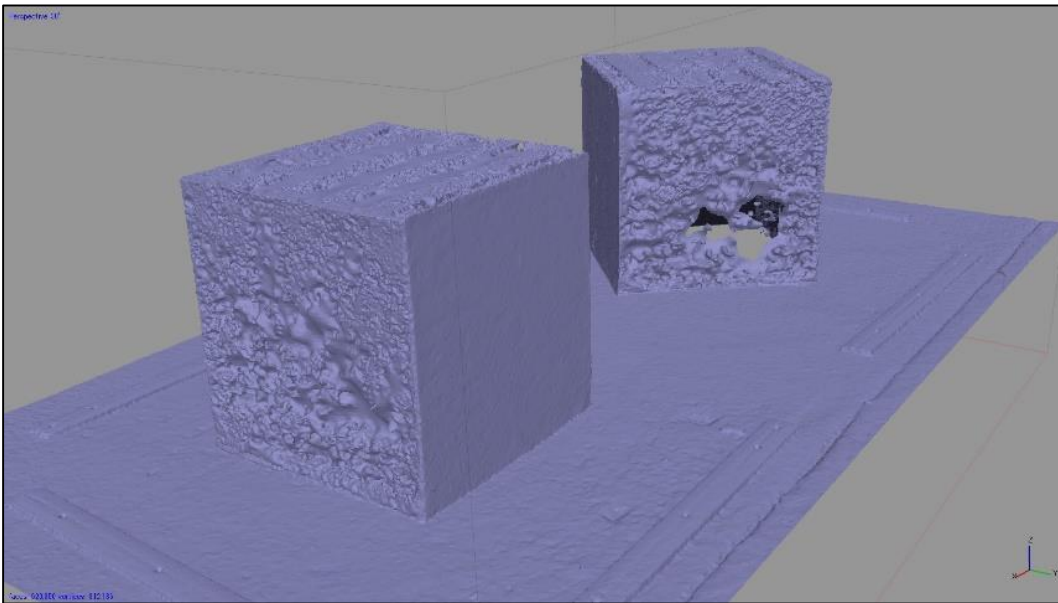


Figure 3-20. Build Mesh process with Interpolation: Enabled setting. (Image: Yamafune)

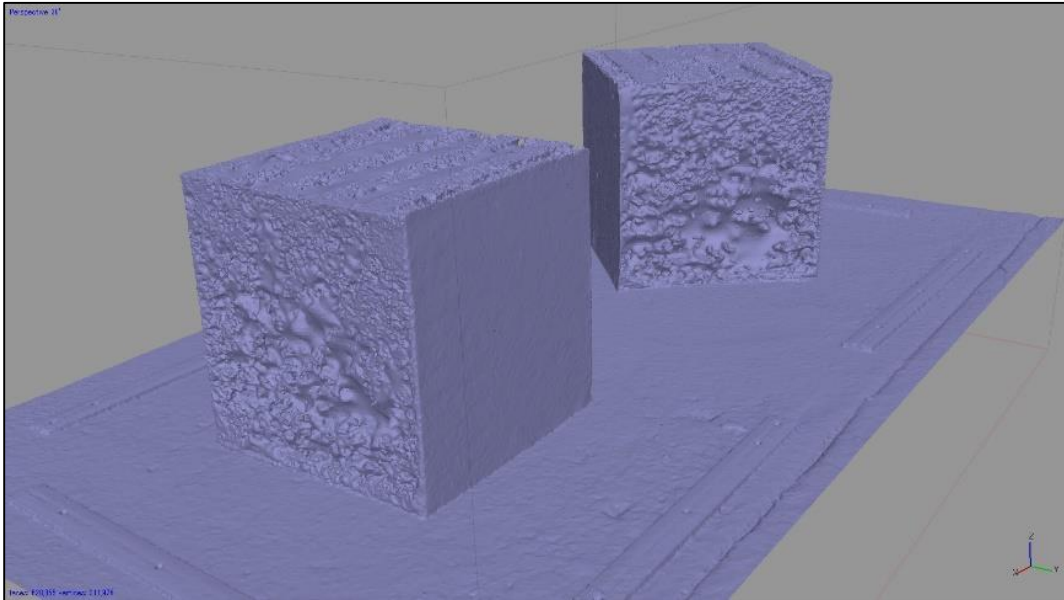


Figure 3-21. Build Mesh process with Interpolation: Extrapolated setting. (Image: Yamafune)

The last sub-setting is Point Classes. This sub-setting is for GIS-based mapping software; it allows point clouds to be imported from mapping software. They can be classified into different categories, such as Ground, Vegetation, Building, Water, etc. This sub-setting allows PhotoScan to read the categories assigned by GIS mapping software, and then create meshes of chosen point types.

### *Build Texture*

The final step of the PhotoScan workflow is Build Texture. In this process, PhotoScan creates a photomosaic and places it on the surface of the meshes. The first sub-setting is Mapping Mode; this applies methods of UV mapping of created textures. UV mapping creates a 2D atlas, or a canvas on which textures can be projected. Options for the Mapping Mode sub-setting are Generic, Adaptive Orthophoto, Orthophoto,

Spherical, Single Camera, and Keep UV. The default setting is Generic; with this option, PhotoScan automatically chooses the best photos (based on cubic projection) and composes a UV of meshes into texture atlases in order to convert the 3D structure of meshes into a 2D image format of created textures. This mode is preferred for more complicated models that have 3D structures (Fig. 3-22). Orthophoto creates a photomosaic from a projection plane (generally, a top view plane) and projects a created photomosaic onto the meshes (Fig. 3-23). Differently from Orthophoto, Adaptive Orthophoto detects vertical faces and creates textures independently for those side meshes (Fig. 3-24). Spherical mode creates a UV map for ball-like, spherical structures. A texture atlas is a 2D plane; therefore, texturing a spherical shape requires a unique mapping projection (similar to world maps and globes). However, this mode is only suitable for spherical structures (Fig. 3-25). Single Photo creates texture based on one photo; a photo can be chosen from any photo in the active Chunk. Keep UV is for importing a UV map created in different software. Many modeling softwares allow the creation of texture on meshes. This process also includes creating UV maps. If UV maps that were created in different software are preferred, PhotoScan can use imported UV maps in the Build Texture process.

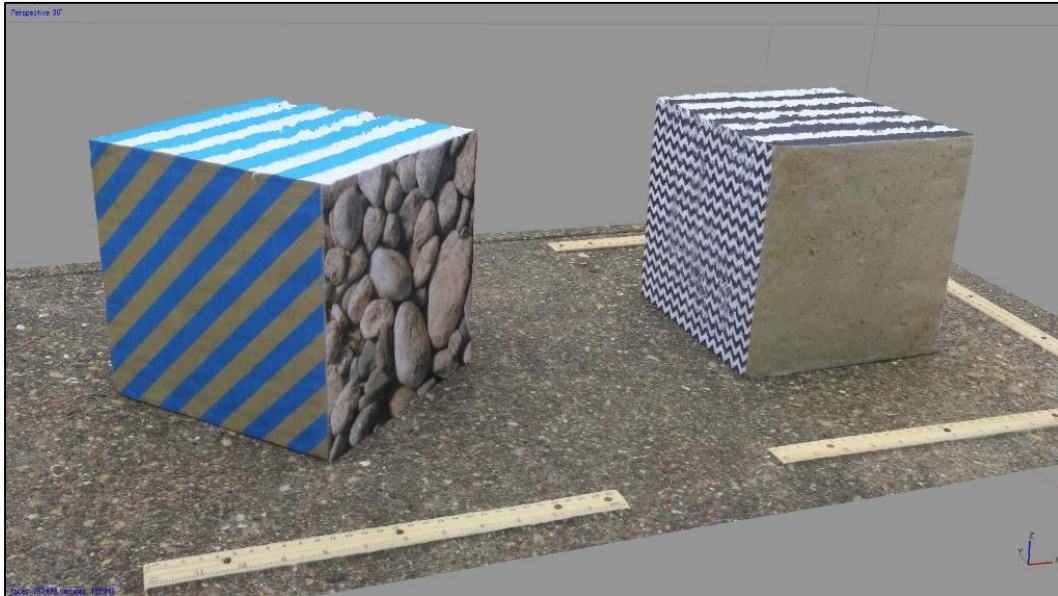


Figure 3-22. Build Texture process with Mapping Mode: Generic setting. (Image: Yamafune)

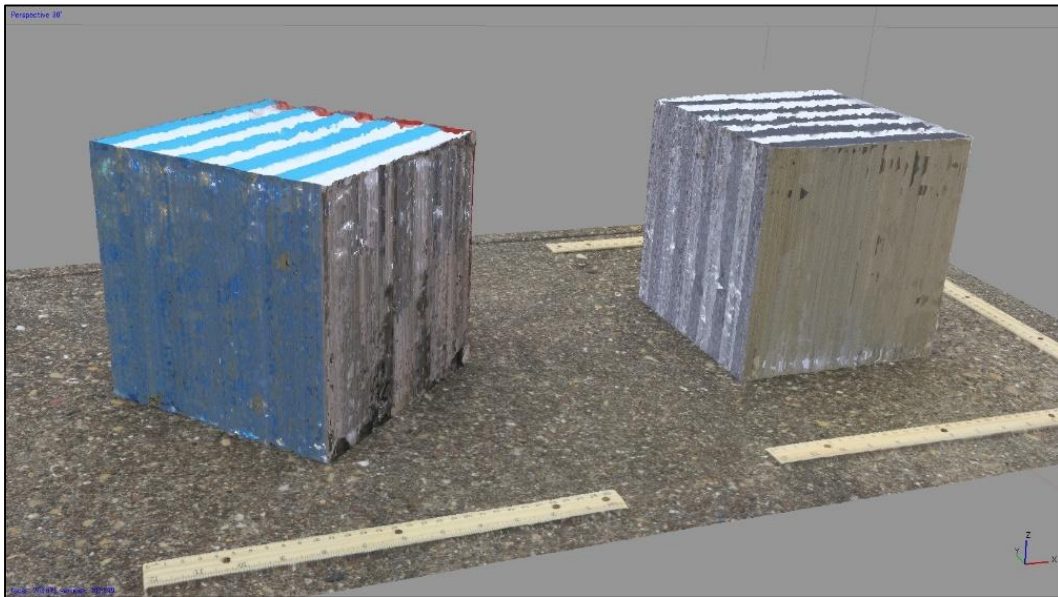


Figure 3-23. Build Texture process with Mapping Mode: Orthophoto setting. (Image: Yamafune)

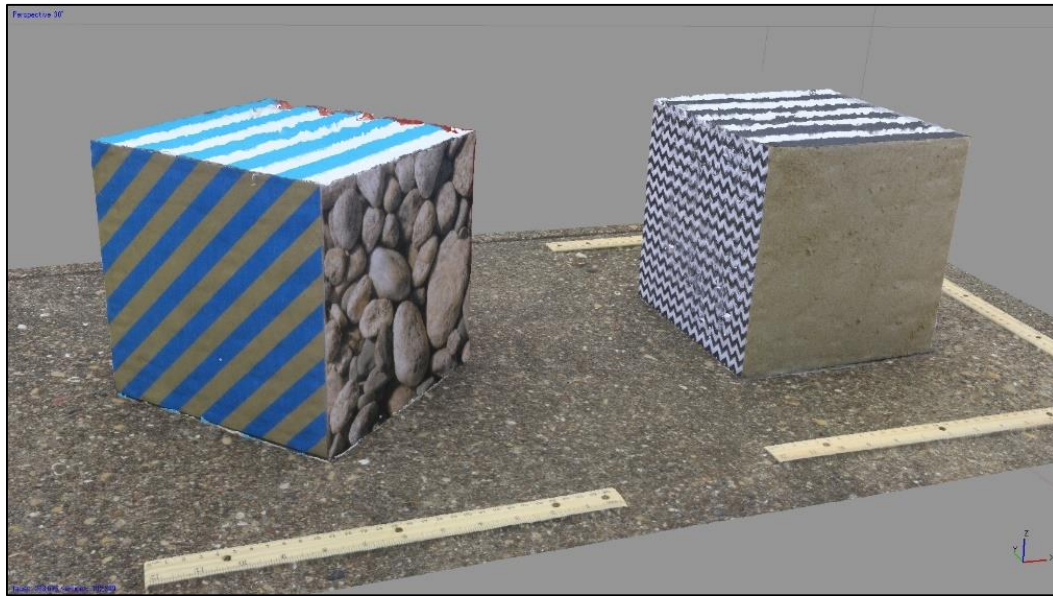


Figure 3-24. Build Texture process with Mapping Mode: Adaptive orthophoto setting. (Image: Yamafune)

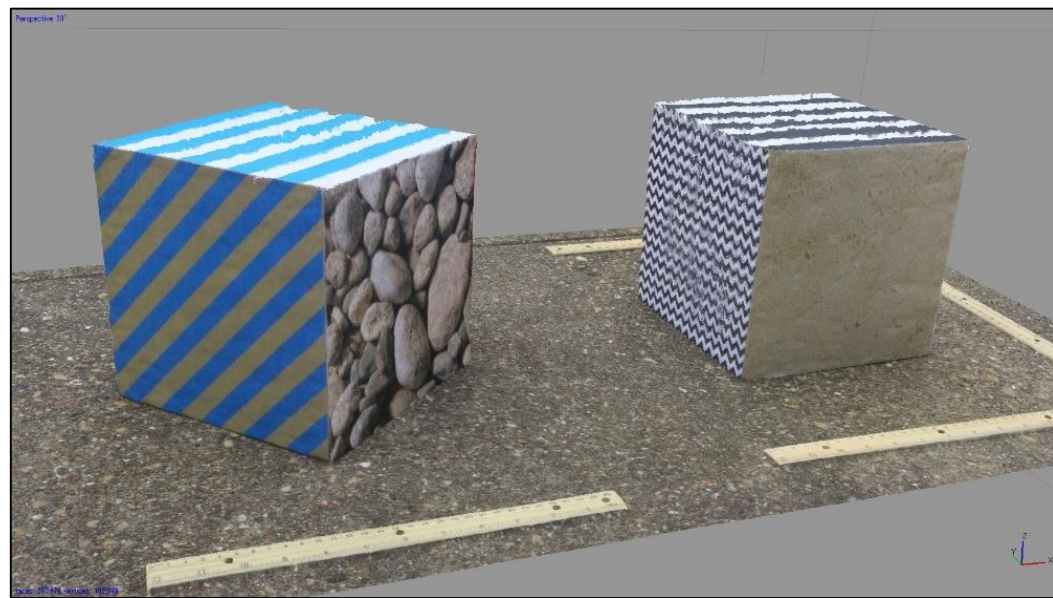


Figure 3-25. Build Texture process with Mapping Mode: Spherical setting. (Image: Yamafune)

Another Sub-setting is Blending mode. To clarify, Mapping Mode is used to compose UV maps, and Blending mode is used to compose selected photo-images on created UV maps as textures. Blending mode has five options: Mosaic, Average, Max Intensity, Min Intensity, and Disabled. The default blending mode is Mosaic. This setting selects the closest photo to corresponding surfaces and uses that image without blending with other overlapping photos. (Fig. 3-26) The Average sub-setting calculates an average pixel value, or RGB value of colors, of overlapping photos and uses those pixel values as textures. (Fig. 3-27) The Max Intensity setting applies images that have maximum intensity, or bright pixels, to corresponding surfaces (Fig. 3-28). The Min Intensity setting is opposite of the Max Intensity setting; it uses minimum intensity images. The Disable setting is, again, for imported models that already have suitable textures (Fig. 3-29). In conclusion, based on the author's experiences, Mosaic provides the best result among those sub-settings; therefore, Mosaic is preferred for creating textures on archaeological photogrammetric models.

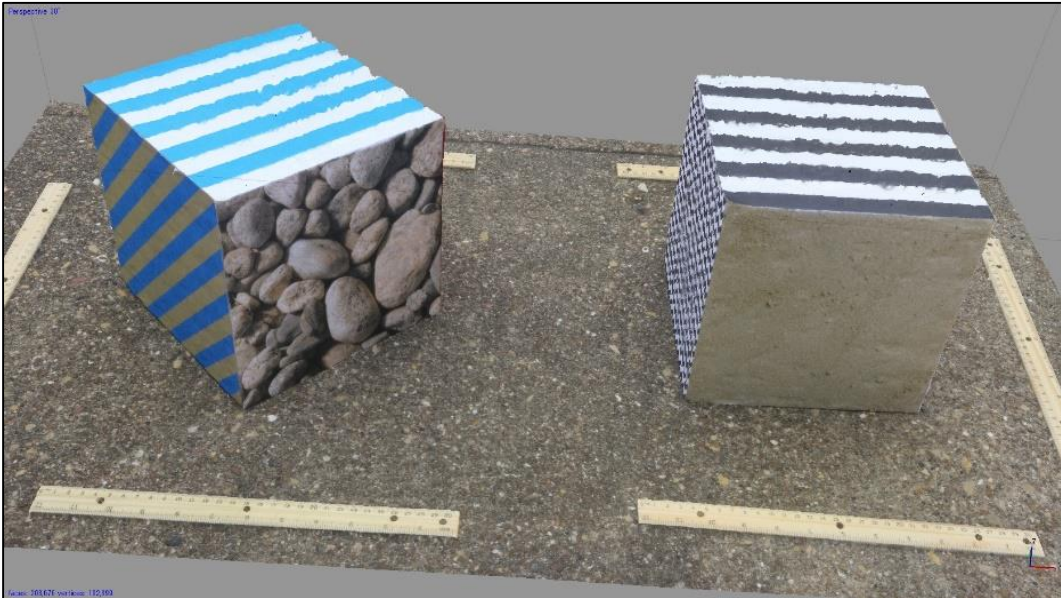


Figure 3-26. Build Texture process with Blending Mode: Mosaic setting. (Image: Yamafune)

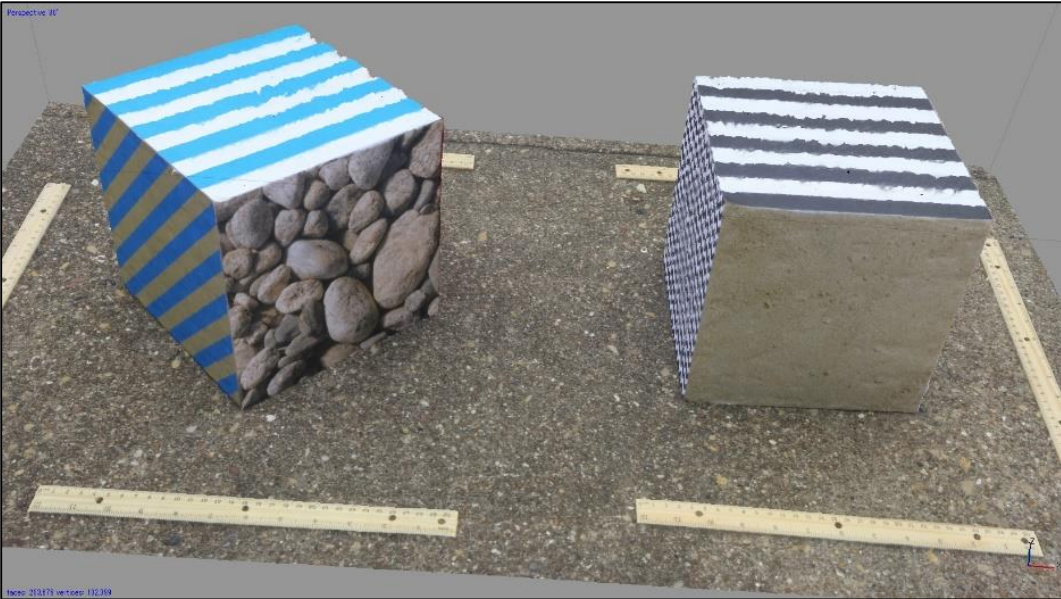


Figure 3-27. Build Texture process with Blending Mode: Average setting. (Image: Yamafune)



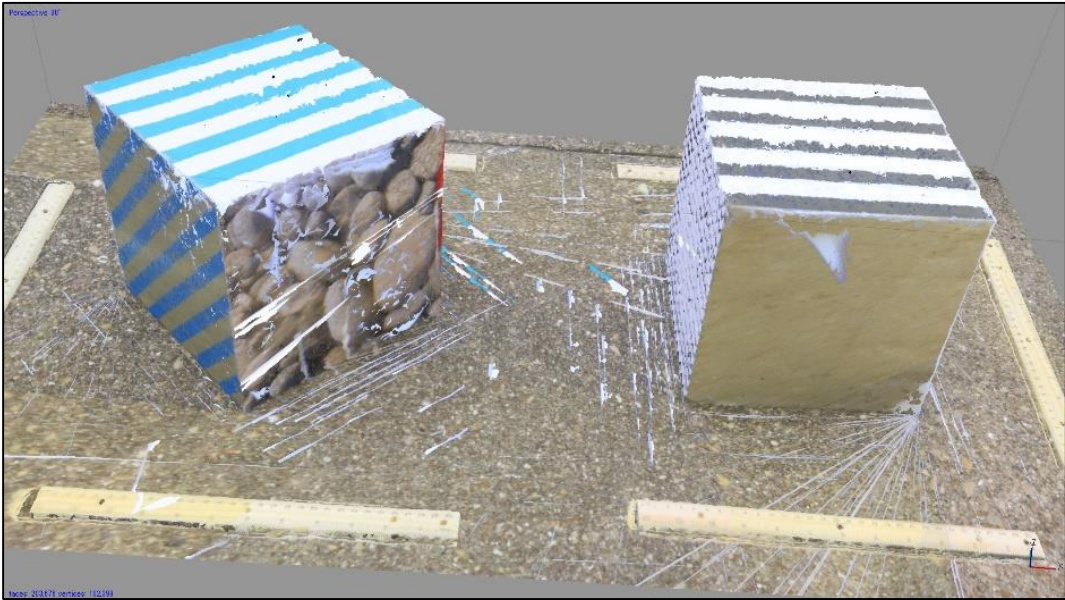


Figure 3-28. Build Texture process with Blending Mode: Max Intensity setting. (Image: Yamafune)

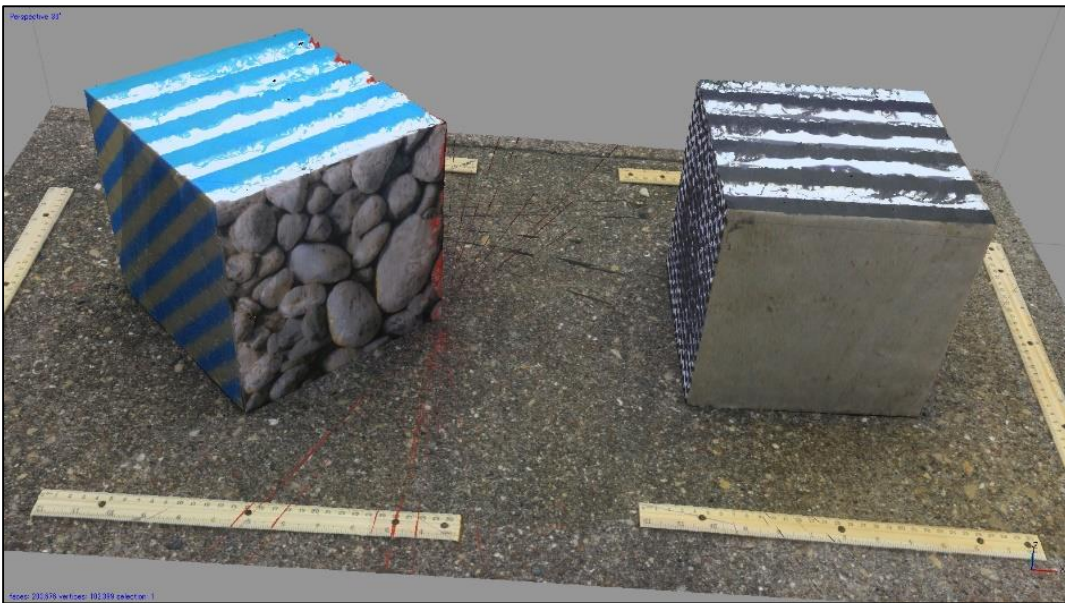


Figure 3-29. Build Texture process with Blending Mode: Min Intensity setting. (Image: Yamafune)

### *Photogrammetric Model of the Saveiro Wooden Ship Model*

With an acquired understanding of PhotoScan workflow and the consequences of its sub-settings, the author tried to create a photogrammetric model of the *saveiro* 1:10 scale wooden ship model. A total of 611 photos were taken and uploaded into PhotoScan. These photos overlapped each other well. Additionally, eight coded targets were placed on the model to aid in photo alignment; consequently, all 611 photos were aligned successfully in PhotoScan. For the Align Photos process, the author used Accuracy: High, Pair Pre Selection: Generic, Key Point Limit: 40,000, and Tie Point Limit: 1000 settings. The next step was Build Dense Cloud. For this process, Quality: Medium, and Depth filtering: Mild settings were applied. However, the result was not successful because unnecessarily dense clouds were created between frames (Fig. 3-30). To avoid the points formed between frames, Disabled depth filtering was applied; however, unnecessary points were still created. All photos were then reviewed, and it was noted that some obliquely taken photos displayed sides of frames as if there were timbers between frames (Fig. 3-31). Subsequently, the author disabled 247 photos that were taken diagonally (hence reducing the total number of active photos to 364).

It must be noted that those disabled photos should not be deleted for the entire workflow process; all 611 photos should be used in the Align Photos stage because maximizing the number of overlapped photos helps PhotoScan align photos. Therefore, disabling photos, if required, should be done after photo-alignment is completed. Accordingly, Build Dense Cloud was applied with 364 photos. The result of this process was drastically improved by disabling obliquely taken photos (Fig. 3-32).

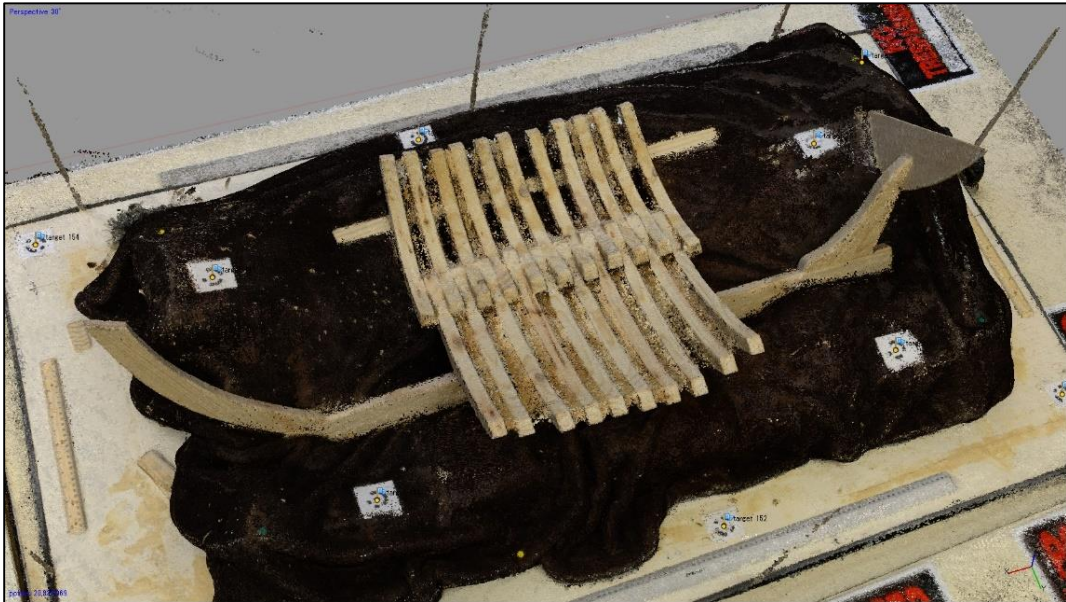


Figure 3-30. Dense Point Cloud of the *saveiro* wooden ship model. Unintended points were created between frames. (Image: Yamafune)



Figure 3-31. An example of photos of the *saveiro* wooden model that were disabled for Build Dense Cloud process. The photo was taken obliquely; therefore it displayed sides of frames as if there were surfaces between frames. (Photo: Yamafune)

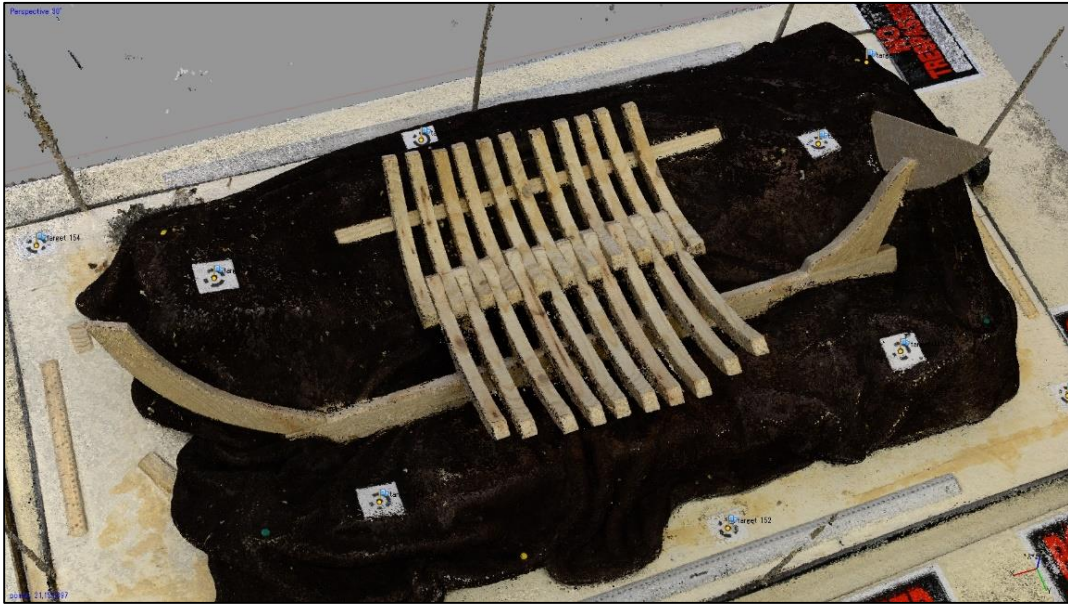


Figure 3-32. Dense Points Cloud of the *saveiro* wooden ship model after 247 oblique angle photos were disabled (processed with 364 photos). (Image: Yamafune)

After manually deleting unnecessary floating points, the Build Mesh process was applied. For this test, the author intended to use the *saveiro* model for two different purposes: 1) visualization purposes (local coordinates system in Chapter II) and 2) archaeological data purposes (section profiles in Chapter III). Therefore, two different sub-settings were chosen and applied on two duplicated dense cloud models. The visualization model sub-settings selected were Surface Type: Arbitrary, Source Data: Dense Cloud, and Interpolation: Enabled. The archaeological data model sub-settings selected were: Surface Type: Arbitrary, Source Data: Dense Cloud, and Interpolation: Disabled. Thus the only difference between the processing of the two models was the Interpolation sub-setting. The Interpolation: Enabled sub-setting tends to fill holes on surfaces, yet it sometimes creates meshes among void spaces. Contrarily, the

Interpolation: Disabled sub-setting creates meshes only where points are closely located; therefore, the created meshes contain more accurate archaeological data. The problem with the Interpolation: Disabled sub-setting is that created photogrammetric models tend to contain small floating meshes, or noisy dust-like surfaces. This noisiness makes UV mapping difficult in the Build Texture stage. Consequently, the Interpolation: Enabled sub-setting was preferred for building high quality texture to support visualization.

Before proceeding to the Build Texture process, both models were decimated (simplified). Each model had approximately 2,000,000 faces; the excessive number of faces may compromise quality of textures because face count constrains spaces on UV maps; therefore, total model face counts should be decreased as much as feasible, while still maintaining the original shape of the source. Thus, both photogrammetric models were decimated from 2,000,000 faces to 500,000 faces. Also, to acquire maximum quality textures, the previously disabled 347 diagonally shot photos were re-enabled. Then the photogrammetric model for visualization purposes was processed in the Build Texture stage using the sub-settings Mapping Mode: Generic, Blending mode: Mosaic, and Texture size/count: 6000 x 3. The result was satisfactory (Fig. 3-33).

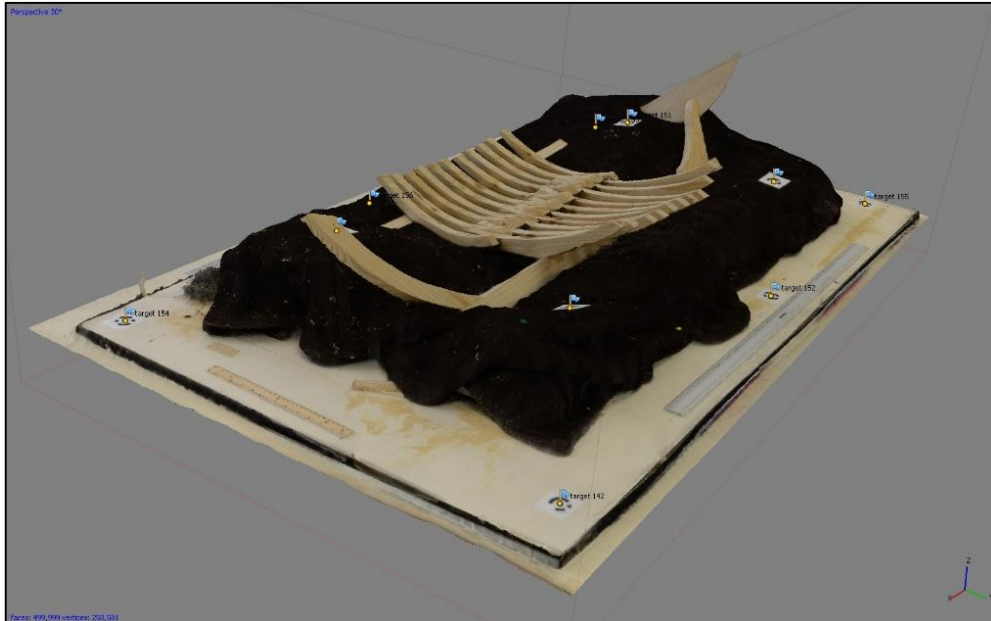
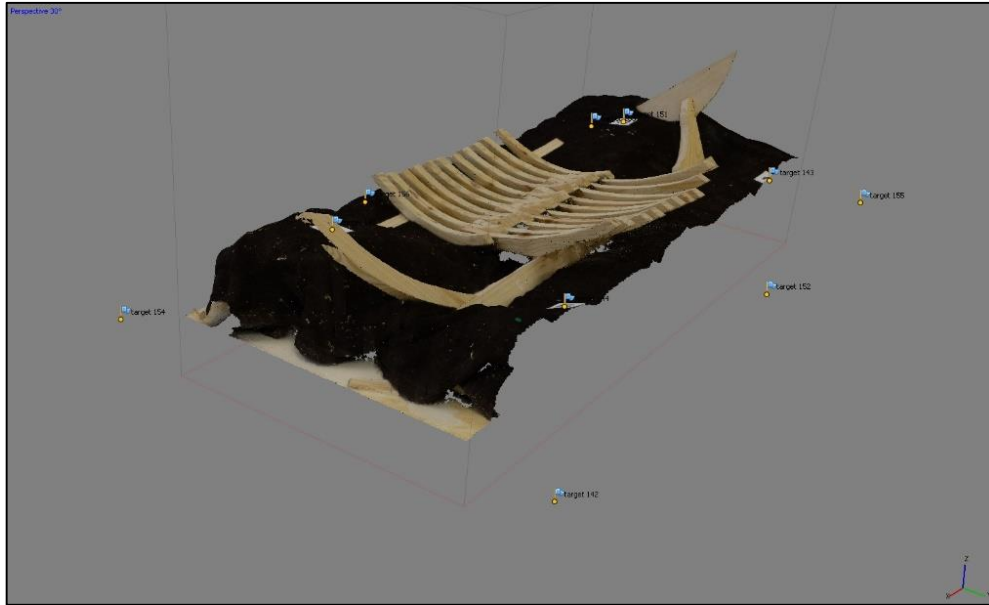


Figure 3-33. Finished Photogrammetric model of *saveiro* wooden ship model that is intended to be used for visualization purposes. (Image: Yamafune)

Another photogrammetric model made for archaeological data purposes was first processed with the same sub-settings as the visualization purposes model, but the result was not good. The poor texture was caused by noisy floating meshes because these tiny faces required individually separated spaces on UV maps. In other words, to acquire good archaeologically diagnostic textures on the created 3D model, meshes of the model must have a clean appearance. To solve this problem, the author deleted peripheral parts of the photogrammetric model. Then the Build Texture process was applied with Mapping Mode: Generic, Blending mode: Mosaic, and Texture size/count: 6000 x 3 settings. The result was satisfactory (Fig. 3-34).



*Figure 3-34.* Finished Photogrammetric model of the *saveiro* wooden ship model that is intended for use as a source of archaeological data, or a reconstruction of the original shape of the frames. In order to get better texture, peripheral meshes were removed. (Image: Yamafune)

To summarize the above discussion, photogrammetric modeling in PhotoScan is not always successful on the first attempt. However, by disabling or enabling appropriate photos before each process, many problems can be addressed. Additionally, the results of processes differ based on selected sub-settings; therefore, the ultimate purpose of the model must be taken into account when creating a photogrammetric model. In the following section, the author shall introduce other ways to solve problems of photogrammetric modeling by using exporting and importing tools in PhotoScan.

#### *Modeling a Sail (Mesh Replacement Techniques)*

It is difficult for Computer Vision Photogrammetry to recognize thin objects and monotone objects. However, using the exporting and importing features of PhotoScan,

created models can be exported to different software to add desirable meshes. Then, the modified models can be re-imported to PhotoScan to apply textures. For example, PhotoScan has great difficulty constructing meshes to model the sails of a ship. The author copes with this difficulty by employing the exporting and importing features of PhotoScan. When the author applied Computer Vision Photogrammetry on a Chinese junk ship model, meshes cannot be created on the sail because it was too thin (Fig. 3-35). Similar failures of photogrammetric modeling often occur when subjects contain monotone faces. When this failure happens, PhotoScan cannot solve these problems automatically in the software. However, using export mesh and import mesh commands, void spaces can be filled with desirable mesh from a different software (Fig. 3-36). However, it is important to maintain the models original spatial position; then, the model can be re-imported to PhotoScan at the exact same location as before it was exported.

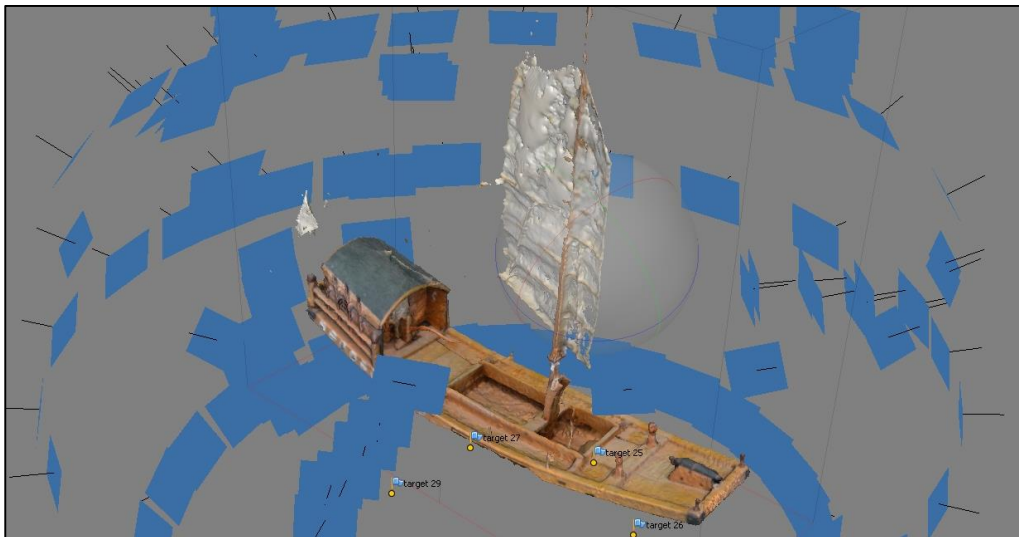


*Figure 3-35.* Photogrammetric model of a Chinese junk model with unsuccessfully reconstructed sail. Often sails are too thin to be reconstructed by photogrammetric software. (Image: Yamafune)



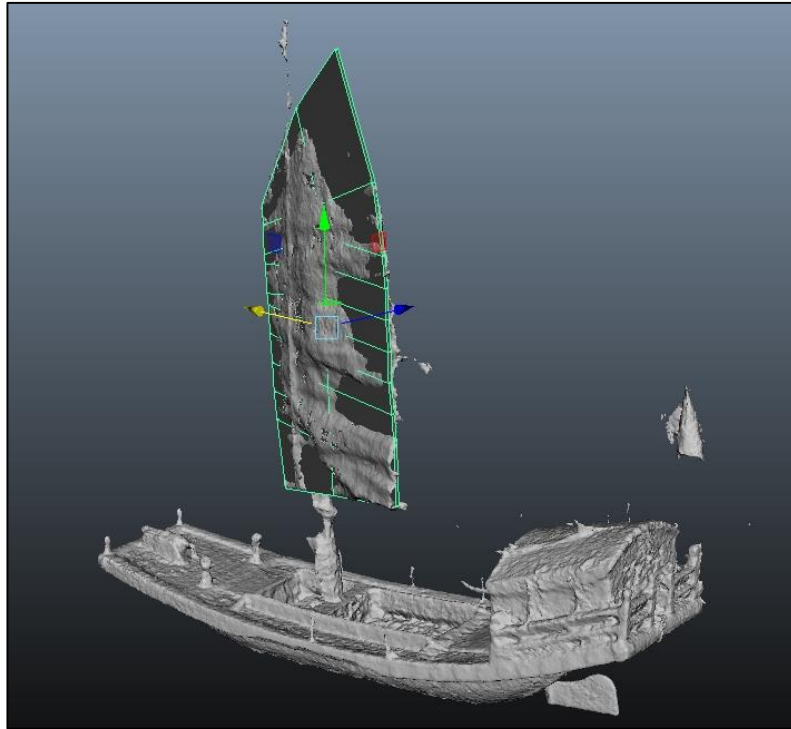


*Figure 3-36.* Sail of a Chinese junk model reconstructed in Autodesk Maya modeling/animation software. Also, this can be done in other modeling softwares, for instance Rhinoceros 3D CAD modeling software. (Image: Yamafune)

As a result of this export and import void filling and mesh processing, the Build Texture process can now adequately process the original photos and new texture will be created on the edited meshes (Fig. 3-37). This technique is also useful when the created mesh has holes because of the monotone coloration problem. This technique may be useful when photogrammetric modeling of ships models or actual sailing ships is desired. Moreover, this export and re-import technique can be used for any photogrammetric model; if some parts of an object's model cannot be created, these parts can be added in another modeling software, and then textures can be created on re-imported models in PhotoScan.

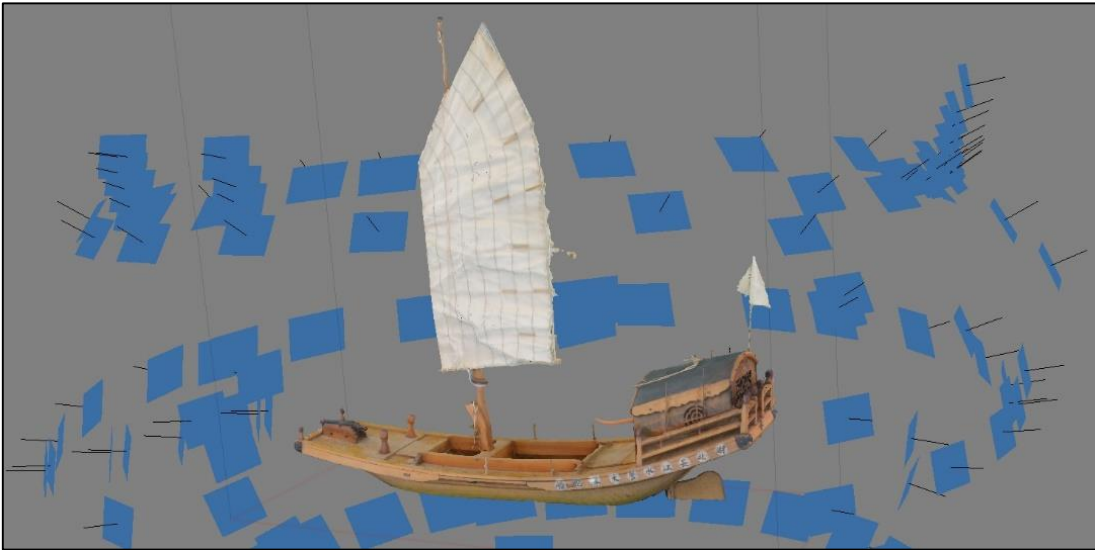


Figure 3-37. Photogrammetric model of a Chinese junk with edited sail after re-importing to PhotoScan from Maya, then “Build Texture” was applied to the model. (Image: Yamafune)

### **Video Frame Photogrammetry**

Another potential use of Computer Vision Photogrammetry is Video Frame Photogrammetry. The idea of video frame photogrammetry is to extract still frames from video footage and use those frame images as photos for Computer Vision Photogrammetry. The basic Workflow of photogrammetric modeling in PhotoScan is the same; the difference is in the source and preparation of images. The author used two different techniques to extract still frames from video footage: selective extraction and automatic extraction.

Automatic extraction is a way to automatically select still frames based on video frame quality and the position of the camera. Selective extraction is a more flexible method in terms of photo alignment because the video processor has total control over

the selection of crisp still frames and the overlap between frames. Since cameras shooting video do not control shutter speed, some still frames are subject to motion blur; therefore, selecting crisp still frames from video footage is important. For the selective extraction, the author used Adobe Premiere Pro CS6 video editing software. Using this software, any still frame can be extracted and saved in Jpeg format with one click (Fig. 3-38). A major disadvantage of the selective extraction technique is its labor intensity because frames have to be manually selected. Based on the author's experiences, extracting still frames from a ten minute long video takes approximately one to two hours; video footage has 24 to 30 still frames per second, thus a ten minute video will have in excess of 14,000 embedded still frames.

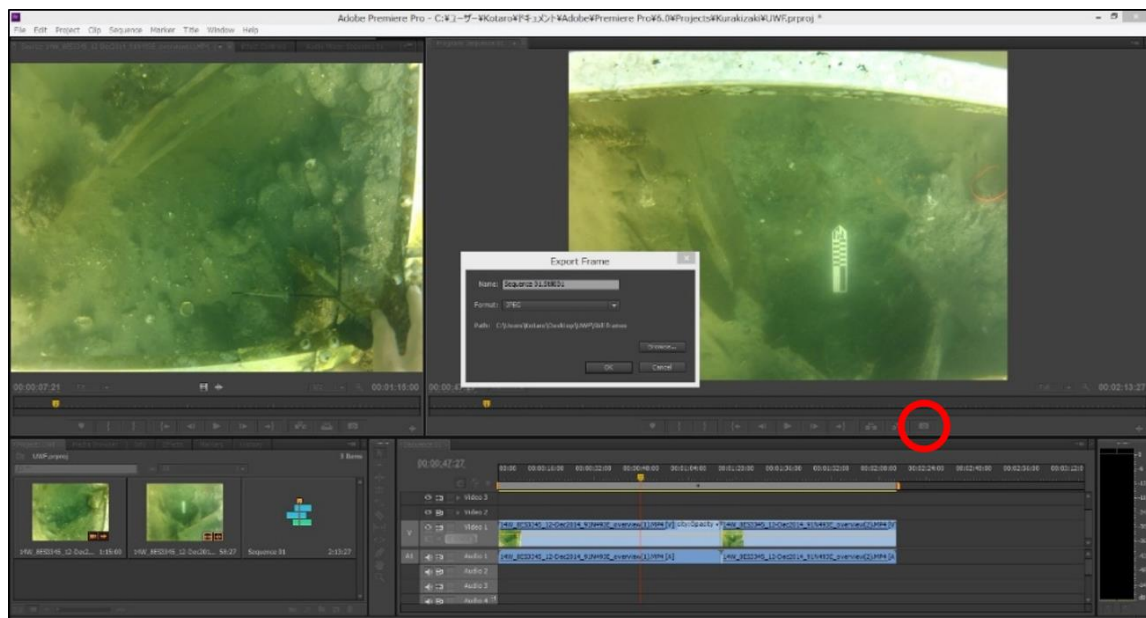


Figure 3-38. Manual extraction of still frames using Adobe Premiere Pro CS6. (Image: Yamafune)

Automatic extraction is another video extraction option. Using this method, still frames can be extracted automatically. The author used Adobe Photoshop CS6 for the automate extraction. The Photoshop software series is typically employed as image editing software, yet it can also edit video files. Using Photoshop, lengths of video footage may be trimmed, and still images from video footage may be exported at a controlled frequency (i.e. the number of frames extracted per second of video is selectable) (Fig. 3-39). This extraction is an automated process; thus, specific frames cannot be chosen for use in Computer Vision Photogrammetry. Consequently, some of the still frames automatically exported may be subject to motion blur.

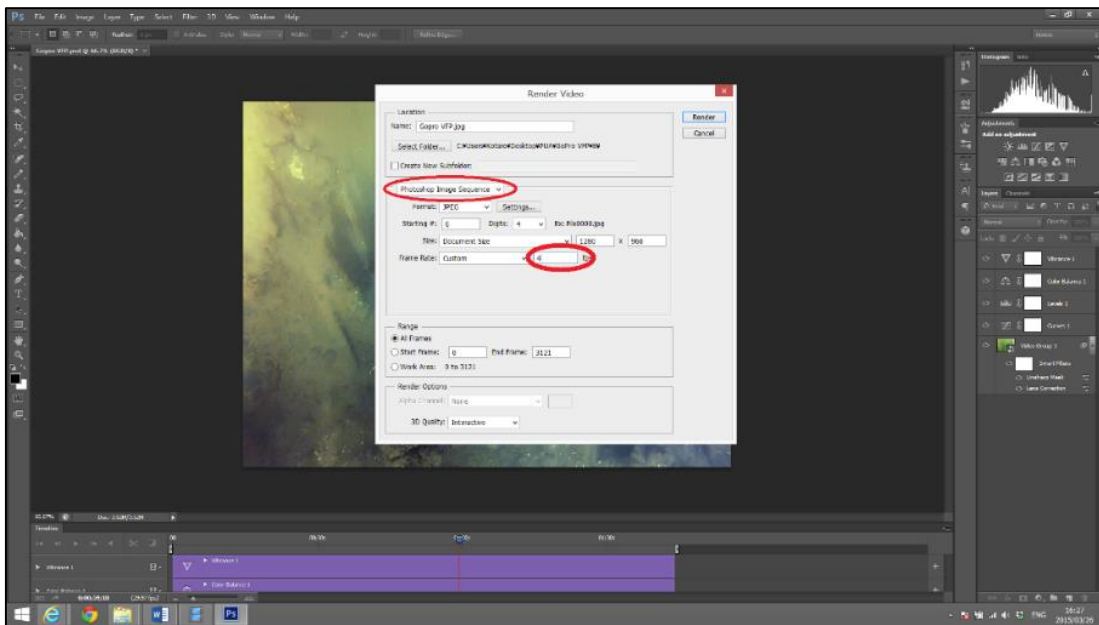


Figure 3-39. Automate extraction of still frames using Adobe Photoshop CS6 (Image: Yamafune)

The images that suffer motion blur have poor pixel information, and this may confuse PhotoScan and become a factor in the failure of photogrammetric modeling. To avoid this failure, poor quality images have to be removed beforehand by using image quality estimation in PhotoScan. To use this detection, the Photos Pane is opened after images are uploaded (Views > Panes), and then the display mode must be changed to the Details view. After selecting all photos, the Estimate Image Quality command is shown by right clicking on selected images. This command estimates the sharpness of images and calculates crispness as quality. When the process is completed, images may be re-organized based on quality by clicking on the Quality tab (Fig. 3-40). Then images that have quality below a certain threshold value should be removed. Unfortunately each photo must be opened and checked carefully, because the calculated value of quality and sharpness also depends on image size. As a starting threshold value, the author has found that rejecting images below a quality value of 0.45 produces satisfactory model results captured from video frame images. Employing this procedure allows photogrammetric modeling using video frames to proceed without poor quality images.

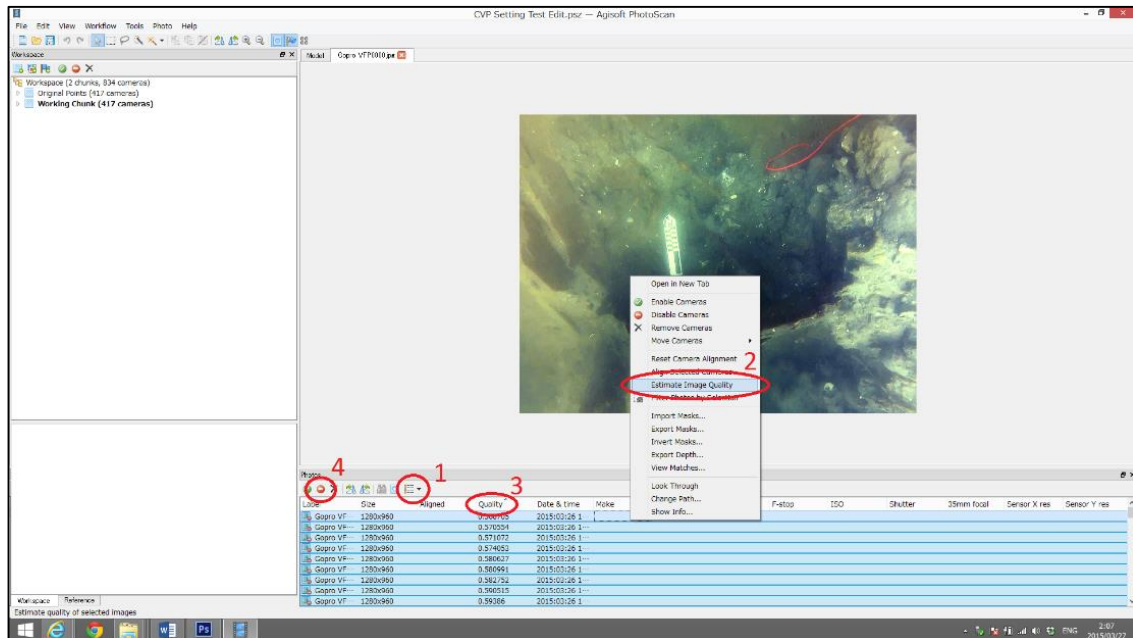
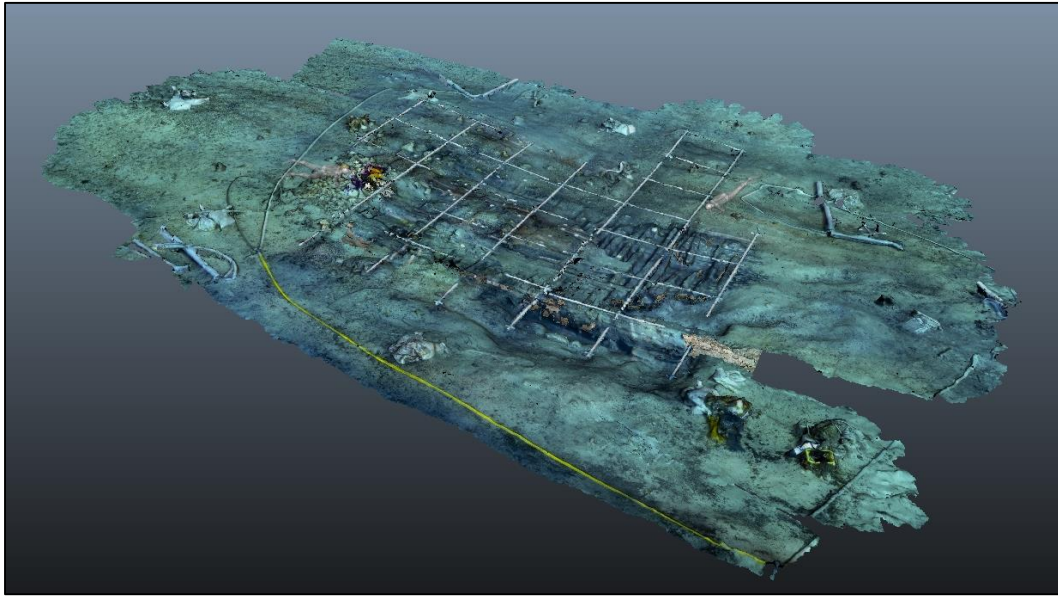


Figure 3-40. Process for removing blurred images in PhotoScan. (Image: Yamafune)

Video Frame Photogrammetry has both advantages and disadvantages. Two major advantages are wider coverage areas and better image overlapping. Since video recording does not require careful camera positioning, it tends to have much larger coverage areas than photo-shooting. During the Gnalici 2014 field season, one diver recording the site with video could cover an area four times larger than a diver shooting photographs in the same amount of time (Fig. 3-41 and 3-42). Another advantage is better image overlapping. Because one second of video footage is composed of 24 to 30 still images, the overlapping of consecutive images is marvelous. Therefore, Video Frame Photogrammetry tends to have excellent results in the Align Photos process. Balancing these advantages are the disadvantages of lower image resolution and fewer original colors. Lower image resolution often results in poor quality textures in the Built

Texture process. This is because most high-definition (HD) resolution video footage only has 1920 x 1080 pixels per frame, while a photo from a DSLR camera (with an ACL-S sensor) contains approximately 6000 x 4000 pixels. Thus, a frame captured from HD video camera footage contains less than 10% of the pixel information of the equivalent photo taken by a DLSR camera. Another disadvantage is less original color. As discussed in chapter II, auxiliary lighting can preserve the original colors of subjects; however, underwater environments require strong auxiliary lighting sources to penetrate water. This strong lighting can easily be obtained by employing strobe lights while taking photographs; however, it is nearly impossible to apply strong lighting as effective as strobe flashes while video recording. Even if a video camera has strobe lights that can provide auxiliary lighting, the power obtained from continuous spot-lighting is not strong enough in terms of original color retrieval. Consequently, photogrammetric models developed via Video Frame Photogrammetry tend to have a bluish-tone (Also see Fig. 3-41 and 3-42).



*Figure 3-41.* Video Frame Photogrammetry of the Gnalić shipwreck site. Photogrammetric models based on video footage have a much larger coverage area than photogrammetric models based on photos. However, without strong auxiliary lighting, created models tend to have bluish and greenish colored textures. (Image: Yamafune)

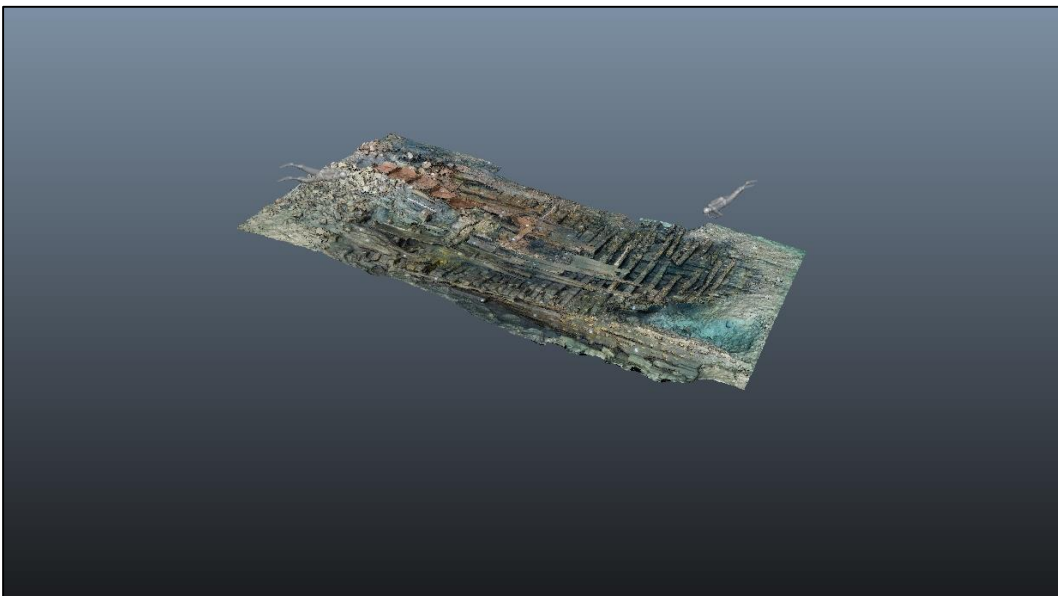


*Figure 3-42.* Computer Vision Photogrammetry of the Gnalić shipwreck site. The coverage area of photogrammetric models is limited because of the nature of photo-shooting. However, created models tend to contain more detailed and diagnostic archaeological information due to their use of high-resolution images. Also, thanks to the use of strobe lights, created models can display more original colors. (Image: Yamafune)



In short, Video Frame Photogrammetry can be a good option for photogrammetric recording, especially when a project does not have DSLR cameras or is time-constrained when performing photogrammetry. Nonetheless, the most important point is that whoever applies Video Frame Photogrammetry must understand both the advantages and disadvantages of using video footage as the source for photogrammetry.

#### *Underwater Video Frame Photogrammetry Using GoPro*

As described above, Video Frame Photogrammetry is beneficial in many ways, especially for novice underwater photographers and divers who do not have knowledge of photogrammetry. One reason is that it does not require complicated camera and strobe lights settings. Additionally, less expensive cameras with good High Definition (HD) underwater video recording capability are becoming commercially available.

Among these cheaper camera options, the most popular product today is likely the GoPro series. GoPro cameras have HD video recording systems that are very easy to handle in water, though their fish-eye lenses create distortion on captured images. However, using the Adobe Photoshop series (CS6, CS5, and CC), distortion in frames captured from GoPro video footage can be easily corrected. Not only does Photoshop have image correction tools, it additionally has the processing ability to automatically extract still frames from video footage at a specified frequency. Also, Photoshop allows color and haze correction over the entire video clip before still frames are extracted. In the end, satisfactory photogrammetric models can be created using GoPro cameras.

The following steps are a recommended workflow for Video Frame Photogrammetry using GoPro. The original GoPro video footage used for concept validation was taken by Charles Bendig, a graduate student at the University of West Florida. The videos were recorded by a GoPro Hero 3. The total duration of the video was 2 minutes and 15 seconds and frame dimension was 1280 x 960 pixels. In this workflow, Adobe Photoshop CS6 was used. To begin, the view window of Photoshop was shifted to Motion workspace, then the video footage was imported (Window > Workspace > Motion > Add Media). Next, the video clips were trimmed to the desirable proportions to be used for Video Frame Photogrammetry. Before applying distortion and color correcting processes, each video clip had to be converted to a Smart Object (Filter > Convert for Smart Filters) for image editing. Then, the “Lens Correction filter and Unsharp Mask filters were applied to the video clips in order to correct distortions and to sharpen video images. After these two filters were applied to the video clips, adjustment layers were applied to enhance the quality of the video clips; these adjustment layers were Curves, Levels, Color Balance, and Vibrance. Curves adjustment enhances the contrast in an image while Levels adjustment enhances color-distributions of the image. Color Balance adjustment restores original colors by reducing greenish and bluish tones in the water, and the Vibrance adjustment enhances the natural colors of the subjects in the images (Fig. 3-43 and 3-44). After satisfactory results were acquired with these corrections, still frames were extracted from video clips using the Render Video command. With this command, the number of extracted frames (per second) can be

controlled (File > Export > Render Video > Photoshop Image Sequence > Frame Rate: number of frames per second).

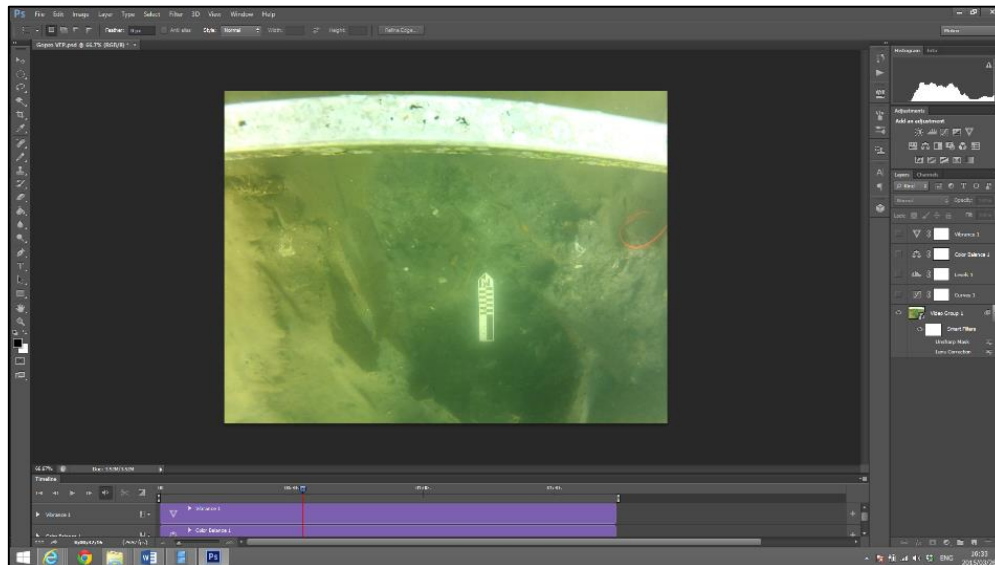


Figure 3-43. The original GoPro video footage before the color and distortion correction (Image: Yamafune)

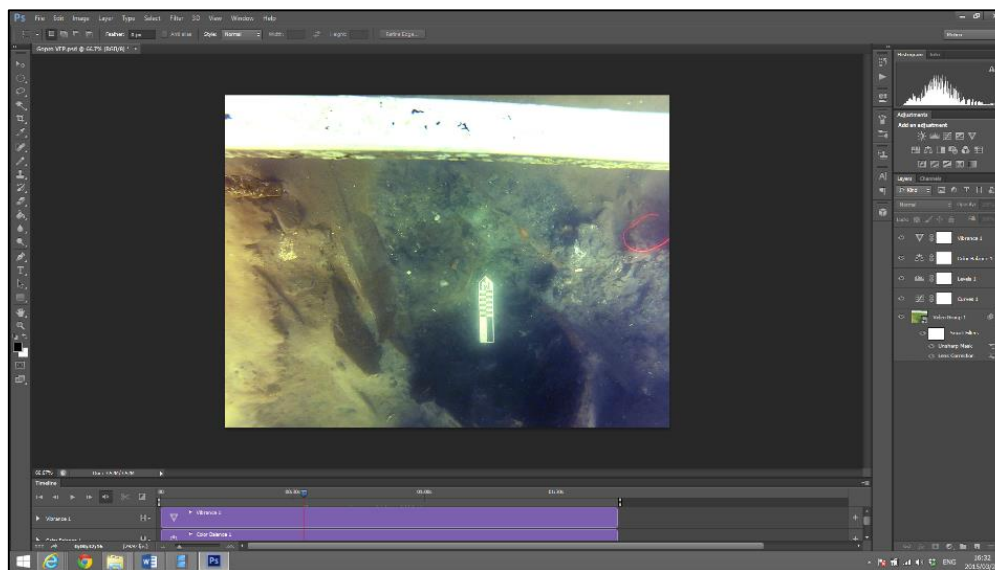


Figure 3-44. GoPro video footage after the color and distortion correction (Image: Yamafune)

After those images were prepared, the extracted frames were uploaded to PhotoScan as photo images. However, as noted earlier, these frames were automatically extracted from the video clips in Photoshop and were not selected carefully with photogrammetry in mind. Consequently, some images were subject to motion blur. Therefore, bad quality photos needed to be excluded before photogrammetric modeling could begin. To do so, the Estimate Image Quality command was applied (on Photo Pane, change view mode to Details views > select all cameras > right click on selected cameras > “Estimate Image Quality”); low quality images were noted and disabled. Then, once the Align Photos process was started, all of the following photogrammetric processes were identical to the PhotoScans basic workflow for Computer Vision Photogrammetry. In addition to Photoshop there are many other open source software packages that can extract still frames from video footage, such as *Free Video to JPG Converter*. However, to retrieve original colors and correct distortion, the use of Photoshop or a similar image editing or video editing software is recommended. Figure 3-45 displays the photogrammetric model with the pre-processed image corrections in Photoshop and Figure 3-46 shows one without any image corrections (Fig. 3-45 and 3-46).

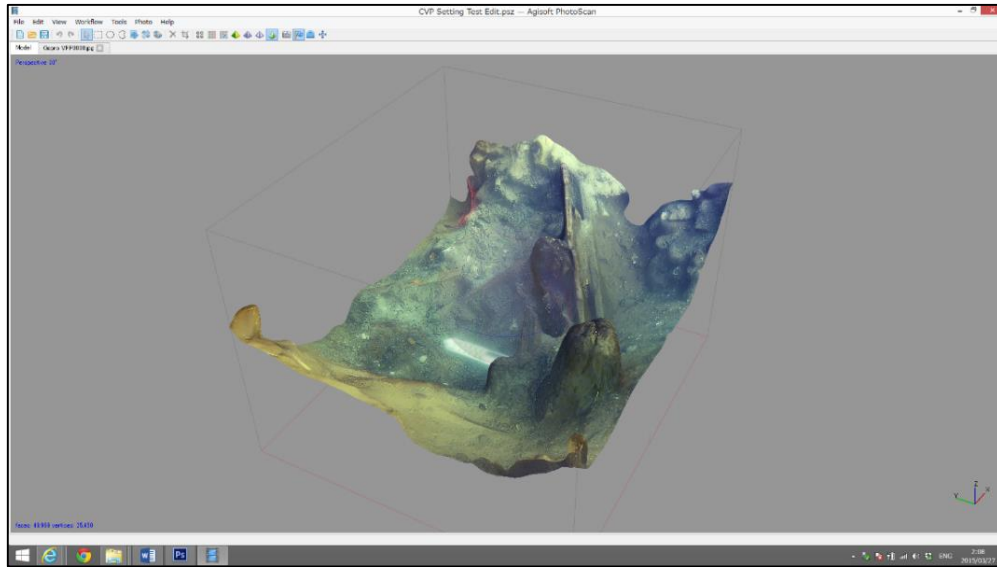


Figure 3-45. Photogrammetric model based on video footage with color and distortion corrections applied in Photoshop. (Image: Yamafune)

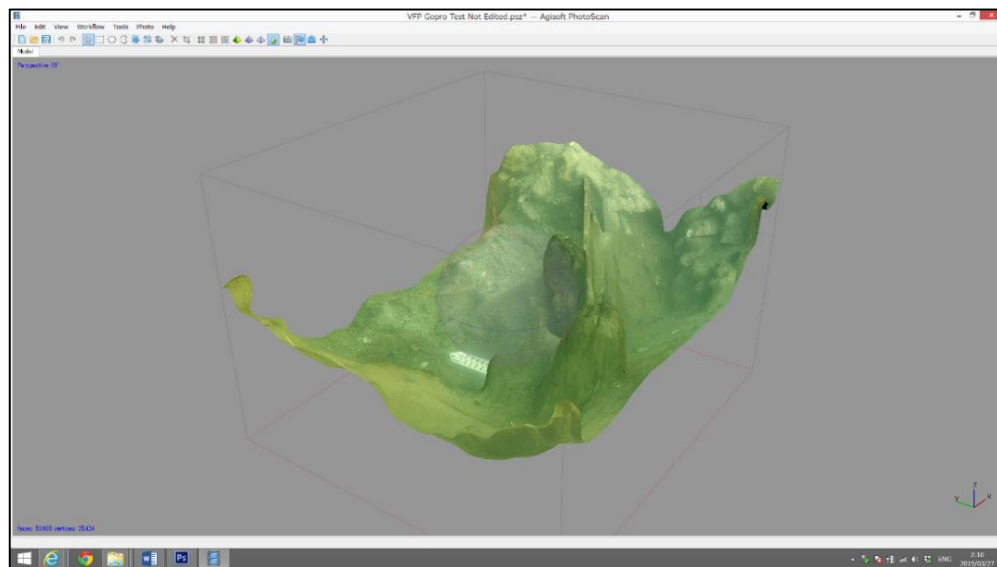


Figure 3-46. Photogrammetric model based on video footage with color and distortion corrections applied in Photoshop. (Image: Yamafune)

## **Georeferenced Orthophotos**

One of the prominent features of PhotoScan is its ability to produce orthophotos. Orthophotos are high-resolution photomosaics, and PhotoScan can compose them based on calculated camera positions. Orthophotos are more accurate than traditional photomosaics because they do not have optical distortion. Moreover, when an orthophoto is created of a scale-constrained model, the exported orthophoto will also have correct proportions. PhotoScan also has an ability to create GeoTIFF images; this file format contains georeferenced information. This image is also 1:1 scale. GeoTIFF orthophotos are very useful, especially when archaeologists need to create a photomosaic for a larger area, such as an entire shipwreck site. When archaeologists have to create detailed photogrammetric models, the photo coverage area may be limited. This situation can be caused by constrained diving time on the area, the number of photos needed to capture the entire area, or the limited computing power of available computers. The author suggests that when a photogrammetric model of the whole archaeological site needs to be created, it is easier to focus on small areas and piece the separated parts together later. When a model of a shipwreck site is created in separate batches, it is impossible to produce one complete orthophoto of the entire site from separated models (though it may be possible if the project computer has substantial computing power and graphic cards to create one complete 3D model of larger coverage area, for instance 100m x 25m shipwreck sites), yet this is less likely on most archaeological projects because of budgetary constraints. However, as long as the photogrammetric model's scale is based on local coordinate systems as the author

explained in Chapter II, exported orthophotos can contain georeferenced information. As briefly mentioned above, GeoTIFF orthophotos have georeferenced data; in other words, the image is a 1:1 scale of the actual shipwreck site and images can open in correct scale and position in GIS software. Consequently, even if orthophotos of the archaeological site were created in separate areas or on different dates, they will merge automatically based on georeferenced information. The method used to create GeoTIFF orthophotos is simple. First, the model must have georeferenced data, such as markers with XYZ coordinates. Then, within the Export Orthophoto command in PhotoScan, a checkbox that says GeoTIFF will appear in the exported orthophoto window. If it is selected, the exported TIFF image contains georeferenced information.

Four different orthophotos in GeoTIFF format were created during the Gnalić Project's 2014 field season. These orthophotos were exported to ArcGIS mapping and spatial analysis software. Once there, the orthophotos opened automatically in the correct positions and with the correct scale; therefore, no manual adjustment was required (Fig. 3-47). Since orthophotos have 1:1 exact scale and have no optical distortion, exported orthophotos are tremendously useful for archaeological analysis; orthophotos can be used as templates for the creation of conventional 2D site plans and special analysis.

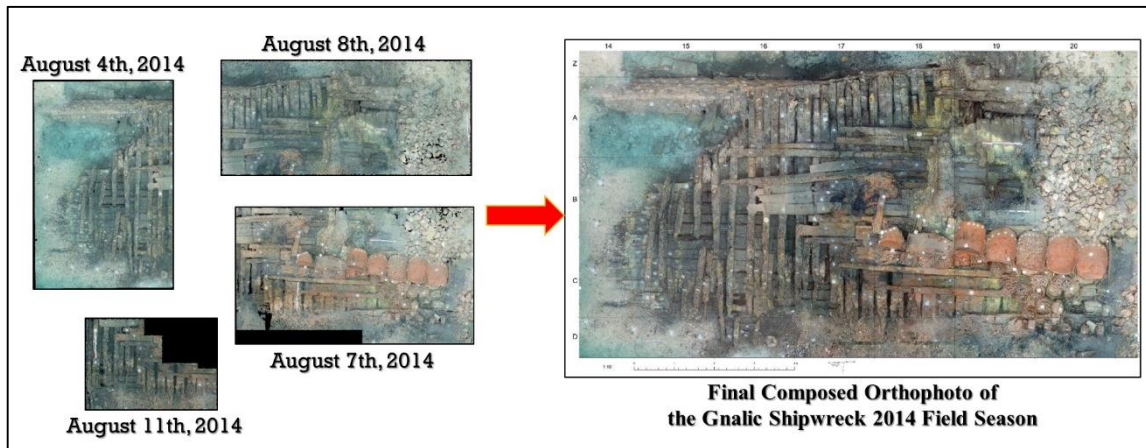


Figure 3-47. Composed Orthophotos of the Gnalic shipwreck site from the 2014 field season. As the final result, four orthophotos were produced from different data. These georeferenced orthophotos were merged automatically in ArcGIS software. (Image: Yamafune and Torres)

Even without georeferenced information, exporting normal orthophotos is useful.

When a GeoTIFF orthophoto is created, the projection plane must be a top view.

Although the exported orthophoto will not be at 1:1 scale, the projection plane of an ungeoreferenced orthophoto can vary. In other words, it can be a photomosaic of a top view, side view, front view, and so on (Fig. 3-48). Additionally, if the rotation of a photogrammetric model is controlled before the orthophoto is created, an orthophoto that is parallel to the archaeological site can be created. This orthophoto based on a parallel projection plane may be useful when the archaeological site lies on a sloped seabed (Also see Fig. 3-48. The red plane refers to a projection plane that is parallel to the shipwreck site). Actual usage of orthophotos shall be discussed in following sections.

Scale of exported ungeoreferenced orthophotos can be corrected in CAD software and Photoshop to match the desired scale. Therefore, archaeologists can choose to create a georeferenced orthophoto or a non-georeferenced orthophoto depending on their needs.



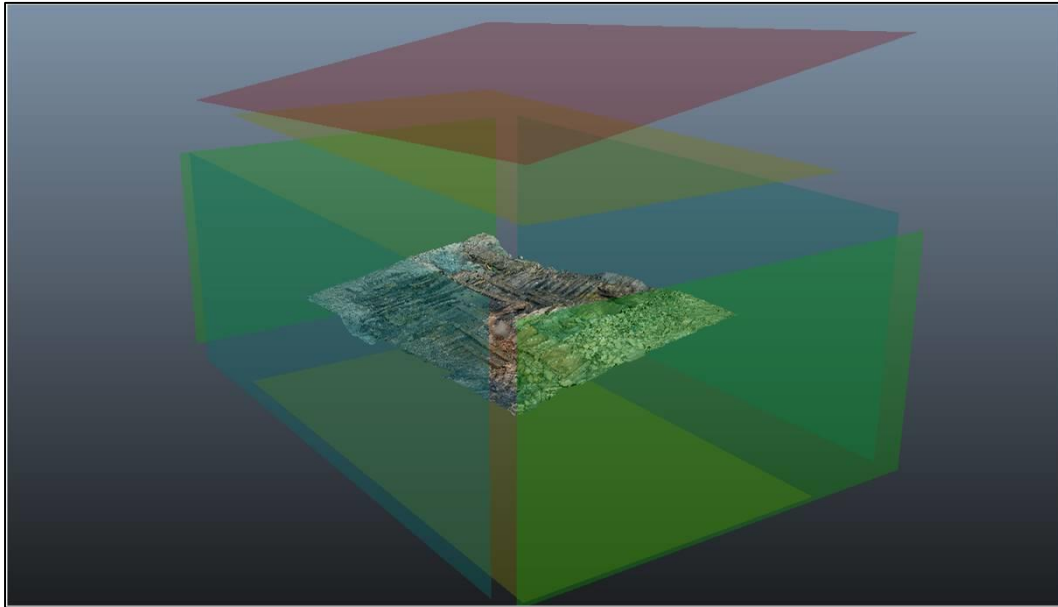


*Figure 3-48.* Image of the visualized projection planes of orthophotos. The projection plane can be chosen from six different orthogonal directions. Moreover, by controlling the rotation of the photogrammetric model, the projection plane can be made parallel to the archaeological site (the red layer). (Image: Yamafune)

### **GIS Based Spatial Data Archive**

Once the information and photos from the excavation are organized and stored in the database, work can proceed (see Chapter II). Now, using georeferenced orthophotos, archaeologists can merge their manually collected information with the georeferenced information to create a database that can be used for spatial analysis. Spatial analysis of a shipwreck site is vital for understanding the original shapes of the ship; Dr. George Bass and Dr. Frederick Van Doornick, and their research team reconstructed the hypothetical original shape of the seventh-century Yassı Ada shipwreck based on meticulously recorded positions of artifacts even though actual wooden remains of hull structure were sparse (Van Doornick, 1967; Bass, 1972; Bass and Van Doornick,

1982). During the Gnalić 2014 project, Dr. Torres, a ShipLab research associate (and Texas A&M University Ph.D candidate at the time) was in charge of GIS analysis, organizing the database, and the production of 2D site plans. He used ArcGIS mapping software for those tasks. The author is currently learning his skills first hand.

Henceforth, the following discussions are based on Dr. Torres idea of using archaeological data from the excavation team to perform spatial analysis based on georeferenced orthophotos.

During the Gnalić Project 2014 field season, Dr. Torres introduced ArcGIS mapping software to the excavation team. ArcGIS is a mapping and spatial analysis software. During the project, georeferenced orthophotos created by the author were imported into ArcGIS. Because of the georeferenced information, orthophotos created in PhotoScan opened in the correct global position. Additionally, orthophotos that were created on different dates and in different areas automatically georeferenced and produced a completed one-piece orthophoto that encompassed the entire archaeological site. What is more, information about the site's artifacts, photos of the artifacts, and sketches and annotations by archaeologists were connected to ArcGIS. Therefore, all the information that was collected by the excavation team was linked to georeferenced spatial information. Henceforth, orthophotos and artifacts can be linked and used for spatial analysis, such as understanding cargo distribution and site formation processes.

Also, ArcGIS and other basic GIS software packages have basic drawing capability. Therefore, archaeologists can trace imported orthophotos to produce 2D site plans (Fig. 3-49). Dr. Torres periodically produced 2D site plans and printed out partial

plans on mylars; therefore, archaeologists and divers could bring these site plans on their dives and use them as templates upon which they could add additional information.

After the field season, Dr. Torres produced a 2D site plan in ArcGIS based on imported orthophotos (Fig. 3-50).

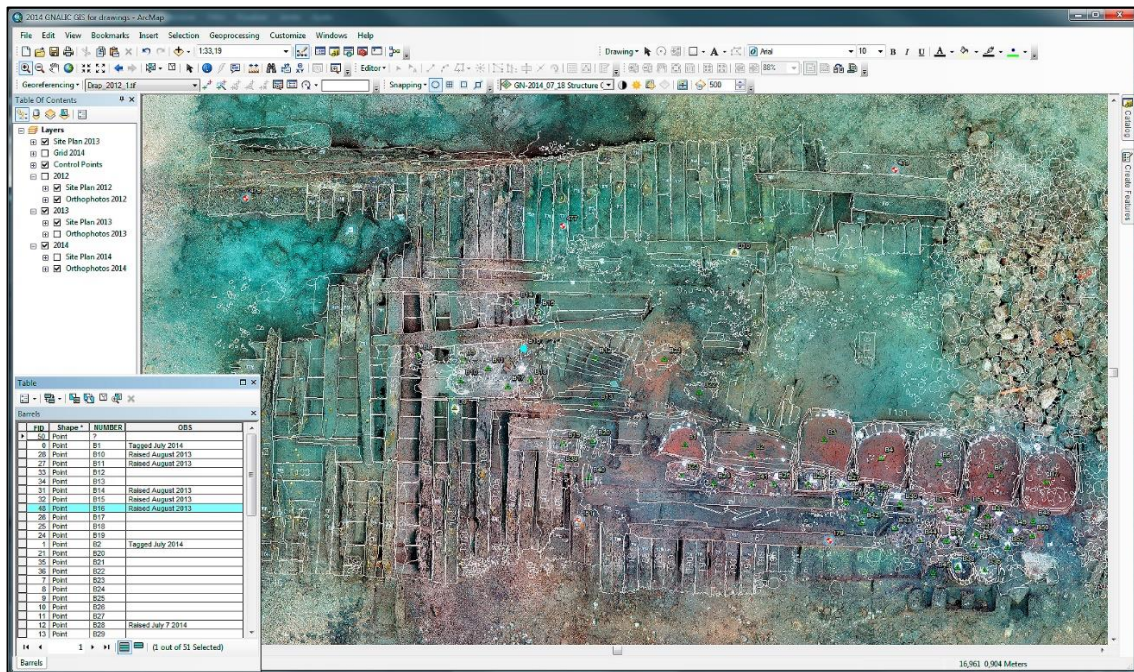


Figure 3-49. The Gnalíć shipwreck site in ArcGIS software. All corrected data by the excavation team is connected to georeferenced orthophotos. (Image: Reprinted with permission from Torres, 2014b)

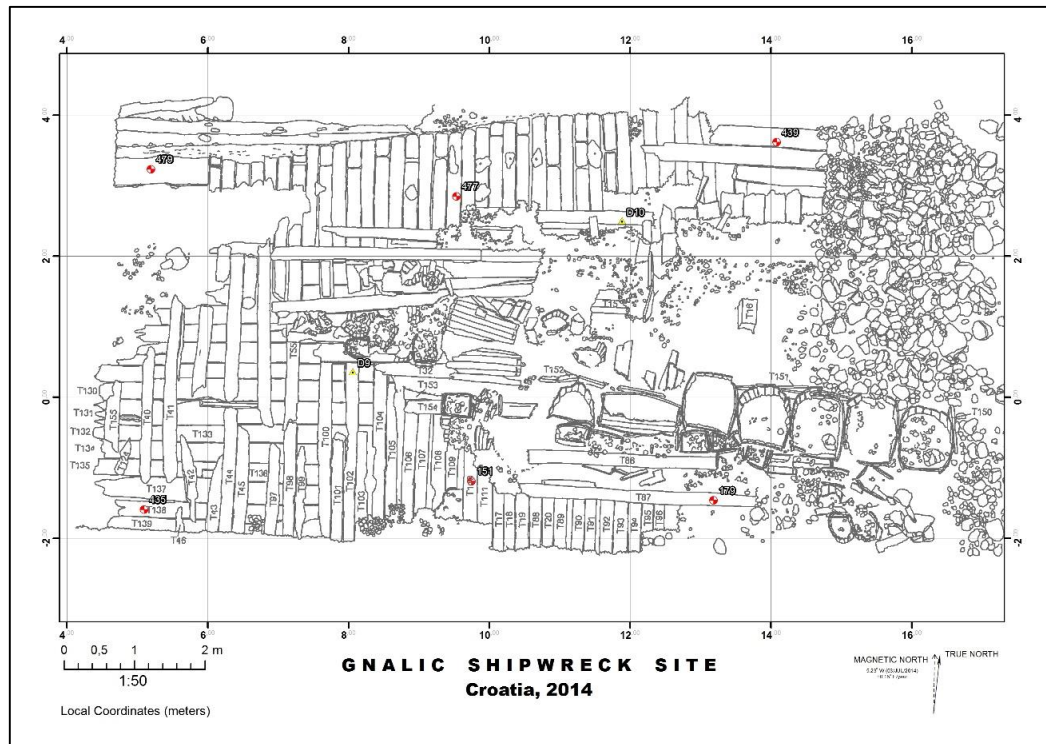


Figure 3-50. 2D site plan of the Gnalici shipwreck based on the 2014 field season. This 2D site plan was produced in ArcGIS mapping software. (Image: Reprinted with permission from Torres, 2014c)

## 2D Site Plan and Timber Catalog Templates

In the previous section, the author described a method for creating a conventional 2D site plan using ArcGIS software. Drawing in ArcGIS allows each image to have georeferenced information. Also, 2D site plans can be created in other CAD softwares, such as the AutoCAD series and Rhinoceros series, and in drawing software, such as the Adobe Photoshop series and Adobe Illustrator series. Some archaeologists may prefer to print scaled orthophotos on paper and trace them manually. In short, there are various ways to produce site plans using orthophotos, and archaeologists can choose a method based upon available software and personal preference. However, these methods are all

based on tracing orthophotos of archaeological sites. This tracing method is tremendously quick and easy in comparison to conventional drawing methods that are based on archaeologist's sketches and collected measurements. Nonetheless, based on the author's experience, these tracing methods are not fast enough to follow the ongoing excavation weekly. Indeed, the first production of a 2D site plan is often completed only after the field season is over. Therefore, during a field season, briefings and debriefings for the project proceed using orthophotos or site plans from the previous season. Yet, these orthophotos are often visually too noisy to understand the structure of site, and manually tracing it (either on paper or in a computer program) to create a 2D site plan takes time. After attending six archaeological excavations, including three years on the Gnalić Project, the author began seeking faster and easier methods for creating 2D site plans that could be used for planning the logistics of an ongoing project and help archaeologists understand the excavation as it unfolds. Based on these ideas, the author found what he calls the erasing method.

#### *Erasing Instead of Tracing Method*

Although tracing an orthophoto to create a 2D site plan is a substantially faster and more accurate method than the conventional manual hand drawing method used by archaeologists, it still requires knowledge of software and sometimes knowledge of shipbuilding. Therefore, production of 2D site plans are often done by experienced archaeologists. However, in many cases those experienced archaeologists are occupied by other tasks during the field project, and this is one of the main reasons that production

of a 2D site plan must wait until the field project is over. The author believes that if the production of a 2D site plan does not require special skills and knowledge, this task can be assigned to attending students and divers. Yet, the process must be easy and fast enough to follow the ongoing project. To satisfy those needs, the author developed an erasing method.

The concept of the erasing method is simple; the archaeologist erases the internal parts of timbers on the orthophoto and the product is converted into a sketch-like drawing using Photoshop. Erasing, or cleaning, can enhance the edges of structures. The first converting part of the process (described below) requires special knowledge of the software; however, once it is converted, the rest of the process requires only the erasing tool. Since this erasing method requires only a single tool in Photoshop, it can be done by any team member. The process begins with the conversion of an image into a sketch-like drawing. To determine the best way to create the sketch-like drawing, the author attempted various methods that can be found in training books and videos, and so far the best result was acquired from a method that was found on YouTube (Ch-Ch-Check It, 2011). In the following section, the author explains a slightly modified method of this conversion process using the orthophoto of the Gnalić shipwreck site from the 2014 field season.

First, the composite orthophoto was exported from ArcGIS and opened in Photoshop CS6 (Fig. 3-51). When an image is opened in Photoshop, the original layer is opened as a locked layer called Background. This locked layer has to be unlocked to be an editable layer (Layer > New > Layer from Background). Now this layer (layer 0) can

be duplicated (Layer > Duplicate Layer), and then it needs to be converted into a black and white image (Image > Adjustments > Desaturate). The author recommends that one change the layers name to B&W to avoid confusion (Layer >Rename Layer). Next, this B&W layer must be duplicated again, and then the duplicated layer should be Inverted (Image > Adjustments > Invert). The author also recommends that you rename this inverted layer to Inverted. Then, the blending mode of this layer must be changed from Normal to Color Dodge. Although, this may create the appearance of a plain white image, that is fine. The next step is to extract edges from the original orthophotos. To do so, the Gaussian Blur filter must to be applied to the Inverted layer (Filter > Blur > Gaussian Blur). By this point, the edges of the original orthophoto can be enhanced as a black and white image. The next step is to extract more detailed edges. To extract detailed edges, the B&W layer must be duplicated again (Layer > Duplicate Layer), and the duplicated layer must be moved to the top of the layer panel. Then, the Glowing Edges filter must be applied on the B&W layer (Filter > Filter Gallery > Stylize > Glowing Edges). At this point, the author also changed the layer's name to Glowing Edges (Layer > Rename Layer). After the Glowing Edges layer is inverted (Image > Adjustments > Invert), the blending mode of this layer must be changed from Normal to Multiply. After these steps are applied, the orthophoto of the site plan is converted into a sketch-like drawing (Fig. 3-52). After these layers are flattened to a single layer (Layer > Merge Layers), it is time to utilize the erasing method.

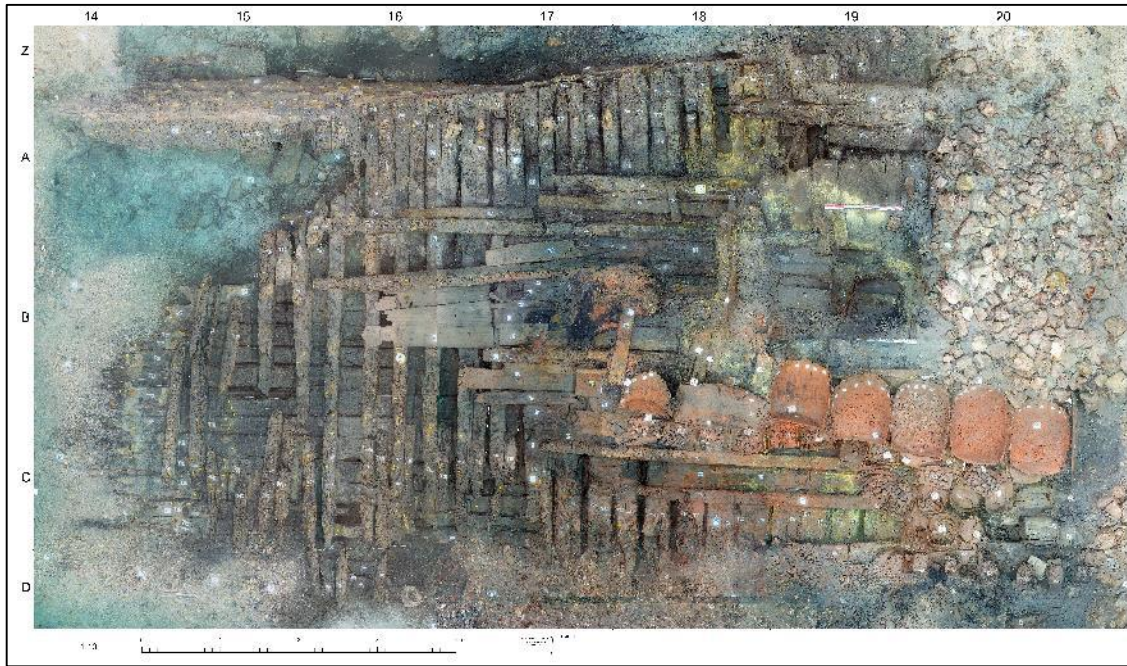


Figure 3-51. Orthophoto of the Gnalić shipwreck site from 2014 field season. (Image: Reprinted with permission from Torres, 2014d)



Figure 3-52. Sketch-like conversion of the orthophoto of the Gnalić site. (Image: Yamafune)



This sketch-like conversion is already visually appealing and can be used as a figure for publication; yet the author aims to create a cleaner and more stylized 2D site plan. Once the orthophoto has been converted to a sketch-like drawing, the following step is surprisingly easy; it only requires an erasing tool that can be found in the tool bar on the left side of the Photoshop screen. The diameter of the erasing tool can be controlled. For example, it took only two hours for the author to clean the structures of the Gnalić shipwreck (Fig. 5-53). This means that a 2D site plan can be acquired within a day. Another advantage of this erasing method using Photoshop is that any mistakes can be corrected afterward (by keeping original images behind the working layer). Additionally, since these images are computer based, they can be updated at any time. Therefore, these images can be printed on Mylar using a laser printer so that archaeologists and divers can dive with these site plans as a template upon which the positions of scarves and fasteners can be drawn. These 2D site plans can be reimported into ArcGIS and additional information can be uploaded. It can then become part of the database. Based on his experiences, the author believes that this erasing method is much faster than the tracing method and it does not require any skills or knowledge of software once the orthophoto is converted to a sketch-like image. This method could be very useful during field projects.

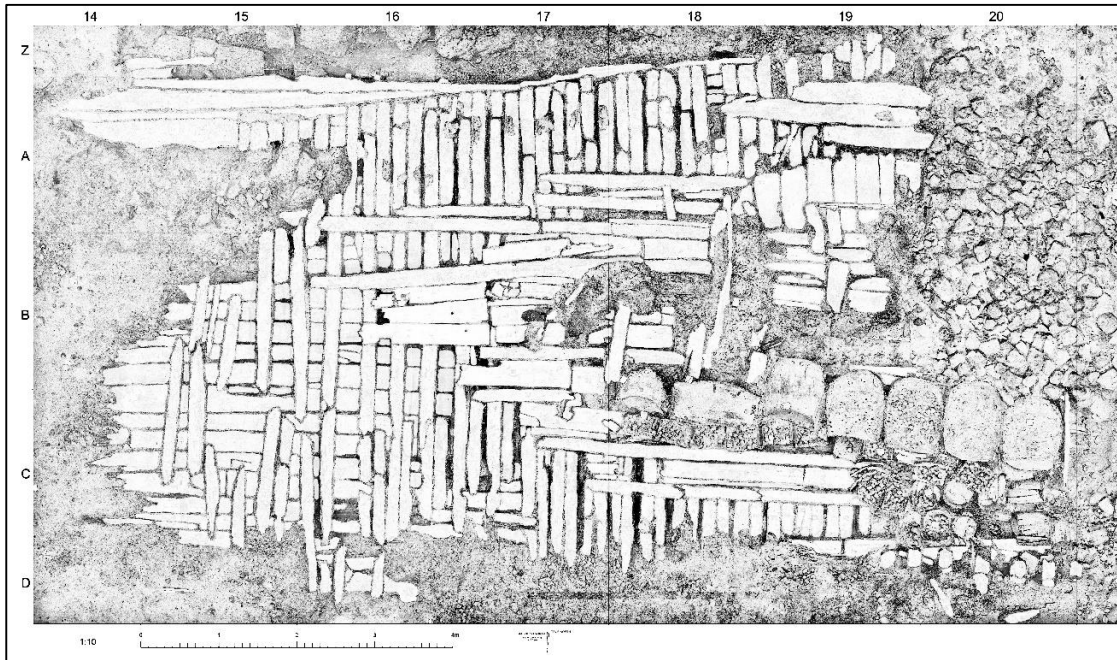


Figure 3-53. Proposed 2D site plan created with the erasing method. The internal depictions of structure were cleaned by the erasing tool in Photoshop. (Image: Yamafune)

#### *Timber Drawing Templates (with Automated Masking)*

The author discussed the sketch-like conversion technique in the previous section. This technique is tremendously useful for timber drawings as well. One of the unique and important tasks of nautical archaeologists is recording timbers. Because ship timbers may contain tool marks and fasteners, the timbers contain important information for archaeologists that sheds light on the construction and design of the original ships (Fig. 3-54). Knowing the dimensions of the timbers is necessary when reconstructing the shape of the original ship. However, waterlogged wood may warp and deteriorate as soon as it is removed from the underwater site. Therefore, archaeologists must record the

timbers as precisely as possible, yet as quickly as possible. However, this timber drawing also requires a great deal of experience and training to do properly.

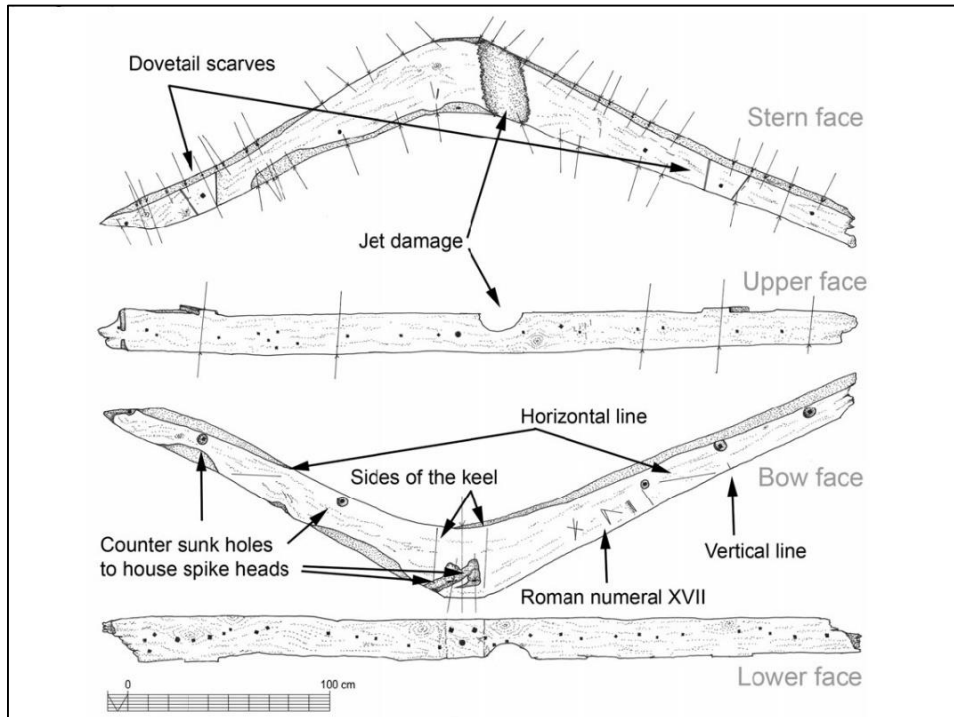
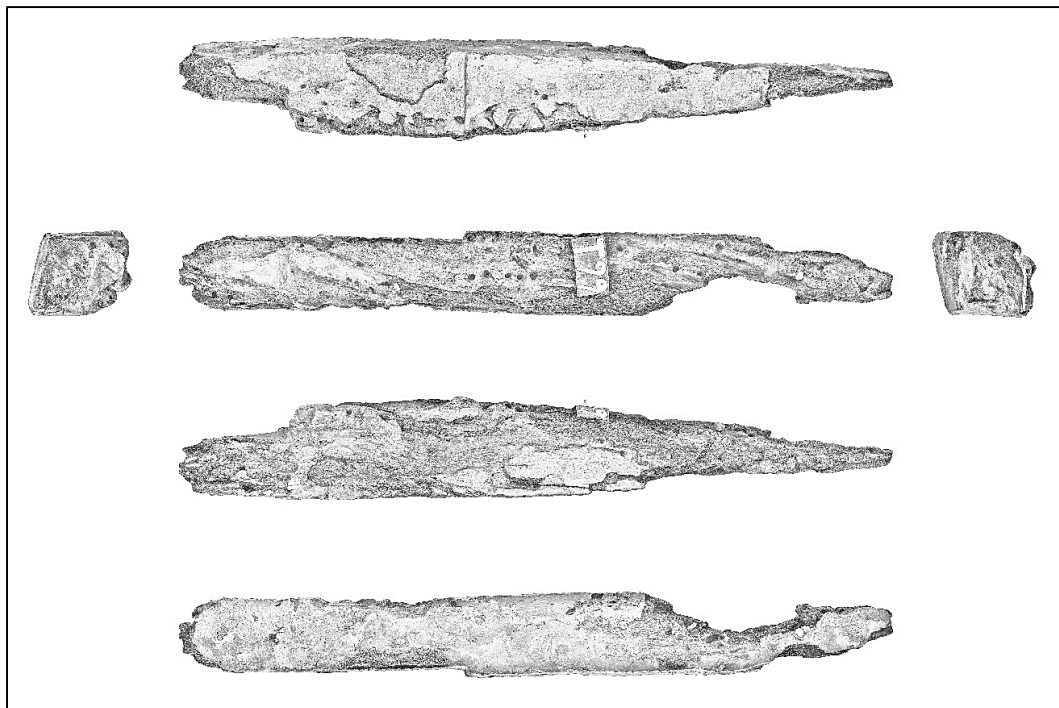


Figure 3-54. An Example of conventional timber drawing (from Cais do Sodre shipwreck) made by an archaeologist (Castro, Yamafune, Eginton, and Derryberry, 2011). (Drawing: Castro, 2011)

During the Gnalíć Project 2014 field season, several timbers were raised, and the conservation laboratory team attempted to produce timber drawings. This attempt was an exercise for university students and was supervised by an experienced historian. However, for most of the students, the drawing training was their first experience with timber recording. As a result, only three timbers were recorded in two weeks by two students.

Because of this difficulty, the author realized the importance of a quick and accurate method for creating templates for timber drawings. Fortunately, the author had an opportunity to create a photogrammetric model of one of the raised timbers. This timber was named T99. After the photogrammetric model was created, the model was re-scaled using a scale bar tool in PhotoScan. Six orthophotos were created based on six different projection planes of orthogonal directions; then, those orthophotos were aligned in Photoshop and converted to sketch-like images (Fig. 3-55). As a result, a template of a timber catalog for T99 was created in four hours. Archaeologists can add tool marks and nail holes on this template based on their observations, which speeds up the recording process.



*Figure 3-55.* An example of a timber drawing template. (Image: Yamafune)

A key to the successful photogrammetric modeling of this timber was the automated masking technique applied in Photoshop. The masking technique for Computer Vision Photogrammetry is often used in PhotoScan. Masking is a technique that hides pixel information in assigned regions. Hiding unnecessary regions in images facilitates the photo alignment process. Therefore, it is useful when turntables are used to capture a subject because the background remains the same in photos, which facilitates masking. The masking feature is also useful when archaeologists want to capture all aspects of an artifact's different sides because an artifact can be rotated and masking can hide the background. Although PhotoScan has various ways of creating masks in the software, the author believes that the best results can be acquired by using Photoshop for masking before importing the images into PhotoScan for processing. Photoshop has very precisely controlled selection tools and the selected area can be saved as an alpha channel (transparency pixel data) with TIFF image formats. What is more, using Action commands, this masking process can be automated. The author shall explain the automatic masking method using Photoshop in the following section.

To apply automated masking, photos have to be taken under controlled conditions. This masking process uses a selection tool in Photoshop; therefore, a monotone background is required. Green screens used by the motion picture industry are based on the same masking idea. For T99 from the Gnalić shipwreck, a white sheet was used as the background. Theoretically speaking, any monotone colored background can be used as long as it is a different color than the subject. Once photos of all sides of the artifact are taken, the photos are transferred and stored in a temporary folder. One photo

must be opened in Photoshop to create an Action command. If the Action command window is hidden from the workspace, it can be reopened from Window menu (Window > Action). After the Record command of the Action command is activated, the masking process must be applied to the image. To mask an image with a monotone background, the best selection tool is the Magic Wand. The background must be selected by clicking on a corner of the image. After confirming that all of the background is selected except the subject, this selection area should be inverted (Selection > Invert). Once selection is inverted so that only the subject is selected, the selection area can be saved as an alpha channel. To do so, select Save as a channel option under the Channels tab, which is located next to the Layers tab. The image now has alpha channel information. Then the image must be saved in the TIFF file format because JPEG cannot carry alpha channel data. When the image is saved as a TIFF file and closed, the recording of the Action command also must be stopped to complete recording. By taking these steps, it is possible to create an action command that can create masks in Photoshop. What is more, Photoshop can apply an action command on a collection of photos that are stored in one folder (File > Automate > Batch, or File > Automate > Create Droplet). Using this Batch Action command, masking can be automatically applied to hundreds or thousands of photos simultaneously. After the TIFF images are uploaded to PhotoScan, the masks should be applied to the images again (Tools > Import > Masks > From alpha) (Fig. 3-56). This masking technique is tremendously useful and fast. Also, this method of automated masking can be applied to any photogrammetric modeling project as long as

the photos are taken in a controlled environment. Moreover, since unnecessary pixel information is hidden from the modeling process, processing time is shortened.

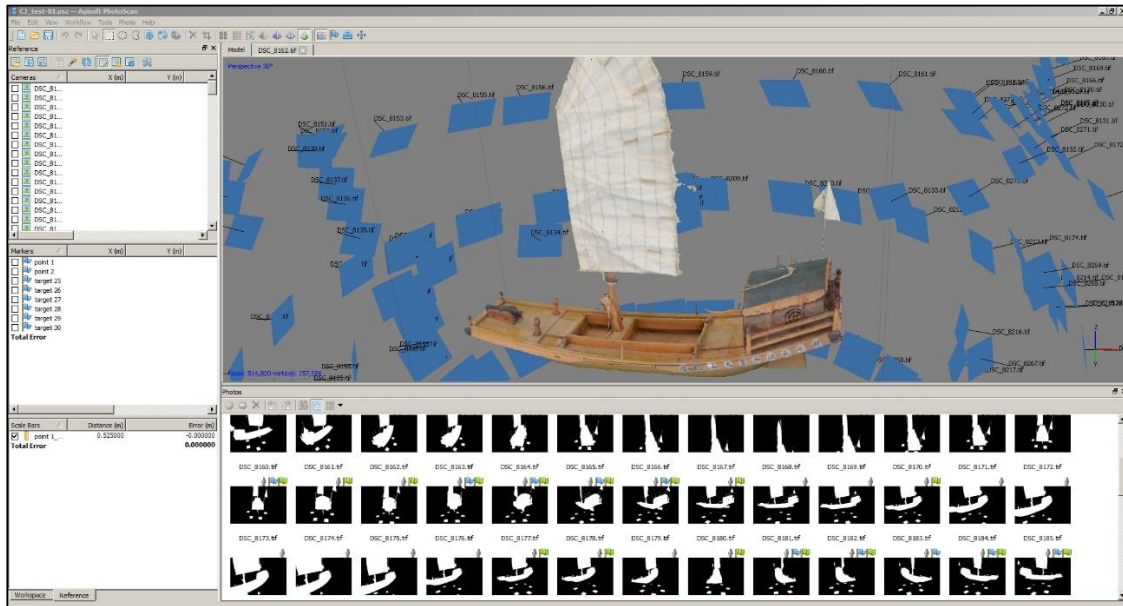


Figure 3-56. Computer Vision Photogrammetry with masked photos. Masked images can be seen in the photo pane on the bottom (the black part of photos were masked). Precise masking improves the quality of photogrammetric models. (Image: Yamafune)

Using this automated masking technique, the photogrammetric model of T99 was created showing all sides of the timber. By association, the timber drawing templates also showed all sides of the timber. One or two timber drawing templates can be produced within a day, after which, archaeologists only need to add fastening and tool marks to the template. This template system substantially accelerates the timber recording process.

The author believes that this timber drawing template method has great potential because archaeologists will only need a quick photo shoot session with the timber to gain a large amount of information. The timber will only need to be removed from the site for 15 to 30 minutes. In other word, as long as the team has a monotone board or sheet on the boat, divers can raise timbers onboard the dive boat temporarily and return them to the underwater site after photos are taken. The rest of the process can be done without timbers, and archaeologists can add tool marks and fastenings using photos and photogrammetric models. This methodology makes it unnecessary for archaeological projects to acquire a budget for conservation and storage, which is often difficult. For these reasons, the author encourages the use of this method to create timber drawing templates for quick and accurate recording.

Before closing this discussion, the author wants to mention that this method of producing timber templates can be used for artifact drawings as well. In addition to the visually appealing drawing and quickness of production, one of the important factors of this method is its accuracy of dimension and details. The author converted orthophotos of a port tiller block from the Red River Wreck *Heroine* (1832) into a sketch-like artifact drawing. From photo shooting to the drawing's completion, the process takes only three hours (Fig. 3-57). The author must note that within these three hours a 1:1 scale photogrammetric model is also created along with the orthophotos.



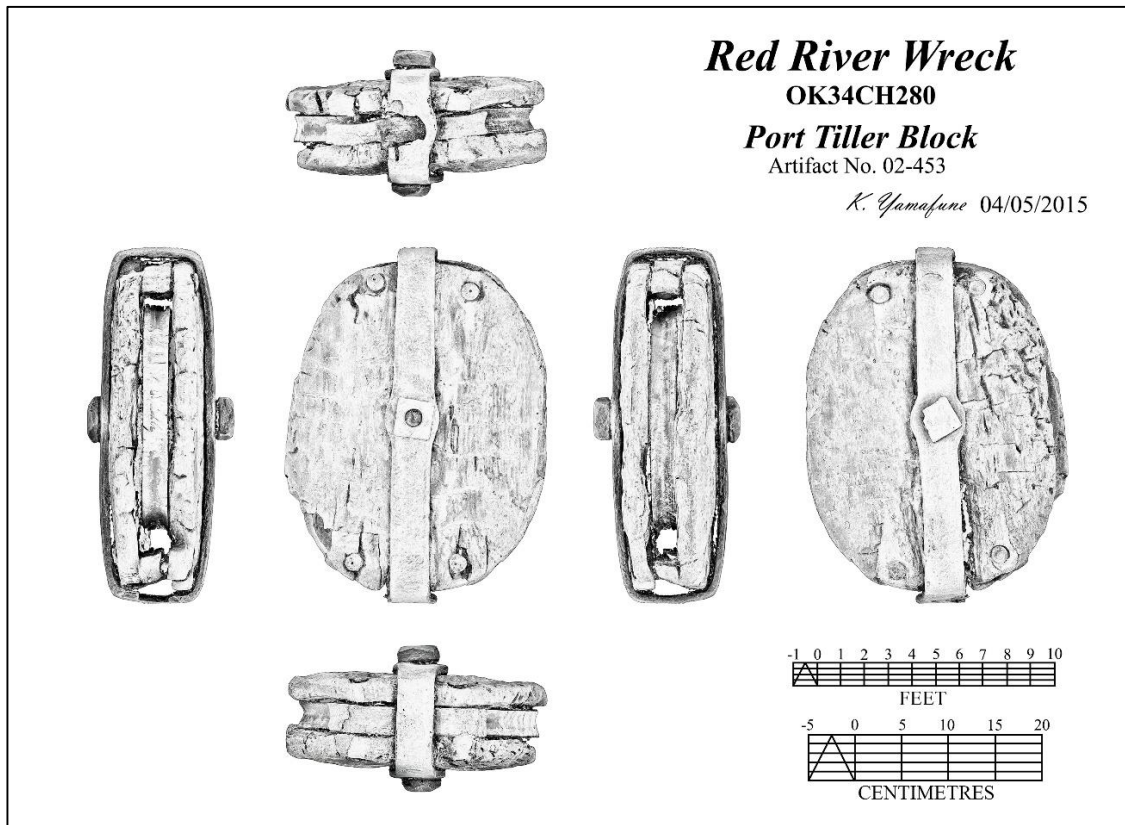


Figure 3-57. Artifact drawing of a port tiller block found in Red River Wreck site based on exported orthophotos. (Image: Yamafune)

### Section Profiles of Shipwreck Sites

Section profiles of the shipwreck site are valuable because they may represent hull lines of the original ship before it sank. One of the most important pieces of information that archaeologists must acquire from the shipwreck site is the curvature of the ship's frames. Since 1960, when archaeologists began to dive to underwater shipwreck sites, many manual methods have been used to extract the curvatures of frames (Steffy, 1994; Bowens, 2009). It is tremendously difficult and requires a great deal of training to measure and draw the correct curvatures of frames. Because of this, many frames have been raised and traced by archaeologists on land in order to record the

curvatures. However, raising frames to record them is time consuming and labor intensive. Additionally, as a result of the 2001 UNESCO Convention on the Underwater Cultural Heritage, the importance of *in situ* preservation has become recognized. Consequently, acquiring the curvature of frames from underwater shipwreck sites has become more difficult than ever.

Fortunately, thanks to Computer Vision Photogrammetry, archaeologists are capable of creating real scale photogrammetric models of underwater shipwreck sites. Since properly created photogrammetric models contain correct measurements, archaeologists can acquire the curvature of frames from photogrammetric models. However, when the author first tried to acquire curvature and section profiles of the Gnalić shipwreck site in 2013, he encountered a problem in the form of heavy data; to extract curvature of the correct locations (at frame positions) unnecessary meshes have to be deleted to clear the desired area. This manipulation takes a lot of computing power, and desired rendered images were difficult to obtain because it is difficult to control the precise location and image scales of the camera in PhotoScan. After experiencing these difficulties, the author found a way to acquire section profiles of shipwreck sites without altering the original meshes of the photogrammetric models. This method is facilitated by Autodesk Maya's unique camera features. During the Gnalić Project 2013 and 2014 field seasons, the author experimentally applied this method to extract section profiles of selected exposed frames on the shipwreck site (Fig. 3-58 and 3-59). In the following section, the author discusses the methodology of section profile extraction that can be accomplished without disturbing the original photogrammetric models.

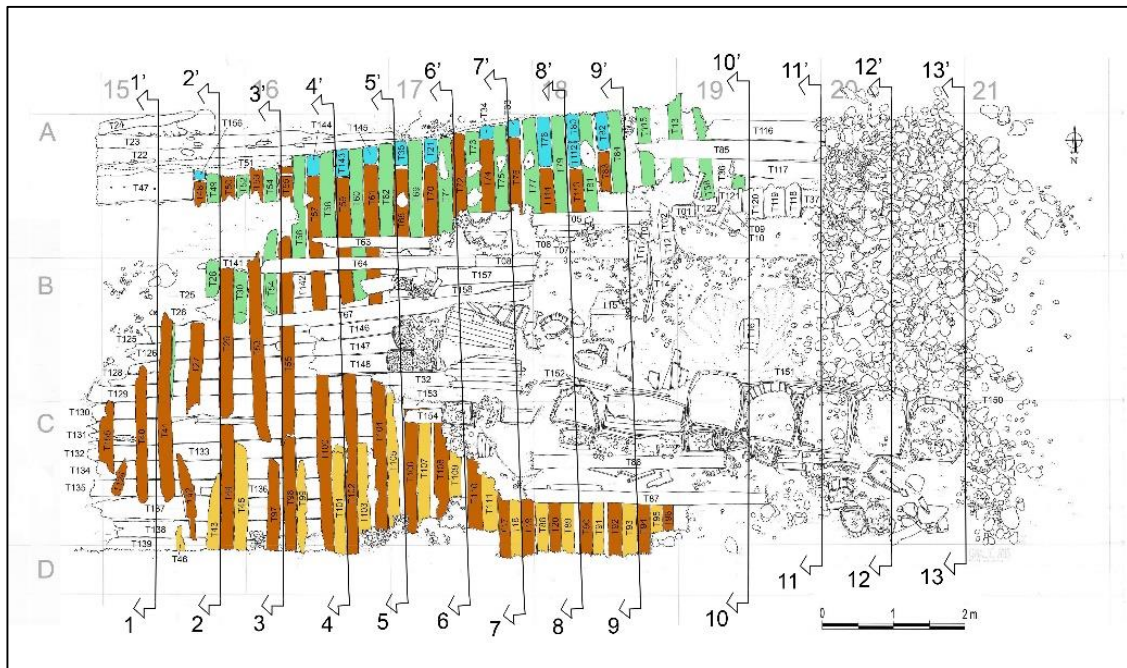


Figure 3-58. 2D site plan of the Gnalčić shipwreck from 2013 filed season with positions of the cross sections. (Image: Reprinted with permission from Castro, 2014b)

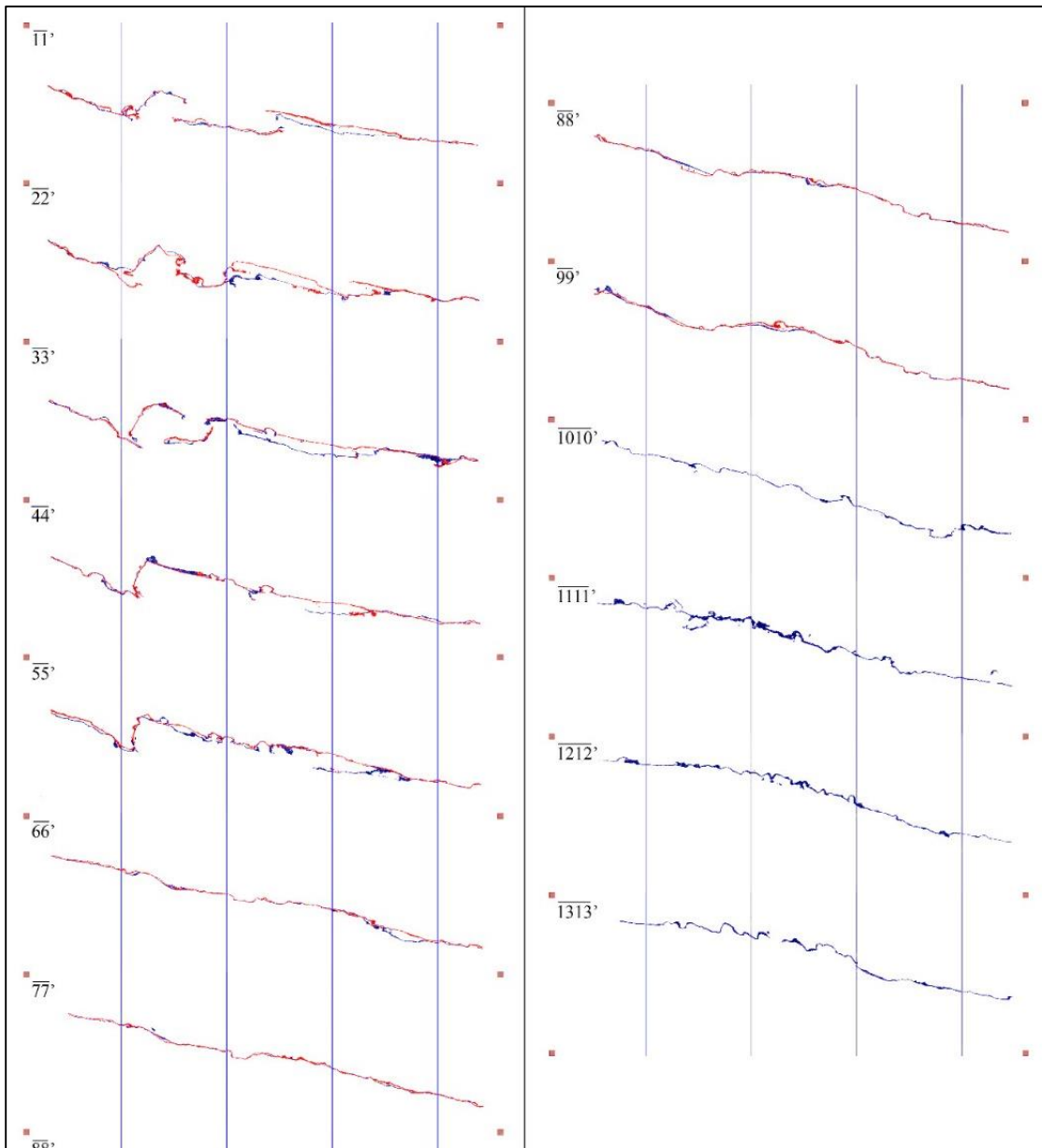


Figure 3-59. Transversal section profiles of the Gnalić shipwreck site from 2013 and 2014 combined photogrammetric models. (Image: Yamafune)

### *Exporting Photogrammetric Models to Autodesk Maya*

The key to this extraction methodology is the camera settings in Autodesk Maya (the author used the 2012 and 2015 versions of Maya for this section profile extraction).

To open photogrammetric models in Maya, it is important to export the file in the correct format. Three exports file formats that are available (April 2015) in PhotoScan that are compatible between PhotoScan and Maya: these are wavefront OBJ (.obj), COLLADA (.dae), and Autodesk FBX (.fbx) file formats. The author strongly recommends OBJ file format. There are several reasons for this recommendation. The first reason is that OBJ is the most commonly used 3D modeling file format, so that exported data can be used in most of the other 3D modeling softwares when needed. The second reason is that the COLLADA and FBX formats are occasionally not recognized correctly by Maya. For these reasons, the author always uses the OBJ format when exchanging files between PhotoScan and Maya. However, there are several important points that must be remembered during the data exchanges. The first is that, when the exporting log is opened in PhotoScan (File > Export Models), the exporting coordinate system must be matched with the one that is currently in use for georeferenced information (Reference pane > Settings tab > Coordinate System). For instance, when XYZ coordinates were input on markers on photogrammetric models using the WGS 84 world coordinate projection system, dialog in export models should be set to be WGS 84 coordinate projection system in order to give the models correct georeferenced information. The second point is that Maya doesn't work well with file names that have spaces between characters. For instance, sometimes Maya cannot correctly recognize files that have spaced names, such as 03 21 Barrel. To avoid this problem, the file name must be 03\_21\_Barrel or 0321Barrel. Thirdly, XYZ axis orientation in Maya is different from the coordinates in PhotoScan. Therefore, once a photogrammetric model is imported to

Maya, it must be rotated -90 degrees on the X-axis. Fourthly, the tone of the imported model may be too bright; therefore, the imported model's Ambient Light on Material Node in Attribute Editor must be corrected manually using Attribute Editor. Also, when photogrammetric models were exported as an OBJ files, PhotoScan also creates an .mtl file along with the OBJ file. This .mtl file designates paths between the exported model and its textures. In other words, without .mtl files, paths between meshes and corresponding UV maps for the texture will be broken; therefore exported OBJ files must always be stored together with corresponding .mtl files. Finally, after exported files are organized in Maya's pipeline directories (also called a projects window files), sometimes links between meshes and textures may be broken (especially when one uses PhotoScan and Maya in different computers). Accordingly, textures must be re-assigned manually using the Color Nodes option on the material tabs on Attribute Editor. By following these steps correctly, exported photogrammetric models will be ready to be used in Maya (Fig. 3-60).

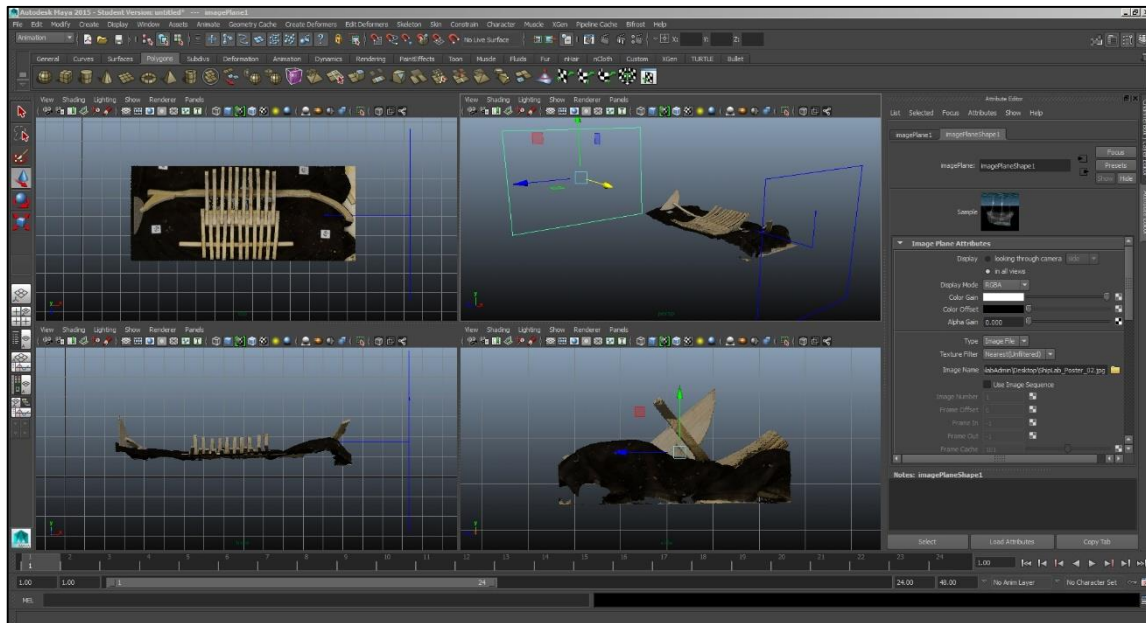


Figure 3-60. Imported *saveiro*'s photogrammetric model in Maya. The screenshot shows orthographic viewports (top, front, side, and perspective views), and Attribute Editor on the right. (Image: Yamafune)

### *Creating CT Scan Cameras in Maya*

The main advantage of using Maya for section profile extraction is that Maya software has the ability to convert its default view port cameras into customized view port cameras which functions similar to medical CT scanner (Computed Tomography scanner/Computerized Axial Tomography scanner) cameras in order to see thin-sliced cross sections of objects, like the human body, or in this case, a shipwreck. Though Maya is not intended to be used for this purpose, there is a way to customize Maya's default view port camera settings to make them into proper CT scan view port cameras. Technically speaking, the CT scan view port cameras are not created from a new camera, rather they are customized from the default side or the front view port cameras of the orthographic view windows. Although new cameras can be created inside Maya

(besides the default orthographic view port cameras), but these new cameras show views in perspective; this means that objects located close to the viewer are shown larger, and objects located far from the viewer are shown smaller (same as human eyes). Therefore, the best way to show objects in correct ratio and scale without optical distortion is to use default orthographic view port cameras that display sheer projections of top, front, and side views. These three default view port cameras show objects in correct scale whether or not an object is located near or far from the camera; in other words, these cameras don't have any optical distortion. Nonetheless, these default orthographical view port cameras are not visible and their position and rotation cannot be controlled. To make these cameras visible and to be able to manipulate them, the author uses Image Plane (View (on side or front view pane) > Image Plane). Once a view plane is created, the camera with an orthographical view becomes visible. However, the created view plane can be visually distracting; therefore, it must be hidden by increasing transparency using Alpha Gain on Image Plane Attribute (Select Image Plane >ImagePlaneShape tab on Attribute Editor > Alpha Gain on Image Plane Attributes).

Once the side or front view port cameras are visible, these cameras are ready to be customized to be CT scan view port cameras. Maya is a modeling software, and its viewport cameras have a function that hides objects from view port windows if the object is located outside of the designated distance of the view port camera settings. For instance, this function is used when a car is being modeled inside a town with many 3D models of buildings; while the car is being modeled, buildings and other objects behind the car should not be displayed in the view port because it makes the view port window



extremely busy. Therefore, visible distance from the camera can be controlled with the settings Near Clip Plane and Far Clip Plane (Select a desired camera > sideShape (or frontShape if you chose the front camera) on Attribute Editor > Near Clip Plane and Far Clip Plane). For instance, when the values of Near Clip Plane is customized as 0.001 and Far Clip Plane as 1.5 for the *saveiro*'s imported photogrammetric model, a camera only displays a mesh that is 1.5cm from the camera (Fig. 3-61). Also this camera's position and rotation can be changed to display desired areas. In short, the 3D model is sliced without disturbing any of the mesh properties. Since this camera has a function that is similar to medical CT scanners, the author calls it a CT scan camera. Also, rendered images of section profiles can be organized in Photoshop afterwards for reconstructions and publications; in order to make the organization and alignment of the captured images easier, the author recommends creating guiding objects around the photogrammetric model. For the *saveiro*'s photogrammetric model, the author placed six long cubic objects on the model that are 30cm apart horizontally and 20cm apart vertically (also see Fig 3-61).

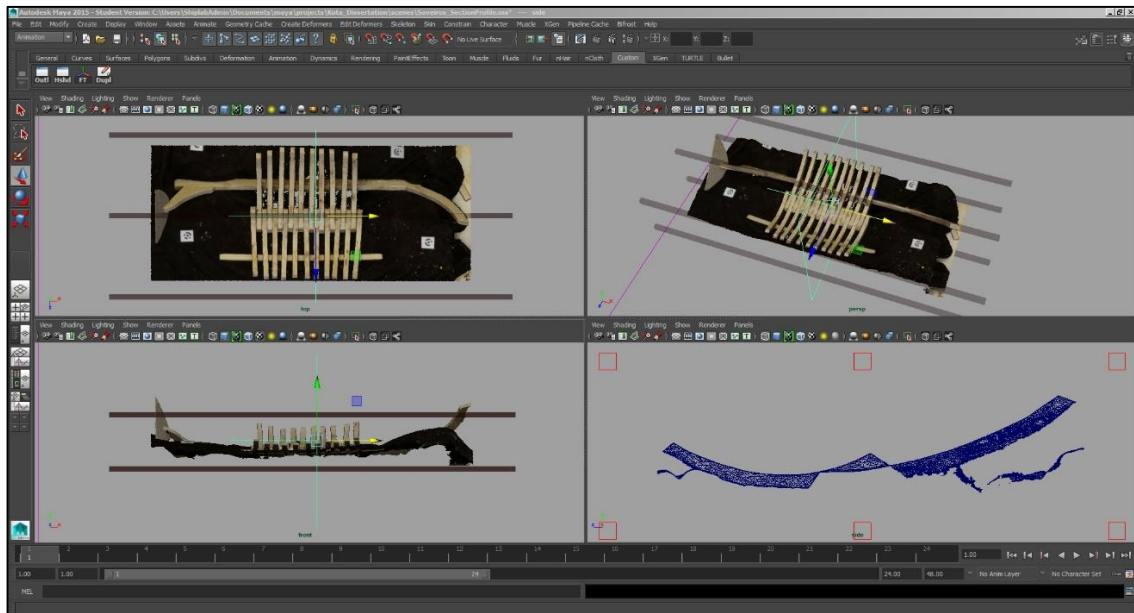


Figure 3-61. Extracting a section profile from the photogrammetric model of the *saveiro* wooden model in Maya. The side orthographic camera (bottom right viewport) has been customized as a CT scan-like camera. Also six guiding objects are created around the imported photogrammetric model. These cubes are positioned at calculated distances, which will help the captured images be correctly aligned and scaled afterword (Image: Yamafune).

A total of 12 section profiles were extracted from the *saveiro*'s photogrammetric models (Fig. 3-62 and 3-63). This time, section profiles between floors and futtocks were taken. However, any values of visible distance from the camera and precise locations of camera can be manipulated; therefore, on a large shipwreck site, the individual curvature of a timber can be taken using this method.

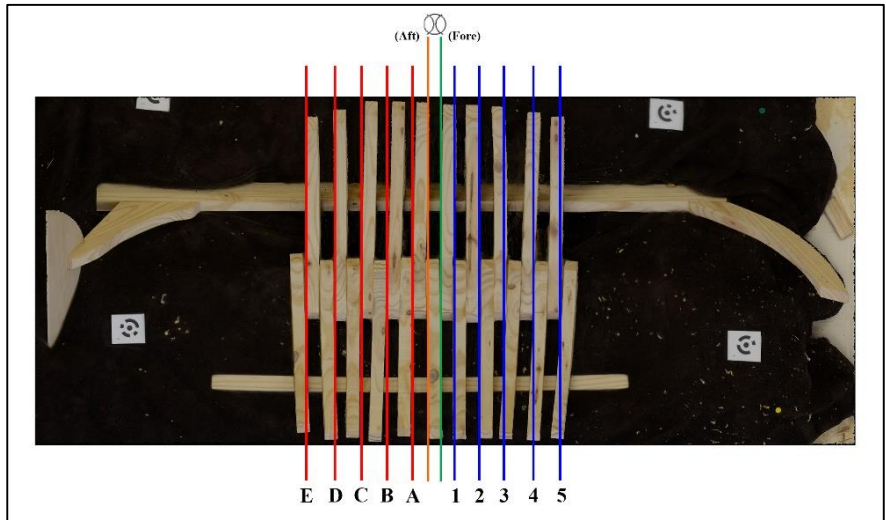


Figure 3-62. Approximate positions of extracted section profiles. (Image: Yamafune)

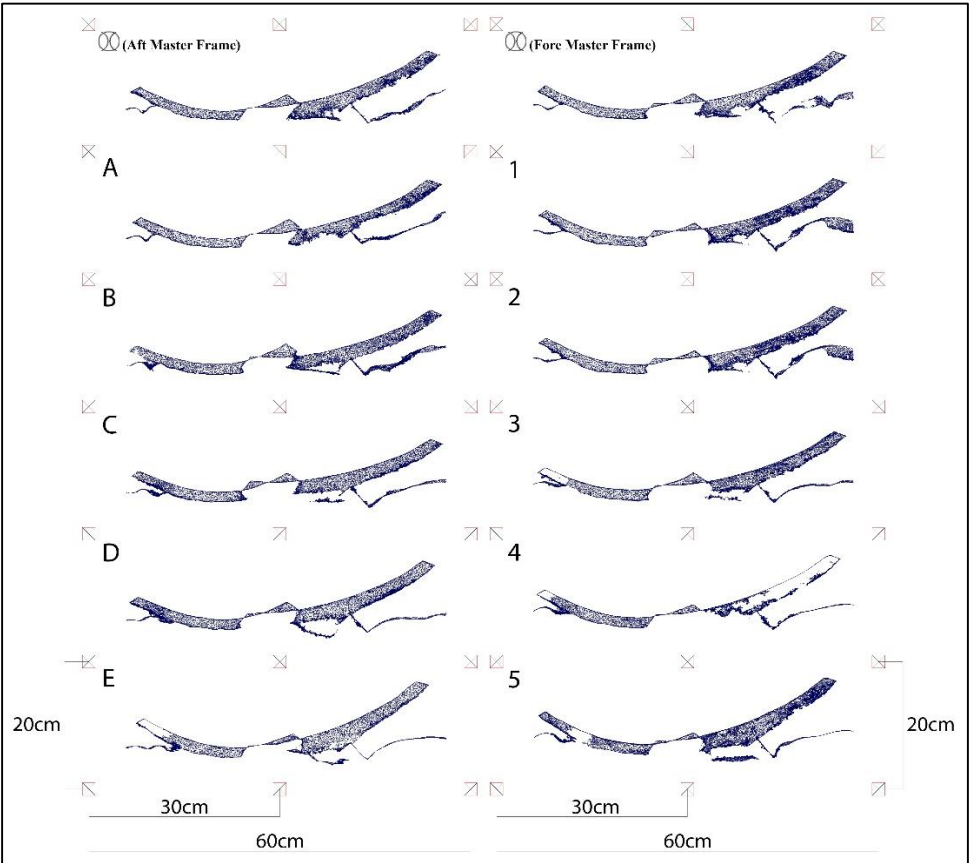


Figure 3-63. Section profiles of the *saveiro*'s photogrammetric model. The twelve captured section profiles are aligned in Photoshop. (Image: Yamafune)

### *Conclusion: Section Profiles*

The curvature of frames on a shipwreck site is one of the most valuable pieces of information that can be used to understand a sunken ship. However, to measure the curvature of frames under water requires good diving skills and extensive experience. The curvatures can be obtained easily once a frame is removed from the shipwreck site; however, removing frames from shipwreck sites is labor intensive and destructive in terms of conservation and preservation. Because of this, the author believes that the previously discussed extraction methodology is tremendously useful because once a real scale photogrammetric model is created and imported to Maya, section profiles of any position on the shipwreck site can be obtained quickly and accurately. Similar to the process of acquiring measurements using scale bars in PhotoScan, extraction of curvature can be accomplished without visiting the shipwreck site. The author believes that this curvature extraction methodology is valuable on any excavation or survey of shipwreck sites. Nevertheless, without proper analysis and usage of these extracted section profiles, this extraction methodology is useless. Accordingly, in the first part of Chapter IV, the author discusses reconstruction of the original ship's shape using section profiles extracted from the *saveiro* photogrammetric model.

## CHAPTER IV

### DATA ANALYSIS

#### **Data Analysis: Legacy of J. Richard Steffy**

After processing the archaeological data (including section profiles, 2D site plans, timber drawings, spatially organized archaeologist's sketches, pictures of the shipwreck site in GIS software, and 1:1 scaled photogrammetric models), archaeologists should begin analyzing the processed data. At this point, methodologies for analyzing and reconstructing shipwrecks are very similar to methodologies that nautical archaeologists have been applying to this discipline for decades. The guidelines for reconstructing hull lines and analyzing shipwrecks were first introduced to this discipline by J. Richard Steffy, one of the founders of nautical archaeology. The author studied the history of wooden shipbuilding in the J. Richard Steffy Ship Reconstruction Laboratory at Texas A&M University (ShipLab) and learned his reconstruction methods from Dr. Luis Filipe Viera de Castro, current director of the ShipLab. With this background, the author composed this proposed methodology using both the new technology to record shipwreck sites and the conventional methods for reconstructing shipwrecks that nautical archaeologists have used since 1960s.

#### **Hull Line Reconstruction**

Once section profiles have been extracted from a shipwreck site, the next step in understanding the shipwreck is to reconstruct the ship's hull lines. Hull lines represent

the tridimensional shape of a ship. They can indicate the capacity of the ship, as well as its sailing ability and stability (Fig. 4-1, 4-2, and 4-3).

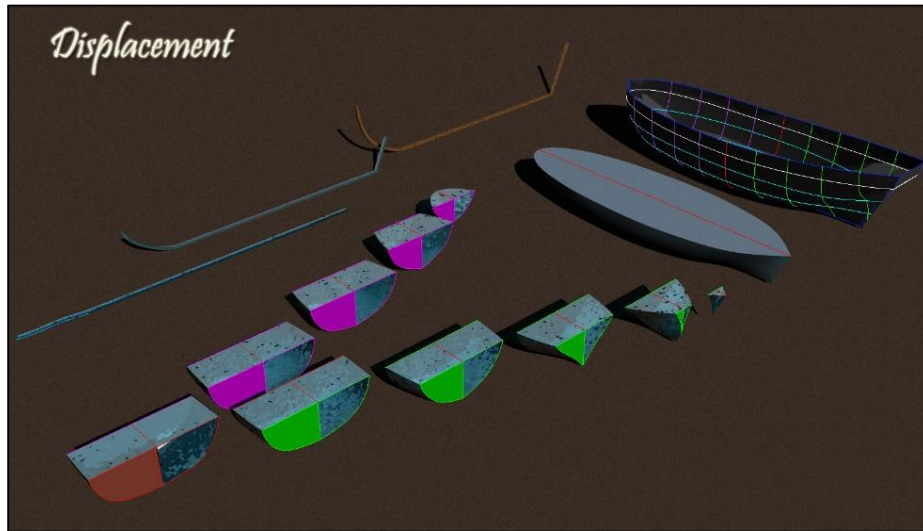


Figure 4-1. Illustration of water displacement calculation based on hull lines. Water displacement can reveal the capacity of a ship (Image: Yamafune)

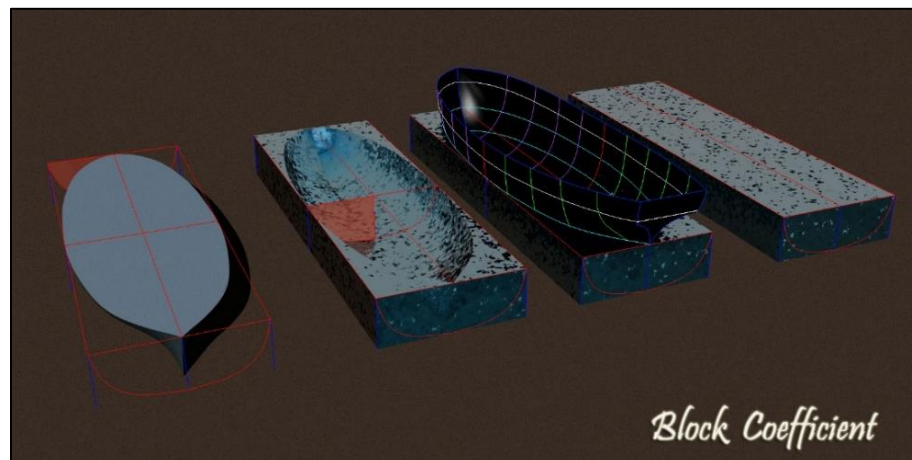


Figure 4-2. Illustration of the block coefficient. The block coefficient indicates the breadth of a ship. (Image: Yamafune)

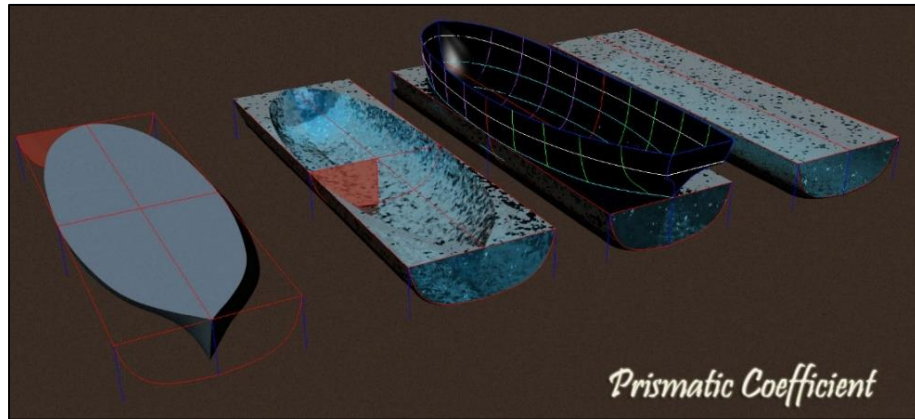


Figure 4-3. Illustration of the prismatic coefficient. The prismatic coefficient can provide a rough estimate of a ship's speed. (Image: Yamafune)

Consequently, when hull lines are reconstructed, archaeologists can understand not only the original shape of the hull, but other characteristics of the ship as well (Steffy, 1994: 253-255). The author learned the methods of ship reconstruction during his graduate studies and also from experience gained while creating the reconstruction of the *Cais do Sodrés* hull lines (Castro, Yamafune, Eginton, and Derryberry, 2011) (Fig. 4-4).

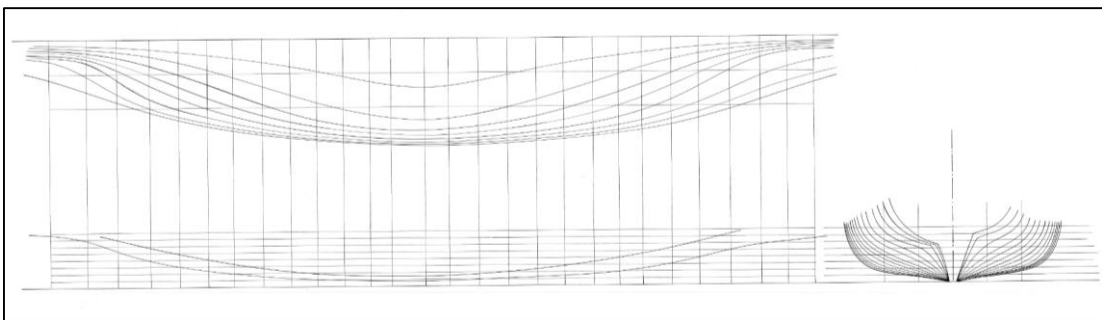


Figure 4-4. Reconstruction of the hull lines of the *Cais do Sodré* shipwreck. The lines were reconstructed based on timber drawings and total station data. The drawing was done by hand in the summer of 2010. (Image: Yamafune)

This method for reconstructing hull lines is similar to what Steffy described in his paper about the reconstruction of the Serçe Limanı shipwreck. Steffy reconstructed the Serçe Limanı shipwreck first using a 1:10 scaled reconstructed diorama of the shipwreck site and its timbers. He reconstructed these fragmented timber models based on tangency of frame curves, shapes of frame joineries, positions of fasteners, tool marks, and so on (Steffy, 1982). To utilize Steffy's hull reconstruction methodology combined with his own methodology for recovering data, the author used extracted section profiles (see Chapter III) for the reconstruction of hull lines.

For the reconstruction of hull lines, the author used section profiles that were produced from the photogrammetric model of the *saveiro* wooden ship model. To recompose the curvatures of the frames, Rhinoceros 3D CAD drawing/modeling software was used. The author often prefers to use CAD drawing/modeling software over hand drawing because its various drawing tools and object snapping modes allow quick and precise drawings. More importantly, the computer-based drawings can be easily converted to 3D surface models and exported to other modeling and analysis software to obtain mathematical data. To begin, the image of section profiles that was extracted from the 1:1 scaled photogrammetric model was imported to Rhinoceros. Then, section profiles were traced and re-oriented based on tangency of curvatures of the floor timber and futtocks (Fig. 4-5). Tracing and re-orienting was applied to all the section profiles in order to reconstruct a body plan of the *saveiro* wooden ship model (Fig. 4-6). After all of the sections lines were reconstructed, these sections can be plotted into the correct locations (Fig. 4-7).



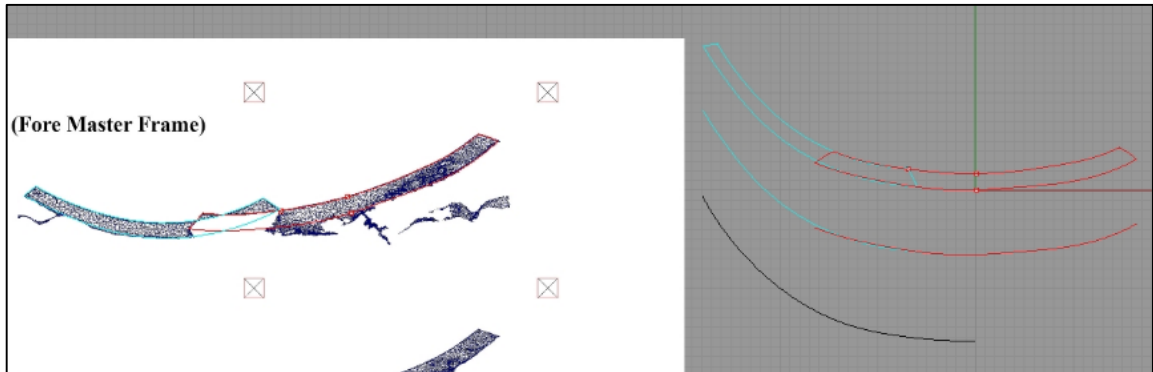


Figure 4-5. The process of reconstructing section lines based on the *saveiro* photogrammetric model. (Image: Yamafune)

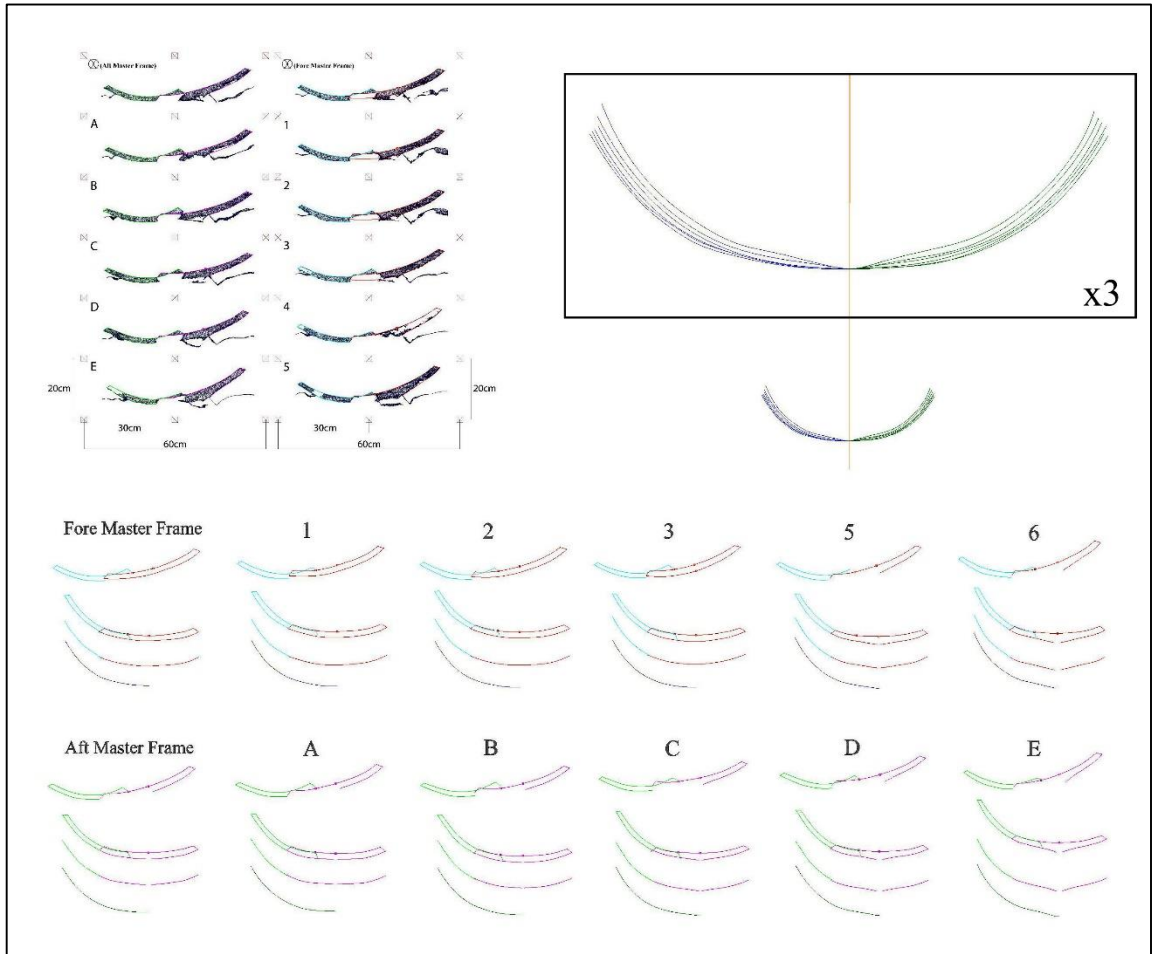


Figure 4-6. The reconstructed twelve master frames of the *saveiro* wooden ship model based on the photogrammetric model and archaeological data. (Image: Yamafune)

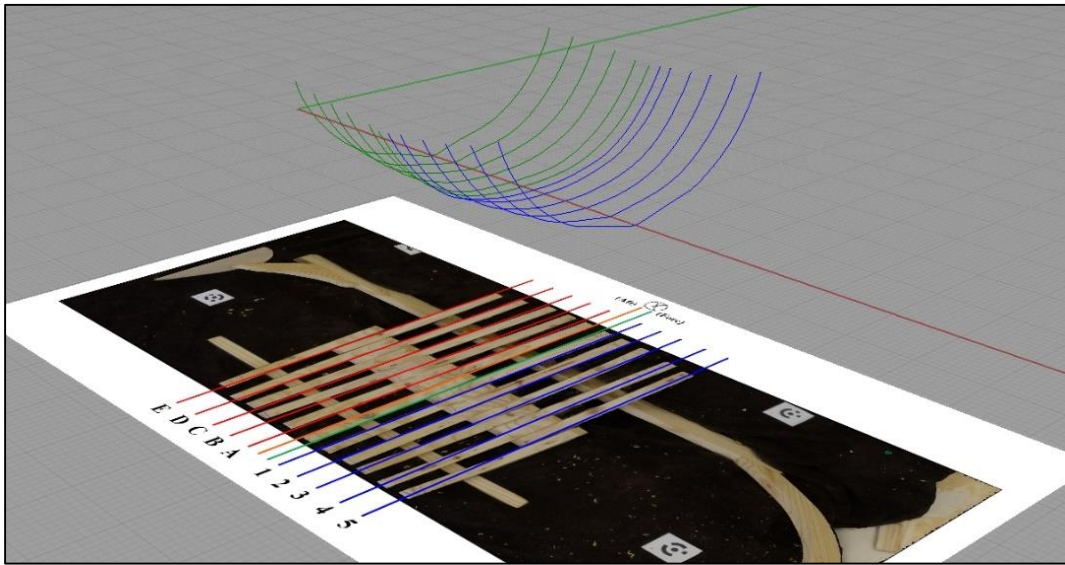


Figure 4-7. Plotted section lines of the *saveiro* wooden ship model. Reconstructed section lines are placed based on frame positions. (Image: Yamafune)

In actual archaeological projects, the hull lines reconstruction is not complete until all water lines and section lines are perfectly fair. More importantly, these hull lines reconstructions are largely dependent on the positions of fasteners and joineries. In addition, the position of curves relies upon construction marks and other ship structure components, such as stringers, keelson, beams, knees, and so on. All of this information gives more precise pictures of the ship, including the hull lines. This is the reason that the author has repeatedly remarked in this dissertation that underwater sketches and any other information must be collected manually by archaeologists along with producing photogrammetric data, and all data must be stored in a georeferenced database, such as a GIS-based mapping software. Reconstruction of hull lines must be based on collective information. Yet, the author emphasizes the advantages of the methodology of using section profiles of photogrammetric models to reconstruct hull lines because

archaeologists can produce hull lines even without removing and conserving the frames.

### *Mold-and-Batten Model Fairing*

The final step that must be applied to this reconstruction procedure before finalizing the reconstruction of the section hull lines is the Mold-and-Batten Model Fairing. The Mold-and-Batten model was originally suggested by Steffy as an initial analysis process of ship reconstruction (1994: 221-224). This method uses molds and battens to analyze fairness of the reconstructed structure (Fig. 4-8). This system is similar to how diagonal lines are used to check fairness when drafting 2D hull lines drawings.

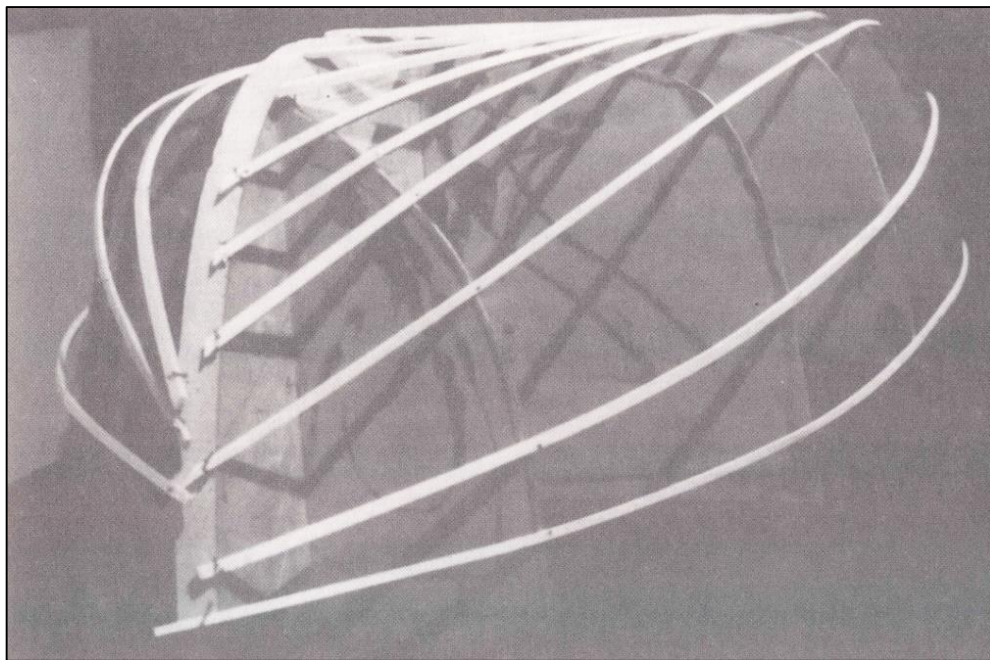


*Figure 4-8. Mold-and-Batten Model reconstruction by J. R. Steffy. (1994: 222)*

The author applied this process on the reconstructed section lines using Rhinoceros 3D CAD drawing/modeling software. Rhino is recommended on Mold-and-Batten Model Fairing because it uses NURBS spline curves. Several diagonal lines that pass section lines were added in order to check its fairness. When the diagonal lines are not fair, reconstructed section lines, or angles of floor timbers and futtocks, should be adjusted using each curve's editing points until the diagonal lines shows fair lines (Fig. 4-9). This Mold-and-Batten Model Fairing converts reconstructed section lines into section profiles of watercraft; therefore, this step should be applied during the course of ship reconstruction.

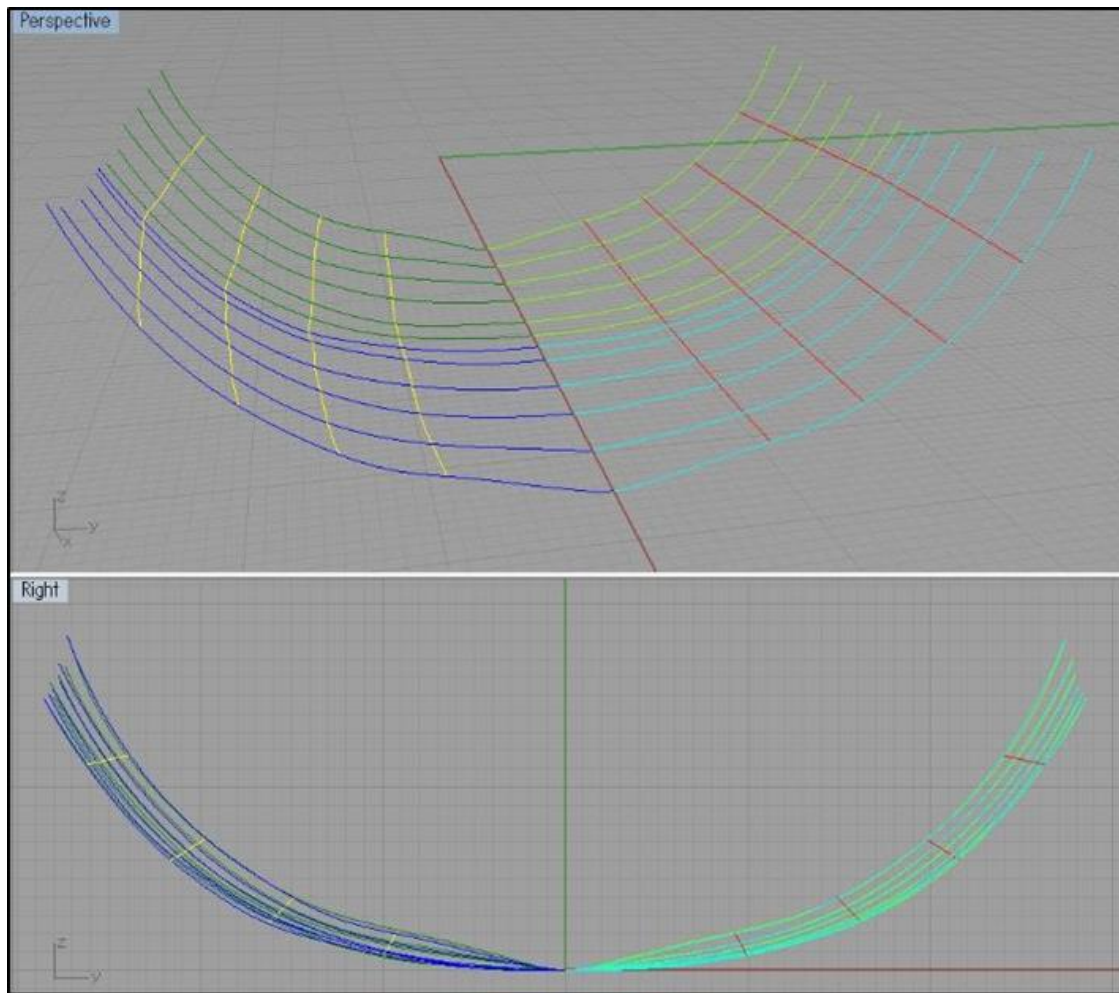


Figure 4-9. Mold-and-Batten Model Fairing in Rhinoceros 3D CAD software. Dark blue and green lines on the left are reconstructed section lines before the adjustment; light green and blue lines on the right are adjusted section lines. Yellow lines are diagonal lines, or simulated battens, before adjustment, and red lines are adjusted diagonal lines. (Image: Yamafune)

#### *Testing Author's Hull Line Reconstruction*

The author chose the *saveiro* wooden ship model for this dissertation's hull line reconstruction because the reconstructed hull lines can be tested. The *saveiro* is a traditional boat type that is still being used today in Bahia, Brazil. The design the *saveiro* was inherited from a type of ship that was used by the Portuguese during the Age of

European Expansion during the 16th and 17th centuries (Sarsfield, 1984; Sarsfield 1985a; Sarsfield, 1985b; Sarsfield, 1991; Castro and Gomes-Dias, 2015). In the 16th and 17th centuries, Portuguese and Spanish shipwrights designed their ships based on simple geometry and ratios of main components of the ship. For instance, the dimensions of many important components of the ship were based on a ratio related to the keel length and breadth at the midship frame (maximum breadth) (Oliveira, 1995; Sarsfield, 1984; Sarsfield, 1985a; Castro 2005a, Castro 2007; Castro, 2008; Castro and Gomes-Dias, 2015). Dr. Castro, the current director of the J. Richard Steffy Ship Reconstruction Laboratory (ShipLab), is very interested in the *saveiro*'s design, and he has acquired original shapes of half molds from his visits to *saveiro* shipwrights in Bahia (Fig. 4-10). Dr. Castro also received several *graminho* from the shipwrights. A *graminho* is a piece of timber that is used for determining the rising and narrowing of pre-designed master frames. The virtue of the Iberian design of ships during the Age of European Expansion and the design of *saveiro* boats today is that the shapes of predesigned master frames were determined by simple geometry that is controlled by three simple timbers: a mold for the floors, a mold for the futtocks, and a *graminho* for the narrowing and rising (Sarsfield, 1984; Sarsfield 1985a; Sarsfield, 1985b; Sarsfield, 1991; Castro and Gomes-Dias, 2015).

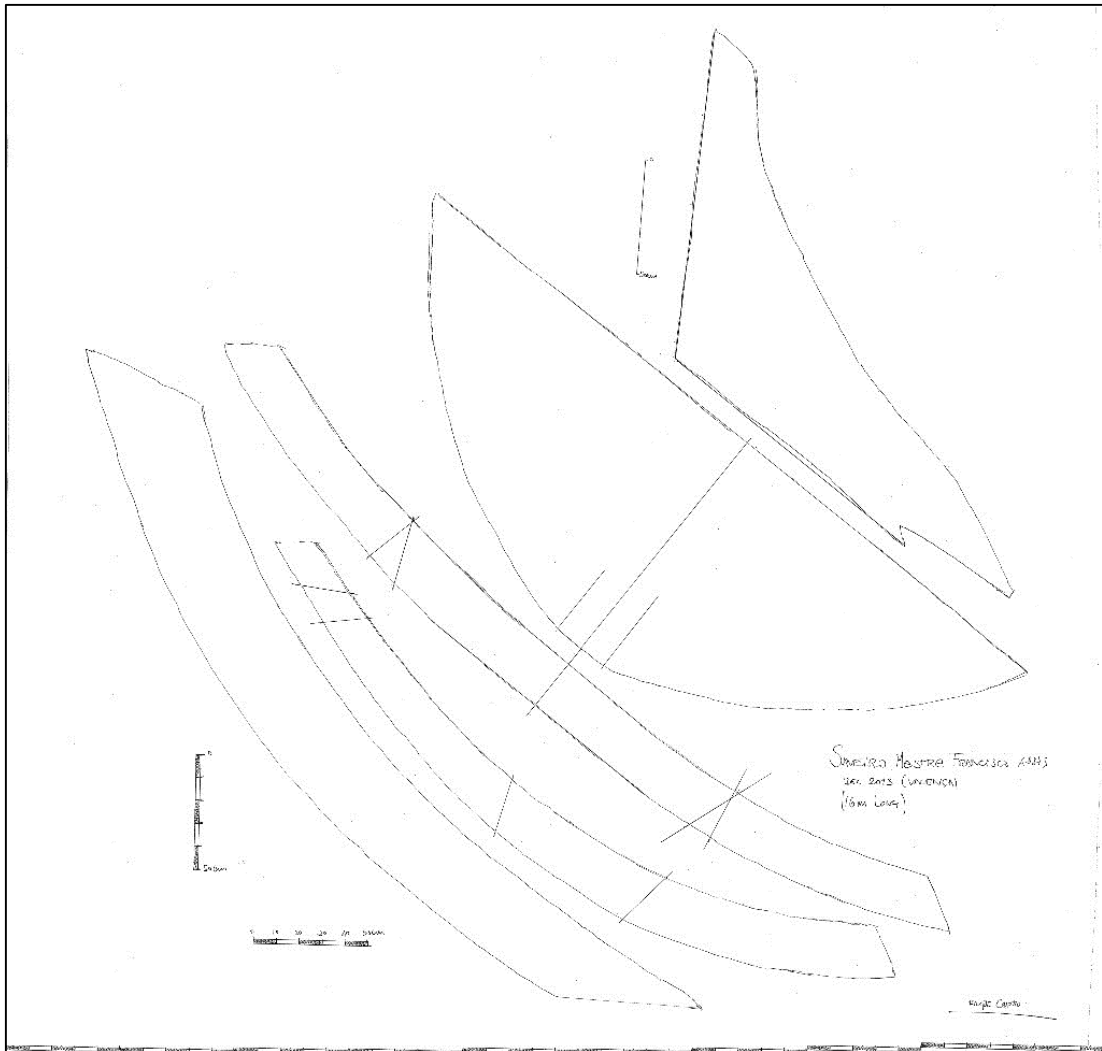


Figure 4-10. A traced and scaled sketch of a *saveiro*'s molds by Dr. Castro. These molds are used for stern knees, transoms, floors, futtocks, and stems (described from the top). (Image: Reprinted with permission from Castro, 2015)

The author also studied these designs and methods in the ShipLab. Using half molds and a *graminho* that was used for the *saveiro* wooden model, the author was able to determine the originally intended complete shape of the master frames. This completed original design of the *saveiro* wooden model was compared to the reconstructed shape that was based on the photogrammetric model (Fig 4-11).

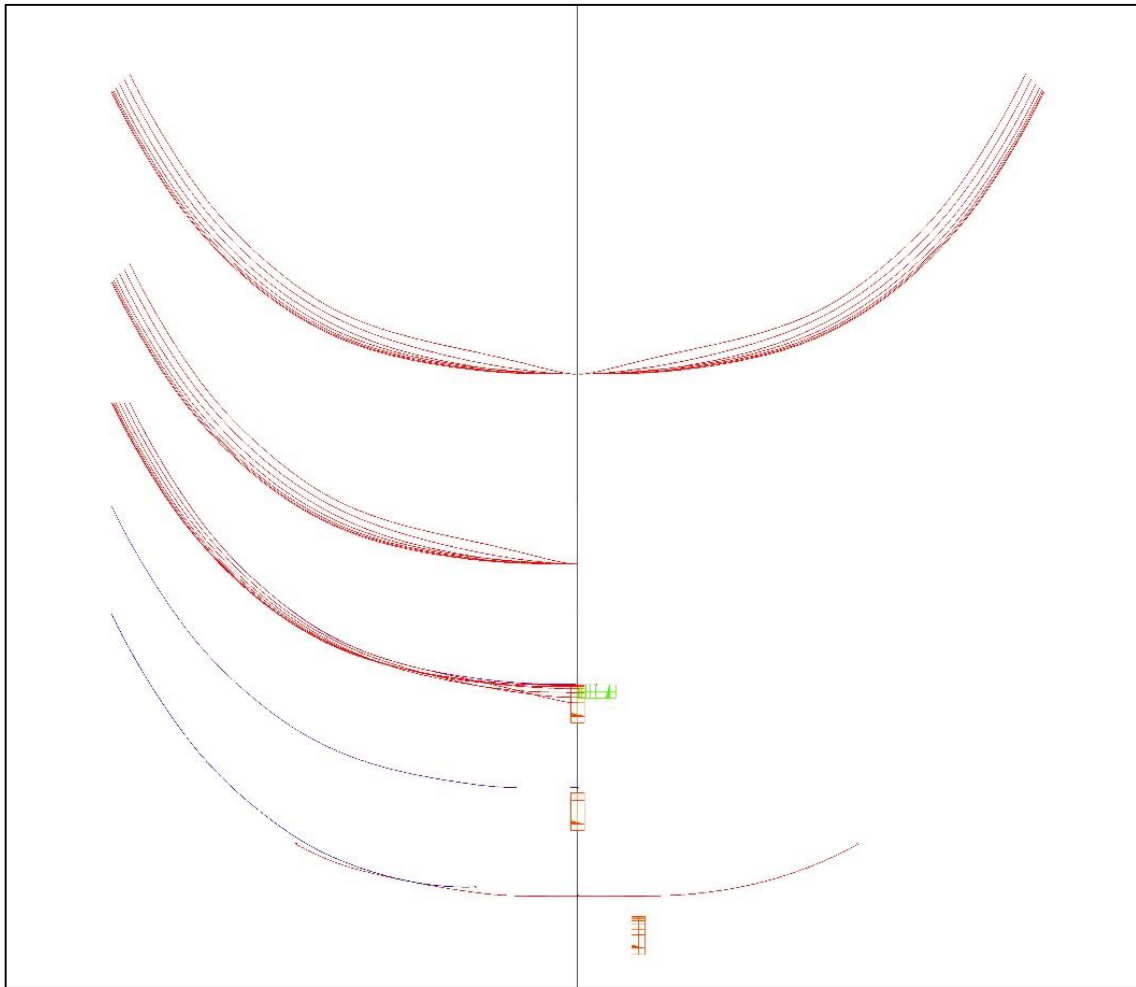


Figure 4-11. The process of designing pre-made master frames of the *saveiro* wooden ship model. Designs were done using three pieces of wood: a mold of the floors, a mold of the futtocks, and a *graminho* to determine the rising and narrowing of the frames. (Image: Yamafune)

After the design of the master frames of the *saveiro* wooden ship model was completed, the author compared them with the reconstructed hull lines of the *saveiro* wooden ship model that was created based on section profiles extracted from the photogrammetric model. Figure 4-12 displays the original design in red and the reconstructed hull lines in blue (Fig. 4-12). The author believes that the reconstruction of the hull lines based on photogrammetric data is successful; the blue lines were drawn



exclusively based on photogrammetric data, or archaeological information, yet the basic dimension of the two lines are very close, especially the curvatures of the floor timbers.

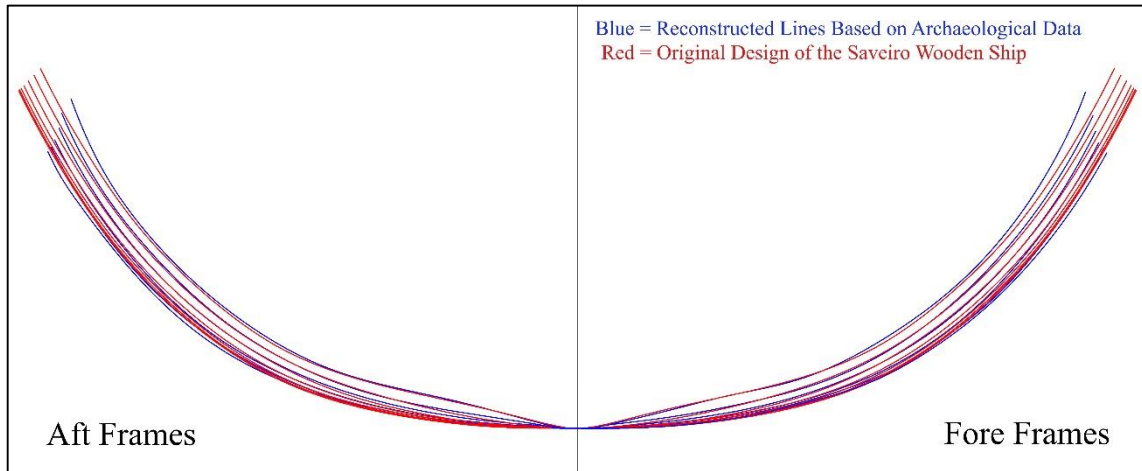


Figure 4-12. Comparison of the reconstructed hull lines based on photogrammetric data and the original design of *saveiro* wooden ship model. The blue lines show the section lines of the reconstructed hull lines of the wooden model, and the red lines show the original design of the wooden model based on its molds and *graminho*. (Image: Yamafune)

Nonetheless, this experiment suggests something very important. The comparison indicates that the greatest misfit between the two sets of lines appears at the extremities of the futtocks. This is because of the fact that when the author was setting up the simulated archaeological site of the *saveiro* wooden ship model for Computer Vision Photogrammetry, the author placed the futtocks on the ground randomly based on relative distance from the edges of the connecting floor timbers. Therefore, while reconstructing hull lines based on extracted section profiles, the correct positioning of the curvatures of futtocks relating to locations of floor timbers was difficult. Aside from

the simulated archaeological site of the *saveiro* wooden ship model that the author used for the hull lines reconstruction, actual archaeological shipwreck sites contain joineries and fasteners in the frame timbers. This information is tremendously important for the reconstruction of hull lines. Computer Vision Photogrammetry is able to capture detailed textures and accurate dimensions of shipwreck sites, yet these are still not as accurate as trained archaeologist's eyes. This information must be collected by archaeologists on the shipwreck site or recorded with timber drawings so that it can be used for hull line reconstruction or data analysis. This experiment confirmed the importance of traditional recording methods. Again, the author must note that new technologies, including Computer Vision Photogrammetry and other software, can improve archaeologist's studies and research, but its effective use relies upon complementary use of traditional methods employed by archaeologists.

### **Archival Research and Shipwreck Analysis**

As a result of the data acquisition processes previously discussed, the author believes that nautical archaeologists should have enough processed data to begin analyzing the context of the shipwreck site. However, nautical archaeologists cannot fully understand a shipwreck without understanding the historical background, the period of shipbuilding, and findings from other contemporary shipwrecks. Archaeology is the discipline of uncovering the human past using material culture. History is the discipline that analyzes the human past based on written accounts. Of course both disciplines often interact with each other; however, the author believes that nautical

archaeology benefits greatly when scholars can utilize both material culture and written record (where available). In this dissertation, the author has discussed only methodologies applied to archaeological excavations. However, it must be noted that archival research both before and after a field season is immensely helpful to understanding the archaeological record.

For nautical archaeology, archival research can vary. Important types of archival research include the identification of shipwrecks and their cargo, finding shipwrights' treatises and iconography of similar ship types, and studying the construction of other contemporary shipwrecks. Historical information and archaeological data acquired in the field can be used to help analyze hull structures and shipwreck sites.

### **Hull Analysis**

Hull analysis is used to understand ship construction and shipbuilding methods. Prior to the invention of aircraft, boats and ships were the only way people could cross water without having to swim. Watercraft remains provide us a window on thousands of years of human seafaring activity and all that it encompasses: technological developments, trade, warfare, and other types of cultural interactions.

There are a variety of methodologies used to analyze shipwreck sites for information about shipbuilding. How an archaeologist reconstructs a ship is largely based on acquired data, and how the ship is interpreted also depends on the ship's known purpose and its time period. Beyond this point, it is impossible to generalize study methods for hull analysis. However, as an example of a way to analyze shipbuilding

techniques based upon data provided by shipwrecks, the author proposes the Interactive Fragment Model method in the following section.

### *Interactive Fragment Model*

When J. Richard Steffy studied the Serçe Limanı shipwreck, an 11th-century A.D. Mediterranean vessel, he carefully recorded fragmented timbers and their locations. First, he created a 1:10 scale diorama of the shipwreck site, and then he moved the fragmented pieces back into their hypothetical original position (Steffy, 1982). Steffy called this the Fragment Model. Then, based on the positions of tool marks and timber fasteners, he revealed his theory about the construction method used to build the Serçe Limanı ship. This was critical information that helped all nautical archaeologists understand the transition of shipbuilding from shell first construction to frame first construction. The author has studied Steffy's method and modified it into the Interactive Fragment Model.

The Interactive Fragment Model is identical to the Fragment Model method in that it attempts to bring the shipwreck structures back to their original position. Based on the positions of structures, including fasteners and joinery, nautical archaeologists can understand the patterns of shipbuilding. The difference between the Interactive Fragment Model and the Fragment Model is that the author uses a 1:1 scale photogrammetric model instead of a 1:10 scale diorama model. In addition, the author uses Deformation (a method of manipulating the shape and geometry of the model without disturbing its original entity) to reconstruct the photogrammetric models using Maya instead of

manual reconstruction of a wooden models. Consequently, the Interactive Fragment Model is a much faster and more reversible method than the Fragment Model method.

The author conducted experiments to determine how the Interactive Fragment Model can be used to learn more about a shipwreck site. For this purpose, the author required a 3D reconstructed model of a ship (created from hull lines) and a photogrammetric model. Due to circumstance and available information, and because an archaeologist often doesn't have an intact version of the ship that is being excavated, the author used a different ship for the 3D reconstructed model (the Pepper Wreck) and the photogrammetric model (the Gnalić shipwreck). For the purpose of exploring the usage of the Interactive Fragment Model, the author created a reconstructed model of the Pepper Wreck using the ship's hull lines. The Pepper Wreck was an early 17th century Portuguese East Indiaman *Nossa Senhora dos Martires*. Based on historical documentation, the ship was 30 m long at the keel with an overall length of 40 m. Dr. Castro studied and reconstructed this shipwreck based on historical documents and archaeological data. (Castro, 2003; Castro, 2005a; Castro, 2005b; Castro 2007). The author reconstructed the Pepper Wreck tridimensionally using Autodesk Maya and information based on Dr. Castro's research (Fig. 4-13 and 4-14).

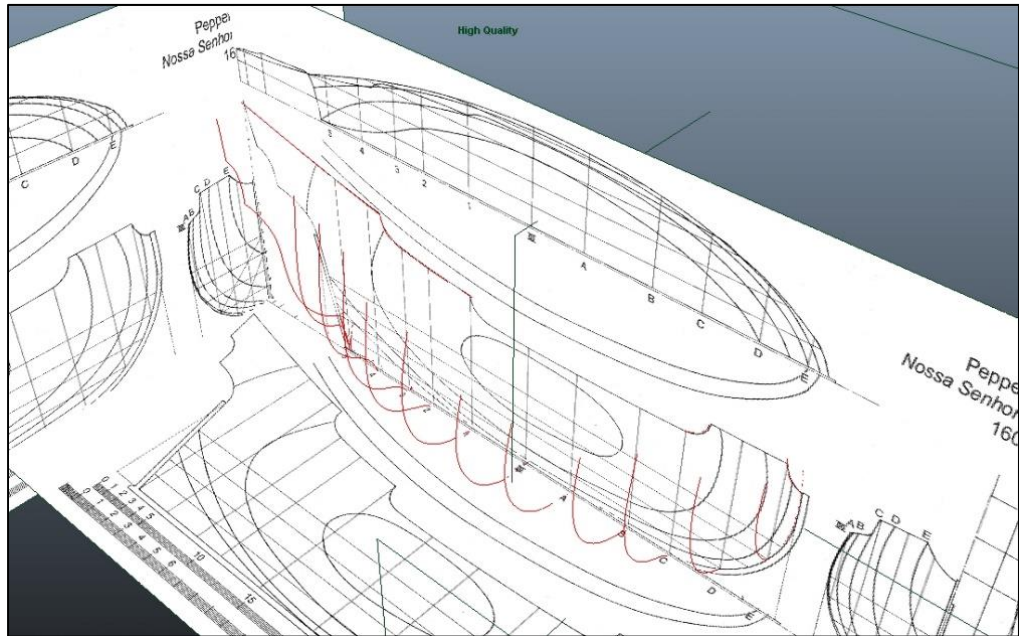


Figure 4-13. An image of the hull of the Pepper Wreck being reconstructed in Maya based on Dr. Castro's lines drawing. (Image: Yamafune)



Figure 4-14. A 3D reconstruction of the Pepper Wreck based on historical and archaeological data. (Image: Yamafune)

Based on archival research conducted by Mauro Bondioli, the Gnalić Shipwreck was a Venetian merchant ship named *Gagliana grossa* with a 30 m length at the keel and 40 m length overall. The ship sank off the coast of Croatia in 1583, about two decades earlier than the Pepper Wreck (Radić Rossi *et al.*, 2013). Despite the fact that the ship was constructed in a different region using different ship building methods, both ships were of similar size and usage (they were round-bottomed cargo-carrying merchant ships), and operated in the same era. For these reasons, the author decided to combine the 3D reconstructed model of the Pepper Wreck with the photogrammetric model of the Gnalić shipwreck site to explore how the Interactive Fragment Model can be used to reveal more information about the Gnalić shipwreck site. The relatively comparable Pepper Wreck is being used to shed light on the Gnalić shipwreck.

The Interactive Fragment Model requires modeling and animation software. The author used Maya. The key factor of this method is a computer function called Deformation, a digital method of manipulating a 3D model. When a 3D model needs to be animated, animators put digital skeletons inside created models and bind meshes of the 3D models to skeletons as skin. Therefore, the 3D models can be animated based on the position of the skeleton (Fig. 4-15).

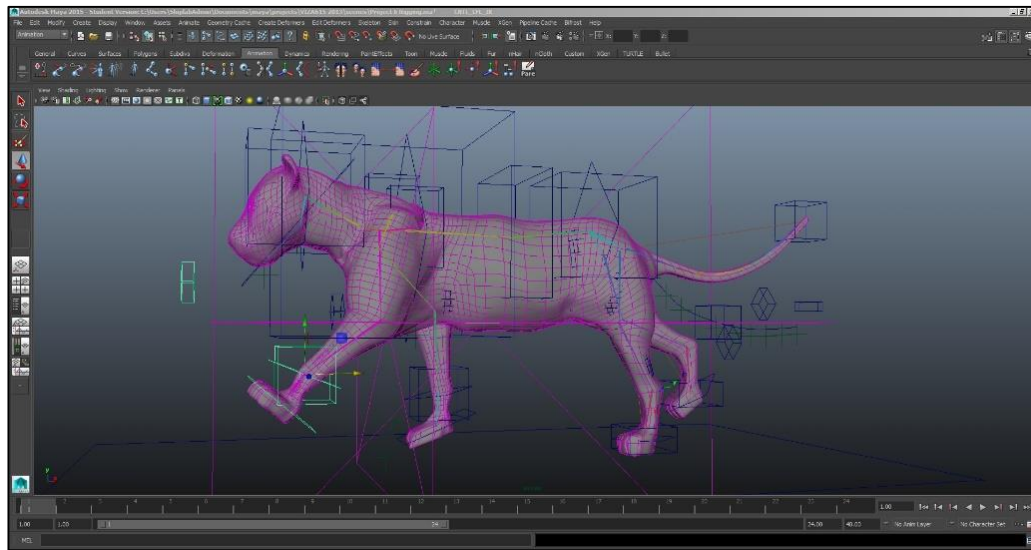
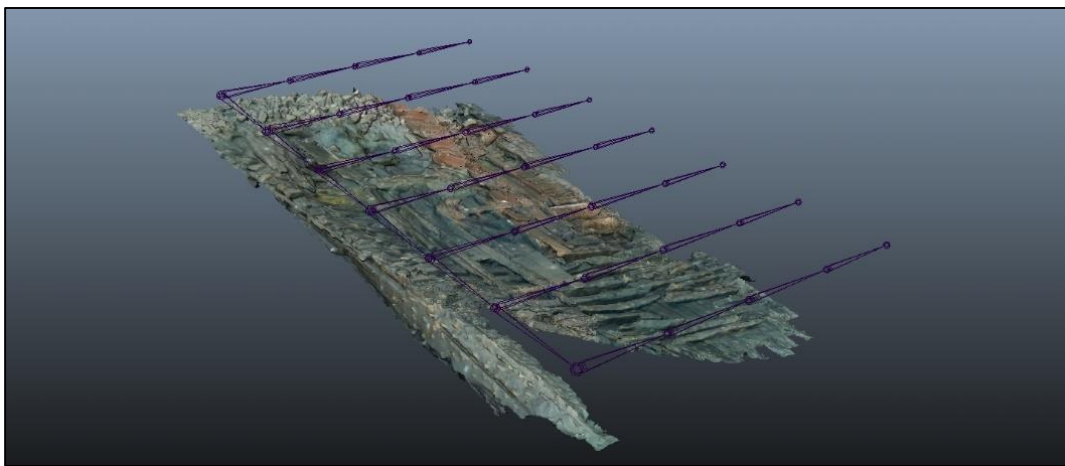


Figure 4-15. Illustration of 3D model Deformation. A rigid 3D model can change its form based on assigned skeletons and rigs. (Image: Yamafune)

When the skeleton moves, the vertices of the meshes follow their assigned skeleton. This alters the shape of the meshes, which is why the process is called Deformation. For the Interactive Fragment Model, the author prepared a simple skeleton for the shipwreck site. Most archaeological shipwreck sites are severely flattened. They must be brought back to their original shapes to enhance their diagnostic components in order to understand the shipbuilding techniques used to build the original vessel. The author used deformation to bring shipwreck sites back into their hypothetical original shape. Once these skeletons were placed in the photogrammetric model, their meshes are bound to the skeleton (Fig. 4-16). As a result, the shipwreck site is now able to change its shape based on the position and rotation of the skeleton (Fig. 4-17). Then, the author imported a 3D model of the Pepper Wreck and juxtaposed it against the Gnalić wreck so that the Gnalić wreck was in its hypothetical position in the ship's hull (Fig. 4-18). Most



likely, when a 1:1 scale photogrammetric model of a shipwreck site is placed on a hypothetically reconstructed ship model, it will not fit perfectly because the ship structures have been flattened (particularly when two different ships are being used, though the process still reveals valuable information as long as the ships are similar enough) (Fig. 4-19). Therefore, the author deformed the photogrammetric model of the Gnalić shipwreck structure until it fit with the reconstructed ship model (Fig. 4-20). Once a photogrammetric model is brought back to roughly the original shape of the ship, many components of the shipwreck site become more diagnostic. For instance, the storage pattern of the barrels on the Gnalić shipwreck became clear after the Interactive Fragment Model was applied, even though it was an experiment using different ships' data (Fig. 4-21).



*Figure 4-16.* Photogrammetric model of the Gnalić shipwreck structures in situ overlaid with the Skeleton tool in Maya. (Image: Yamafune)

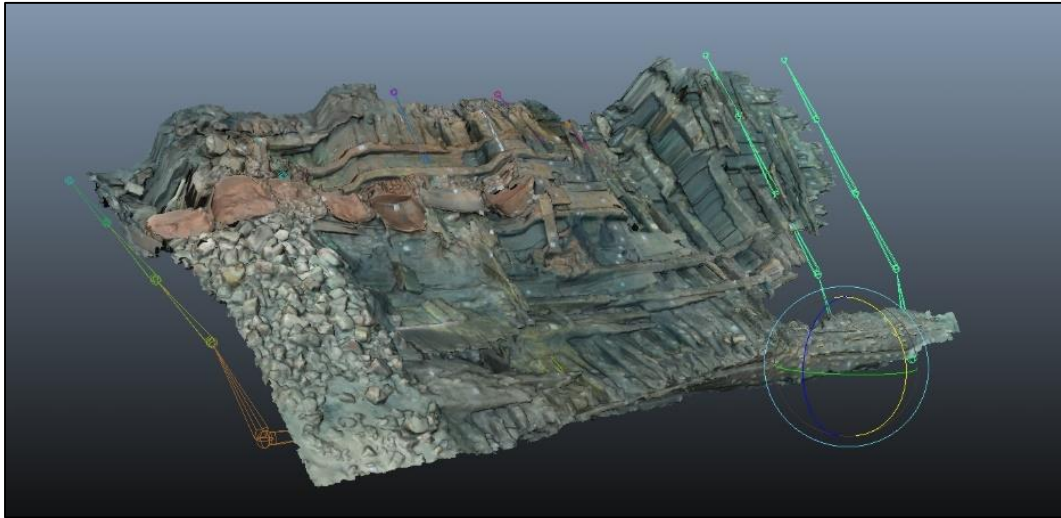


*Figure 4-17.* Deformation of the Gnalčić shipwreck site in Maya. Meshes of 3D models change their shape based on the shape of the skeleton. (Image: Yamafune)

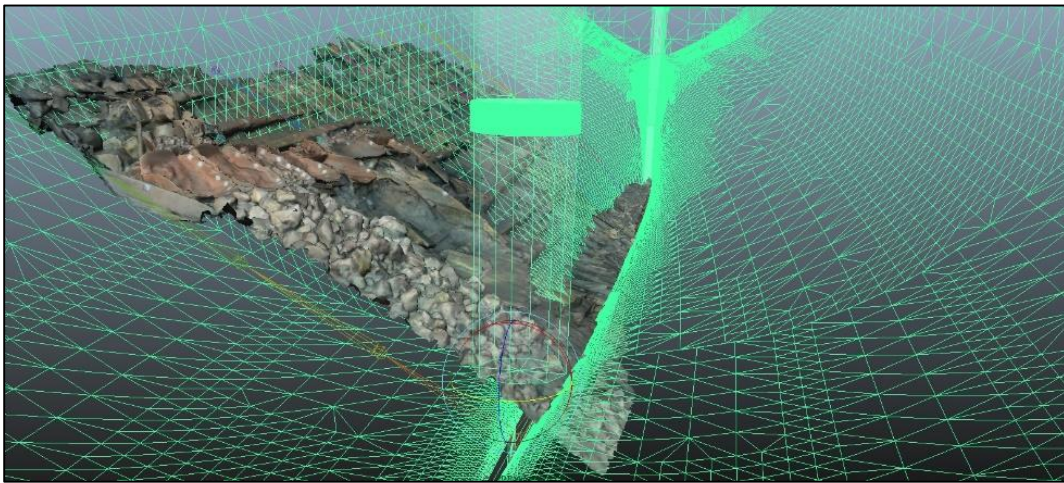


*Figure 4-18.* Photogrammetric model of the Gnalčić shipwreck site and reconstructed 3D ship model in position. (Image: Yamafune)

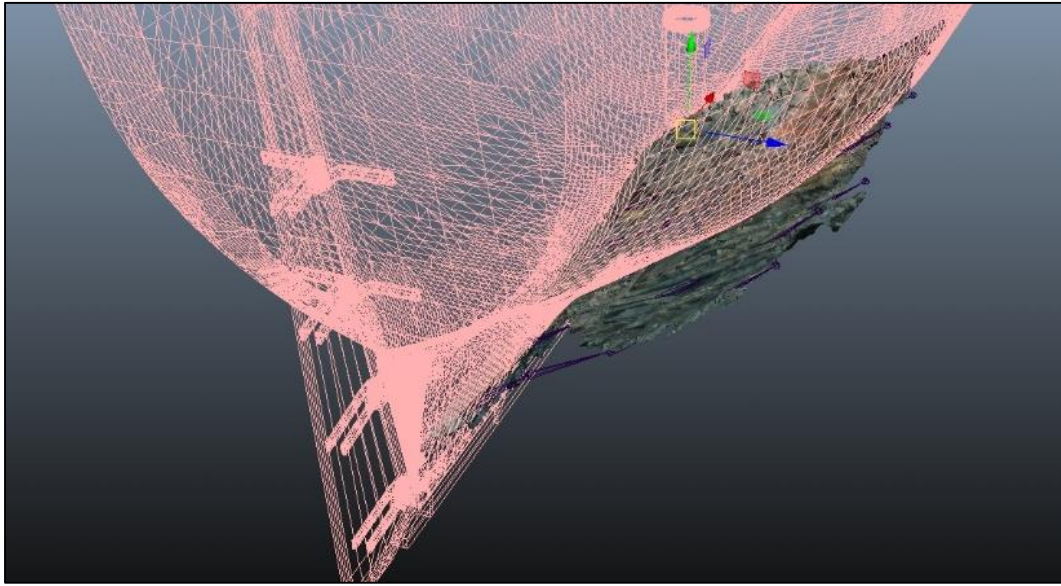


*Figure 4-19.* Flattened Gnalić shipwreck site juxtaposed with hypothetical reconstructed ship model. (Image: Yamafune)

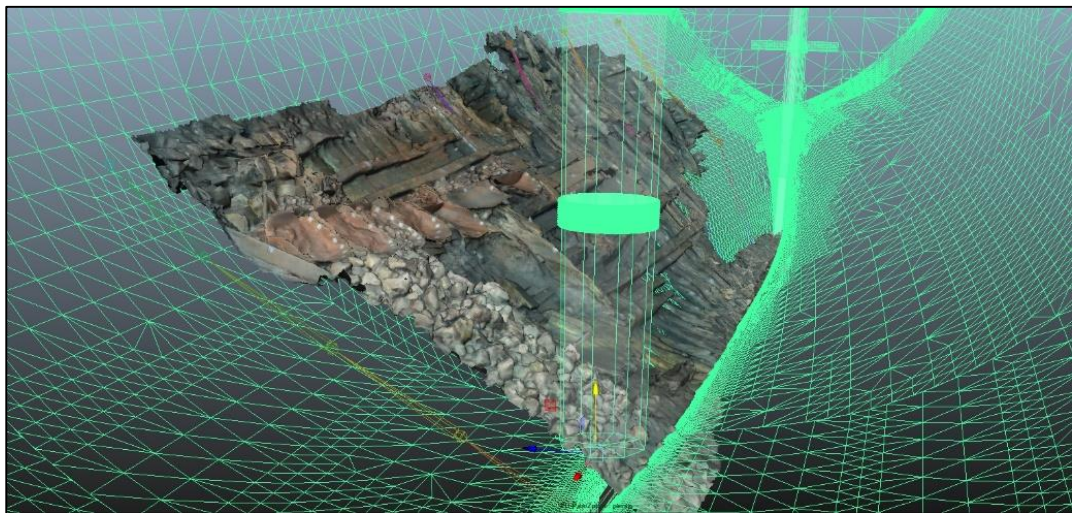


*Figure 4-20.* The Gnalić Shipwreck site brought back to the hypothetical original shape using the Interactive Fragment Model. (Image: Yamafune)



*Figure 4-21.* Storage pattern of the barrels on Interactive Fragment Model of the Gnalić shipwreck site. Diagnostic context became clearer thanks to the Interactive Fragment Model method. (Image: Yamafune)

In this dissertation, the author avoids further analysis of the Gnalić shipwreck site using this method because the reconstructed model used for comparison is from a different shipwreck. The method revealed valuable information about the barrels, but any further analysis would be unreliable. Yet for real archaeological projects, nautical archaeologists must reconstruct the hull lines of the shipwreck once enough frame timbers are exposed and recorded. Hull lines can also be reconstructed based on historical documents that are found during archival research.

Before closing this section, the author would like to remark on one more point; for the experimental Interactive Fragment Model method that was just discussed, the author used the reconstructed 3D model of the Pepper Wreck. However, this application can be used with hull lines instead of 3D models. With proper interpretation, contemporary shipwrights' treatises and 2D reconstructed hull lines drawn by scholars can be converted into 3D hull lines (Fig. 4-22). These 3D lines can be stored in a data

archive so that nautical archaeologists can apply the Interactive Fragment Model method immediately after a photogrammetric model of the shipwreck site is produced. This can be used as a tool to identify the type of ship. In short, the Interactive Fragment Model is very flexible and can be used for a variety of analysis purpose. J. Richard Steffy noted that generating a wooden Fragment Model is a very time consuming and labor intensive method; however, using new technologies, nautical archaeologists can apply his method in very quickly and in a less labor intensive manner.

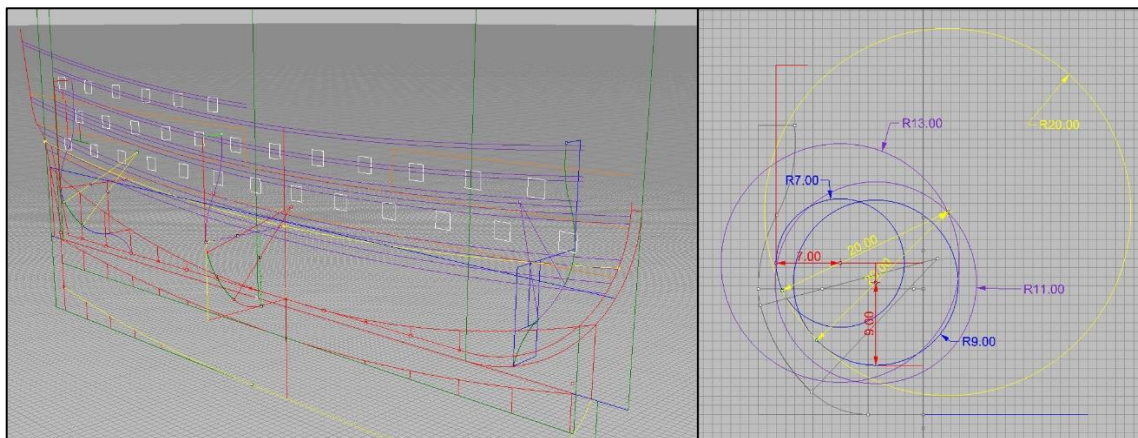


*Figure 4-22.* A reconstructed set of hull lines based on shipwrights' treatises. The figure displays the digital reconstruction of the Deane's 3rd-rate British ship (Deane and Lavery, 1981). Whenever a shipwreck with a similar type is found, this 3D hull line is ready to be used with the Interactive Fragment Model. (Image: Yamafune)

## Site Analysis

Site Analysis includes the study of the site formation processes that occurred during the wrecking event and those that have occurred in the years since.

Photogrammetric models can assist the archaeologist in understanding the layout of both

the ship and the artifacts on the site, which can provide clues about the site formation process. However, site analysis should not be limited to the study of what happened to the shipwreck in the past and what is happening in the present. The proper analysis of a shipwreck site must encompass what could happen to the wreck in the future and develop a management plan to deal with this. However, this only becomes possible when the archaeologists have a clear understanding of the wreck site and comparisons of other shipwreck sites based on several seasons of site recording and monitoring. Here, the author proposes a site monitoring method based on Cloud Compare, a point cloud analysis software.

#### *Photogrammetry Based Site Monitoring*

One of criticisms that underwater archaeologists often receive from terrestrial archaeologists is that underwater archaeology does not match the site recording standards that terrestrial archaeology follows. This is true to some extent. In land archaeology, archaeologists record layers of sediment and their contents. This is called the study of stratigraphy and it is possible because of the nature of terrestrial sites. At the end of a terrestrial field season, the archaeology team may have sequential layers of site plans that help them understand stratigraphy and the site formation processes that have occurred on the site. Contrarily, nautical archaeologists may not try to produce layers of site plans because working time underwater is limited. On some sites, archaeologists can only work on the site for less than one hour per day (for example, when the archaeological site is more than 30 m deep). In addition, running underwater excavations

is tremendously expensive because excavation require special equipment, including a diving boat. Therefore, until present day (2015), nautical archaeologists are usually able to create only one site plan at the end of the field season. In short, it has been nearly impossible for nautical archaeologists to produce layers of a site plan to help understand stratigraphy and site formation processes.

However, several years ago, PhotoScan, a fairly inexpensive and accurate photogrammetry software appeared on the market. Nautical archaeologists realized the importance of its data producing ability. Today, using the correct methods with photogrammetry software and other computer programs, nautical archaeologists can produce archaeological site plans fairly quickly. With this ability comes a clearer understanding of the site formation processes that act upon archaeological sites. Additionally, this clear understanding may help provide accurate predictions of what could happen to the archaeological sites in the future, which can help archaeologists develop reliable preservation and monitoring plans. There are several computer analysis software programs that archaeologists can use to analyze data that was produced during Computer Vision Photogrammetry. The author will briefly introduce this analysis software, which is called CloudCompare. It can be used to support archaeological site analysis and facilitate site monitoring.

CloudCompare is an open source 3D point cloud analysis software. PhotoScan can export dense point clouds in a variety of file formats. Some of the file formats are compatible between PhotoScan and CloudCompare, such as the ASTM E57 file format (.e57) and ASPRS LAS file format (.las). If the photogrammetric model is

georeferenced, the point cloud also automatically contains geographical information, thus, exported point clouds will open in the correct location with the correct scale. The main ability of CloudCompare is deviation analysis; in other words, it can compare two different point clouds and visualize the differences using colors (Fig. 4-23).

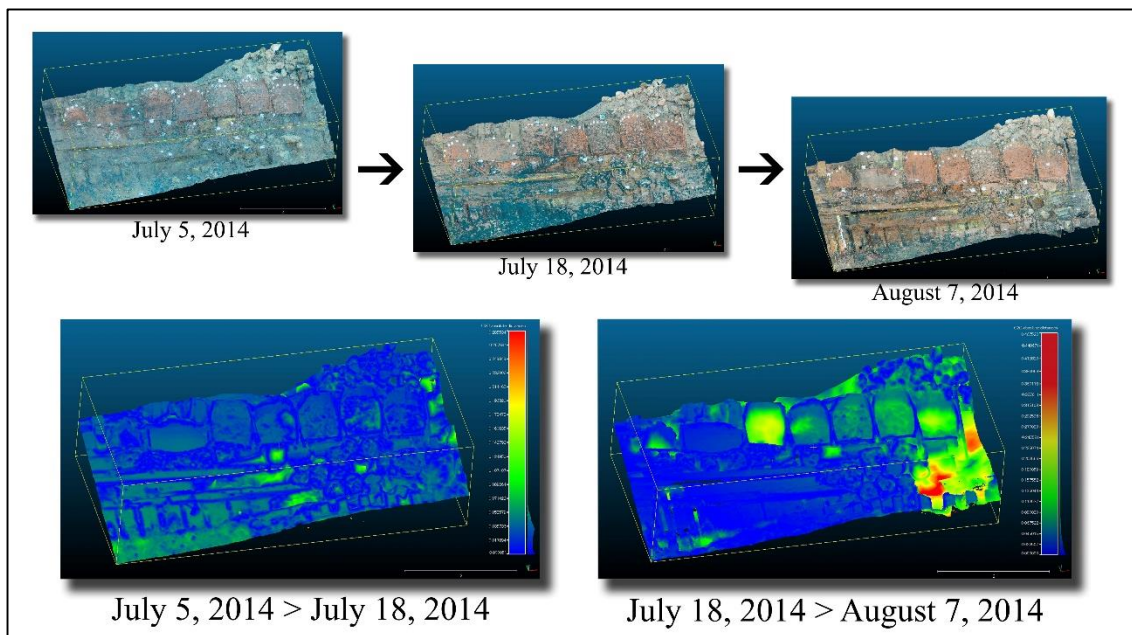


*Figure 4-23.* Visualizing the progression of the Gnalić 2014 excavation using CloudCompare. The photogrammetric point clouds show the area on the shipwreck where barrels were found. (Image: Yamafune)

Using this point analysis software, archeologists can track the progression of the excavation, both short term and long term. Moreover, this can help archaeologists track the accumulation of sediments and other alterations that occur on archaeological sites through the years. This can assist with making predictions about the near-future



conditions of the site in terms of *in situ* preservation. Furthermore, those deviation analysis can be used to monitor long-term condition of both excavated and unexcavated sites. To conclude, using 3D data produced by Computer Vision Photogrammetry and deviation analysis software, nautical archaeologists can track the progression of excavations in order to understand shipwreck sites both in the past and in the future.

### **3D Reconstructions**

Before the workflow completes its final step, which is publication, the author would like to suggest one additional step between hull analysis and publication, which is 3D reconstruction. The author believes that 3D reconstruction is a great way to test a scholar's hypotheses about a shipwreck. 3D reconstructions can be created in a variety of ways. Building a scaled wooden model is a common and traditional method often utilized by nautical archaeologists; some projects even build 1:1 scale operational reconstructed ships. 3D printing is becoming popular as well. In the following section, the author briefly discusses creating 3D reconstructions using 3D computer modeling software. The author often receives questions from colleagues about which computer modeling software they should start learning. For this reason, the author will briefly discuss two different types of 3D computer modeling methods that nautical archaeologists can use to build 3D reconstructions that can be used to test their hypotheses.

### *NURBS Modeling and Polygon Modeling*

Non-Uniform Rational B-Splines [NURBS] modeling and Polygon modeling are two different approaches to computer modeling. The idea behind NURBS modeling is that one can create surfaces based on curves, or wireframes. These curves are shaped based on mathematical formulas, which can create very smooth and accurately measured models. Polygon modeling is based on creating surfaces made of polygons that often have triangular and quadrilateral surfaces. Meshes of photogrammetric models are also categorized as Polygon models. These faces can be manipulated by vertices and edges.

Both NURBS modeling and Polygon modeling have advantages and disadvantages. The biggest advantage of the NURBS system is its precision and accuracy. This is the reason that many industrial CAD drawing and modeling software programs use the NURBS system. The AutoCAD series and Rhinoceros series are two examples. For nautical archaeology, NURBS modeling has advantages in modeling ship hulls because they are designed using curves (Fig. 4-24). NURBS modeling allows archaeologists to draw or trace curves and create surfaces based on these curves; therefore, NURBS modeling is suitable for when archaeologists need to reconstruct their hypothesis based on measurements and precise dimensions (Fig. 4-25). The disadvantage of the NURBS system is that texture mappings are not available on NURBS models. Only the simplest pattern can be used for textures on NURBS models.

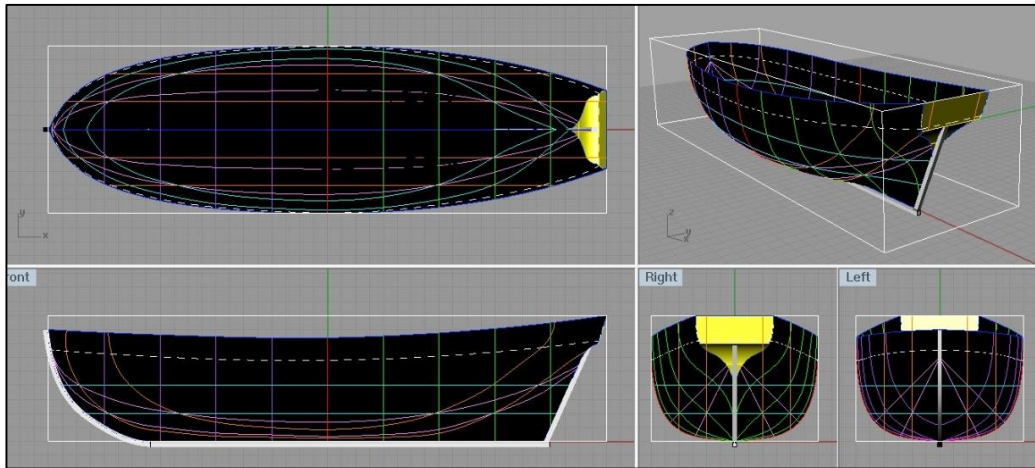


Figure 4-24. A 3D model of a ship's hull as an example of NURBS modeling. Using NURBS modeling, users can model smooth curvatures and surfaces (Image: Yamafune)

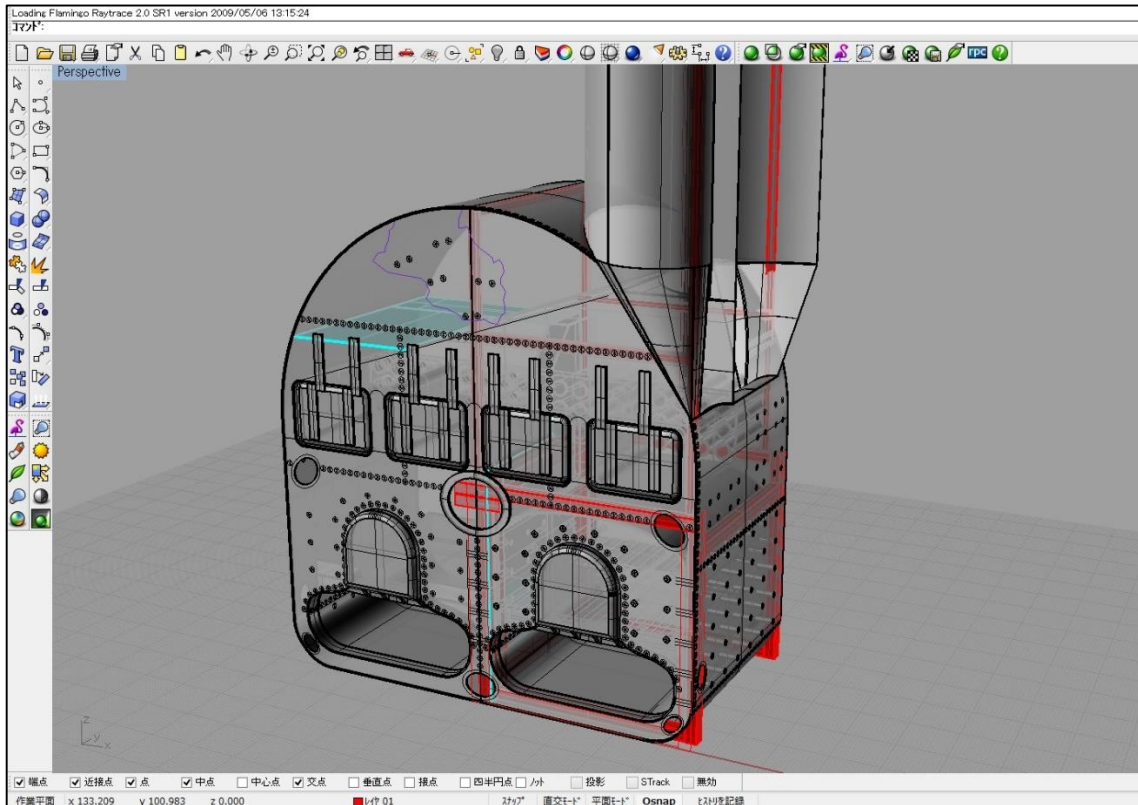


Figure 4-25. 3D reconstruction of a boiler from the shipwreck of the *Westfield* steamship created by Justin Parkoff. The author assisted by creating a 3D model based on Parkoff's reconstruction measurements for a museum installation. Therefore, this 3D model is entirely based on precise measurements. (Image: Yamafune)

The biggest advantage of Polygon modeling is its easy manipulation; the shape of objects can be changed while maintaining closed solid model properties. Additionally, we can apply and position textures using UV mapping (2D atlas, or canvas, for textures to be projected), which makes detailed and controlled texturing possible. The disadvantage of Polygon modeling is that the dimensions of models become arbitrary once you change the basic shape. Polygon models are not mathematically controlled in the way that NURBS models are; therefore, dimension and details of models based on archaeological data may lose their precision once the model is changed. Nevertheless, its ease of manipulating model shapes makes Polygon modeling more suitable for 3D reconstructions when the model is created using site plans and photogrammetric models as data. Using this technique, the site plans or photogrammetric models are traced to create the 3D reconstruction. Modeling by tracing is tremendously easier with Polygon modeling than it is with the NURBS system (Fig. 4-26). Therefore, when modeling does not require exact precision over accuracy in terms of the dimensions of 3D models, the author strongly recommends Polygon modeling (Fig. 4-27). Fortunately, many modeling softwares, including Maya, can convert NURBS models into Polygon models; therefore, nautical archaeologists can create a ship's hull using NURBS curves initially, and then convert it to a Polygon model to assign visually appealing textures if necessary.

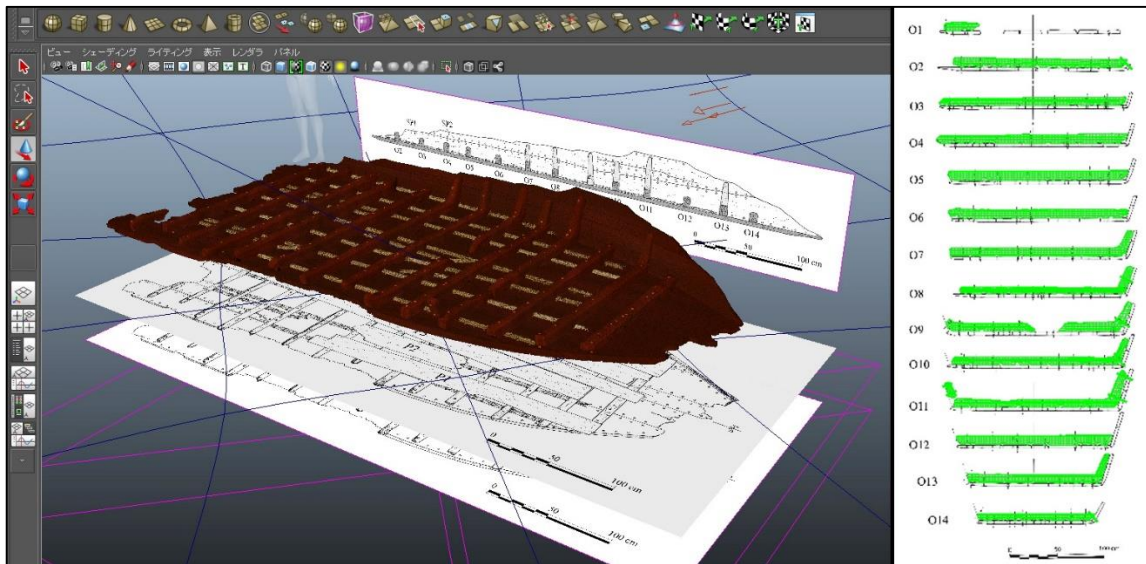


Figure 4-26. 3D model of Stella 1 shipwreck as an example of Polygon modeling. The model was created by tracing site plans. The original site plan of the shipwreck was drawn by Dr. Castro (Capulli and Castro, 2012). (Image: Yamafune)

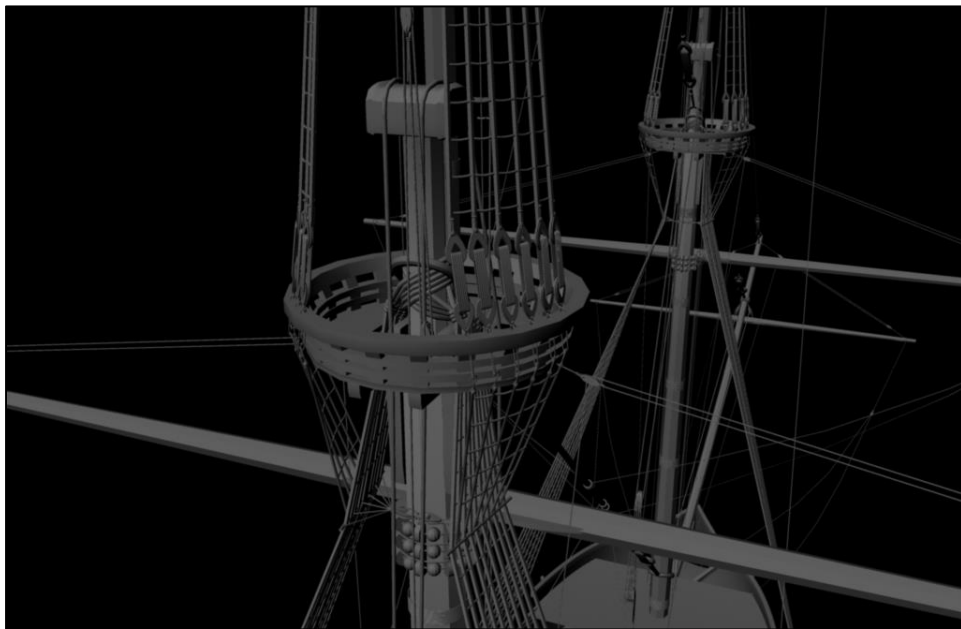


Figure 4-27. Hypothetical reconstruction of an early 17th century rigging arrangement of a Portuguese East Indiaman as an example of Polygon modeling. This 3D model was created based on historical accounts as well as descriptions and iconography about rigging of contemporary ships (Castro, 2003; Castro, 2005b; Castro, 2009; Castro, Fonseca, and Wells, 2010). This information did not indicate exact measurements of the rigging components. Therefore, Polygon modeling is an easier and better choice than NURBS modeling in this case. (Image: Yamafune)

To conclude this section, archaeologists must choose either NURBS modeling or Polygon modeling when creating a 3D model reconstruction to test their hypothesis. The important factor in this decision must be based on the goals of the reconstruction and the methods by which the original data was obtained. In short, when a model will be reconstructed based on the curvature of hull lines or based on precise measurements that archaeologists must follow, the author strongly recommends NURBS modeling software, such as the Rhinoceros series; on the other hand, when modeling must be done based on historical description and iconography, or based on tracing archaeological site plans and photogrammetric models, the author strongly recommends Polygon modeling software, such as the Maya series.

## CHAPTER V

### PUBLIC OUTREACH & PUBLICATION

#### **Visual Tour Animation**

In this chapter, the author will discuss various ways of sharing archaeological research with the public, which is a vital and ethically necessary part of archaeology. The first public outreach methodology that the author would like to introduce is Visual Tour Animation, which is a simple animation that uses photogrammetric models and a flying camera created in Autodesk Maya (this animation can be done in other modeling and animation softwares such as Blender). The author believes that making a Visual Tour Animation is much simpler and easier than creating conventional computer generated animations because it does not require computer modeling and Deformation. Since most of the modeling for the Visual Tour Animation can be done with Computer Vision Photogrammetry software, the required knowledge of computer animation in Maya is Key-Frame Animation for a created flying camera. The basic concept of computer generated animation is the same as that of video recording; one second of animation is composed of 24 – 30 rendered images so that the human eye and a brain see it as a movie instead of consecutive pictures. When the Animation Setting in Maya is set at 24fps (frames per second), a 20 second animation has 480 still frame images. Key frame animation uses these frames as keys of timing (designated timing of actions of the object, such as positions, scales, and rotations of the selected object). When the position of a cube needs to be moved from point A to point B in 20 seconds, the first default key

frame would be frame 1 and a cube would be located at point A. Then, the Set Key command is applied by pressing the S button. This command orders the cube to be located at point A at key frame 1. Then, the current frame on the Time Slider Tab that can be seen at the bottom of the Maya workspace needs to move from 1 to 480 to make time flow in Maya 20 seconds later (24 fps x 20 seconds). Also, the position of the cube must be moved to point B, and then the Set Key frame command should be applied. Consequently, the cube travel from point A to point B in 20 seconds (Fig. 5-1).

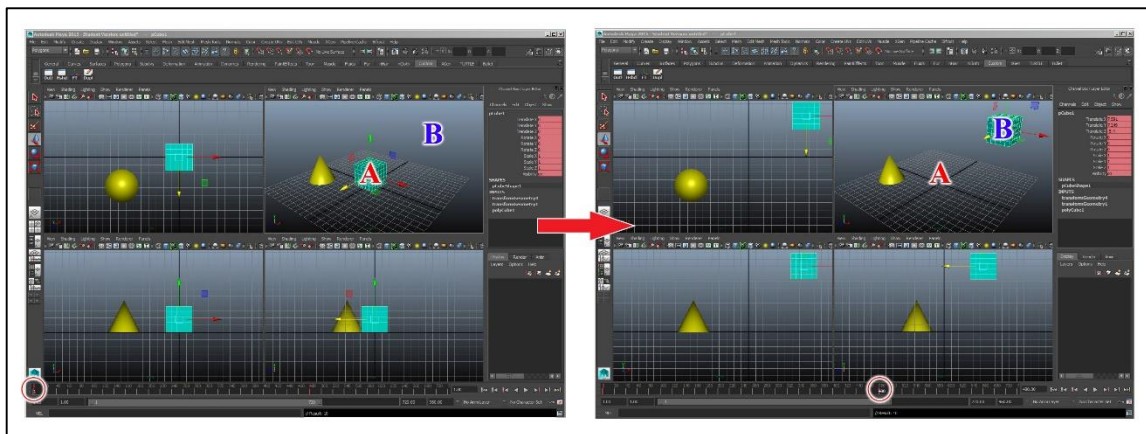


*Figure 5-1.* An example of simple key frame animation. Keys of the cube are set on frame 1 and 480. As a result, the cube traveled between two assigned positions from A to B in 20 seconds. (Image: Yamafune)

Transparency of the material can also be animated so that the visibility of the objects can be easily controlled. Using transparency, objects can fade in and fade out in the animation (Select object or material > material node tab on Attribute Editor > Transparency > Set key by right click on Transparency). This fade-in and fade-out



animation allows archaeologists to show the progress of the excavation to the general public (Fig. 5-2).

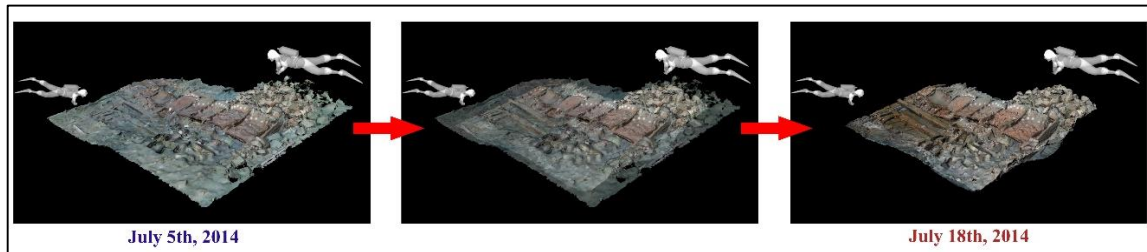


*Figure 5-2.* Key frame animation of transparency of the materials. The photogrammetric model can fade in and fade out using this technique. (Image: Yamafune)

To create a Visual Tour, archaeologists need to animate a camera in Maya. A camera in Maya is not a camera in the traditional sense. It is a way to render specific images from a digital camera that flies around the site (Fig. 5-3). In Maya, new cameras can be created (Create > Cameras > Camera and Aim) and will render images through their viewports (From Rendering work space > Render > Butch Render).

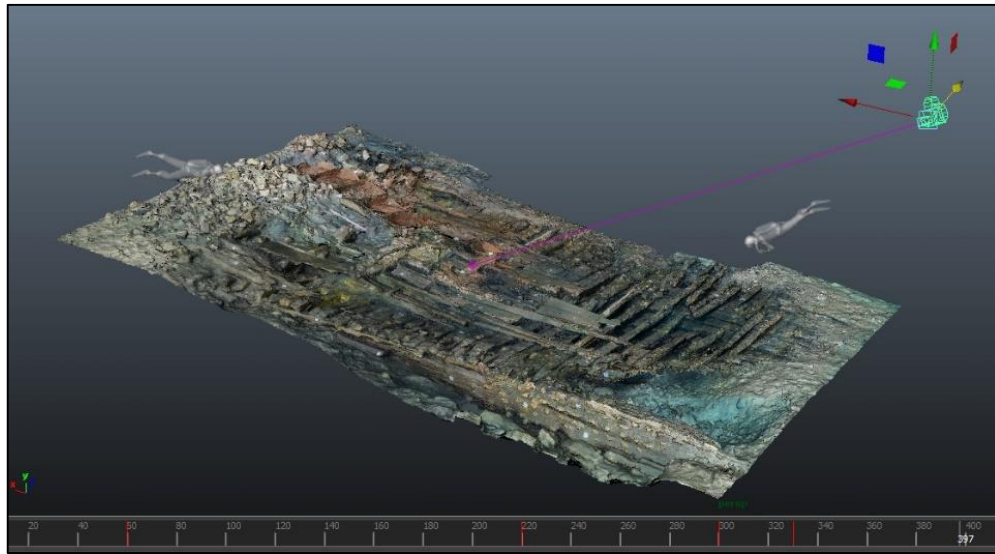


*Figure 5-3.* A created flying camera in Maya. The position of the camera and its aim can be key-animated. Visual Tour Animation can be created through this flying camera's viewport. (Image: Yamafune)

Though rendering settings can vary, the only important settings that archaeologists need to know to create a Visual Tour Animation can be found under the Common tab in Rendering Settings. These commands are File Output, Frame Range, Renderable Cameras, and Image Sizes (Window > Rendering Editors > Rendering Settings). The Butch Render command exports still images created by the viewport of the flying camera. Although Maya can export relatively low resolution movies by choosing AVI file format output in the Render setting, high resolution still images that were exported through the Butch Renderings process are not yet a movie. The images still need to be pieced together to become an animation. The author uses Adobe Premiere Pro CS6 to compose animations because this video editing software also allows composed animations to have visually appealing titles, scene transitions, and various sounds. To compose a movie from still images in Premiere Pro is simple. Once the desired still

images have been selected in the Import window (File > Import), the Image Sequence box at the bottom needs to be checked (Fig. 5-4). Then, the imported selected images will automatically be uploaded as video footage. After titles and other video transition effects are added to the animation, Premiere Pro can export the animation in the desired file format such as MP4 (H.264), AVI, or QuickTime (File > Export > Media). Then, the visual tour animation is ready to be shared.

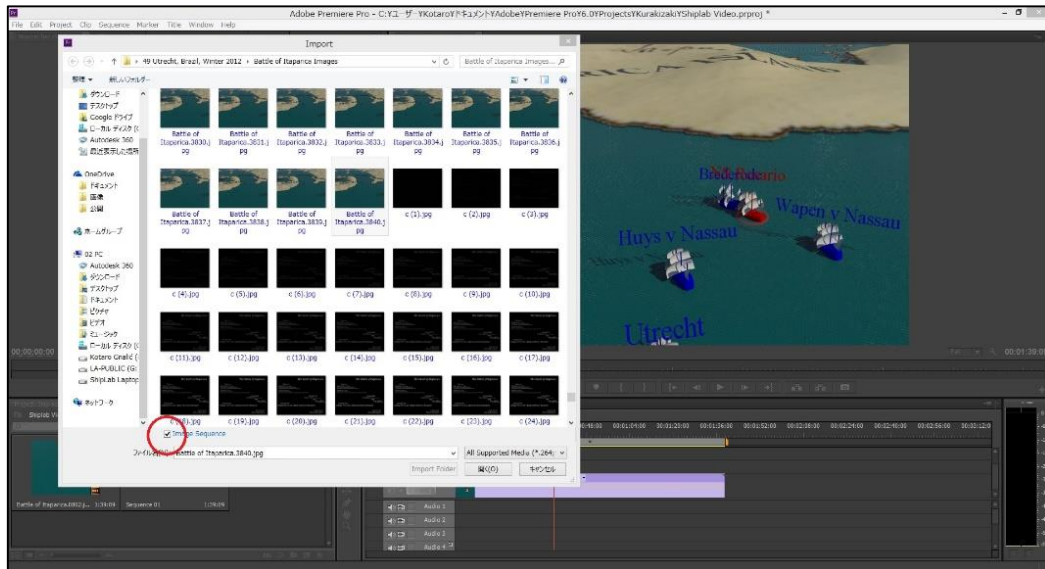


Figure 5-4. Converting still images to an animation using Image Sequence import in Adobe Premiere Pro CS6. (Image: Yamafune)

The author believes that Visual Tour Animation is an excellent method for sharing our discoveries and excitement with the general public because not many people are able to visit the sites, either because they cannot SCUBA dive or because they lack the permission required to visit many underwater shipwreck sites. It is particularly useful

for when an excavation is ongoing. Furthermore, poor visibility on the shipwreck site often prohibits good video camera footage from being obtained. However, computer generated animations can deliver clearer images of the entire archaeological site. Using the transparency key frame animation, the Visual Tour Animation can show the progress of an excavation.

From the archaeologist's perspective, this proposed method does not require any special knowledge of computer modeling or deformation beyond the skills needed to create the original photogrammetric models that are used for archaeological analysis. The animations can be created within a day or two. This means that visual tour animations of the shipwreck's site can be uploaded to the Internet for public viewing on a weekly basis without taking too much time away from archaeological research. Consequently, the public can not only see results of the season but can also follow the progress of excavation. The author created several animations from the 2013 and 2014 Gnalić Project field seasons and received many positive comments from the public as well as from archaeologists.

### **Interactive Virtual Museum**

Another outreach method that can be created using photogrammetric models is an Interactive Virtual Museum. The Visual Tour Animation is a passive way to share archaeological information with the general public; on the other hand, the Interactive Virtual Museum is an active way to do so. One of the benefits of Computer Vision Photogrammetry is its visually appealing 3D models. PhotoScan can export these models

in various file formats, including PDF files. Any computer with an installed PDF reader is able to rotate PDF files, which essentially makes the image on the PDF a 3D model that can be zoomed and rotated by viewers.

There are also webpages that will host 3D models. The webpages, such as [www.Sketchfab.com](http://www.Sketchfab.com) [Sketchfab], can be used by anyone and shared without any special software. The author believes that the trend of uploading and sharing 3D models will become more popular. For example, the author uses Sketchfab. PhotoScan also supports this webpage officially so that created photogrammetric models can be directly uploaded to Sketchfab (File > Upload models > Sketchfab). Also, Sketchfab can host a variety of file formats. The author has often exported photogrammetric models into Autodesk Maya to fix problems or to combine several photogrammetric models. Then, completed models are exported in OBJ file format and uploaded to Sketchfab. Many of the 3D model-sharing webpages allow uploaded 3D models to have annotations and explanations of the models. Viewers can rotate and zoom models by themselves and enjoy 3D models more interactively (Fig. 5-5).

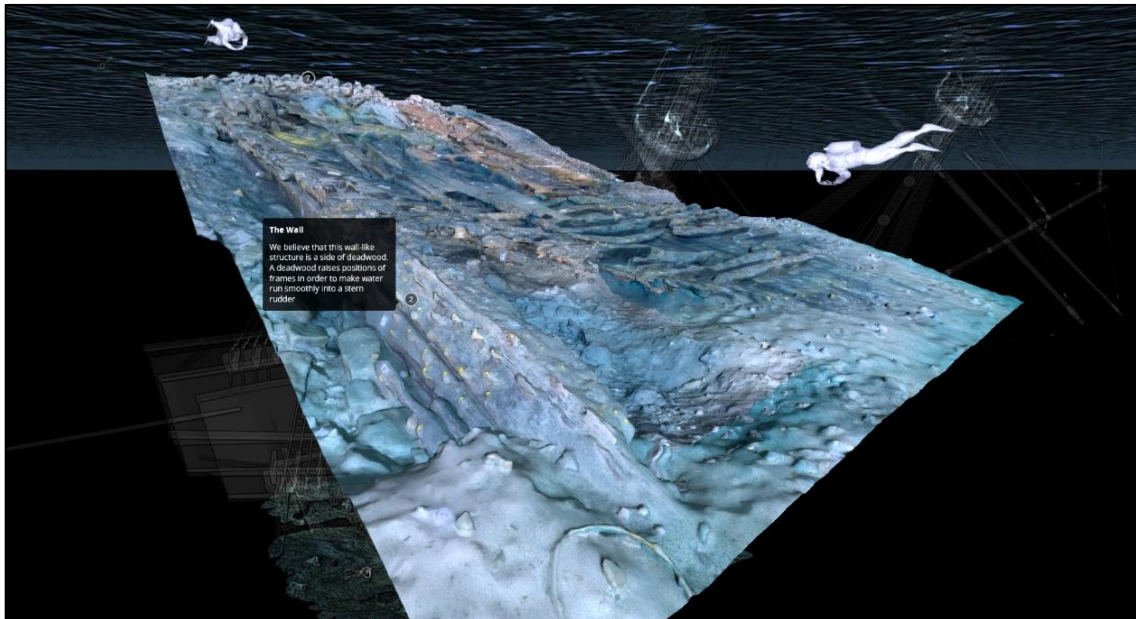


Figure 5-5. Photogrammetric model of the Gnalici shipwreck site in Sketchfab. Users can interactively control the position of the camera, or a viewpoint. Also, its annotations can display information related to the models. (Image: Yamafune)

Using these 3D model-sharing webpages, such as Sketchfab, archaeologists can share our field experiences with the public more easily and quickly without creating an animation using programs such as Maya. Because webpages like Sketchfab don't require any special knowledge or software experience, the Interactive Virtual Museum is an easier method than creating a Visual Tour Animation. Using this method, the public can follow ongoing underwater archaeology projects via these webpages. For these reasons, the author believes that using the 3D model sharing webpages to support an Interactive Virtual Museum is a very effective method for sharing photogrammetric models with the public.

## **Publications**

The final step of the proposed workflow is publication. Since many shipwreck sites are located in underwater environments, it is very difficult for other scholars and the public to have access to archaeological sites. Thus, in many cases, archaeological publications are the only way that other people can access technical information about the shipwrecks. It is very clear why it is vital that all archaeological projects reach the publication phase. Forms of publication can vary; museum exhibitions, newspaper articles, and project webpages can be forms of publication. Yet in this dissertation, the author also wants to note another possible perspective on publishing in peer reviewed journals and scholarly books.

Throughout this dissertation, the author has discussed ways to combine Computer Vision Photogrammetry with traditional research methods for nautical archaeology. The point of this discussion was to replicate real scale shipwreck sites in digital format so that archaeological information could be extracted from the models. The author also believes that 1:1 scale constrained photogrammetric models can contribute greatly to scholarly publications such as peer-reviewed journals. Before explaining how Computer Vision Photogrammetry can contribute to these publications, the author would like to note why he came up with his ideas regarding publication. The author always had questions about the publication of underwater archaeology. Peer reviewed journal articles of natural science have protocols that describe the procedures used in their experiments and research. Therefore, everybody who reads the journal can replicate the experiment that journal article described. In other words, description and research results

of natural science are repeatable and testable. Contrarily, in the field of social science, it is tremendously difficult (if not impossible) to replicate and test the results that are described in publications. The reason for this is very obvious in the field of underwater archaeology because of the difficulty of accessing the underwater sites. However, as the author described in the Interactive Visual Museum section, sharing 3D models with others is becoming cheaper and easier. The author believes it is not difficult for nautical archaeologists to share their 1:1 scale constrained photogrammetric models and 3D reconstruction models using 3D model sharing software with downloadable settings. This should be done with peer-review journal websites acting as data archives or through scholar's personal accounts. An important point is that these 3D models should be accessible to other scholars so that they can test what was written in the journal articles. This could raise the standards of nautical archaeology to same level as that of the natural sciences; as a result, the body of knowledge of maritime history could be much richer.

In short, the author believes that Computer Vision Photogrammetry can also break the paradigm of nautical archaeology as a social science by sharing 1:1 scale constrained photogrammetric data with its peer-reviewed journals. The author strongly recommends that publishers of peer-reviewed journals have 3D model sharing services or accounts in order to share archaeologists' results and data with other scholars so that published archaeological research can be tested and refined. The author may be too naïve about this notion, and there are many processes and obstacles that we have to overcome. But nautical archaeologists are already creating 1:1 scale constrained



shipwreck site models, thus, this is a good time to start thinking about next step of scholarly researches and publications of nautical archaeology.

## CHAPTER VI

### CONCLUSION

#### **Conclusions**

The author has discussed the proposed methodology for recording and analyzing shipwreck sites in four different sections: data acquisition, data processing, data analysis, and sharing knowledge (public outreach and publication). The important point is that this methodology is very flexible and still developing along with advances in technology; the discussed methodology can be fitted to any type of shipwreck as long as the water visibility allows archaeologists to capture fairly clear images. Technology, even PhotoScan, can be replaced by more advanced software when it appears. In other words, archaeologists will have to modify this methodology to make it suit the needs of their projects. This methodology is a philosophy and idea rather than a completed guideline. The author strongly believes that the philosophy behind this methodology can change the standard of traditional underwater excavations in nautical archaeology. To note one more time, the primary idea behind this methodology is to create a 1:1 scale constrained accurate replication of a shipwreck site in digital format and to extract archaeological information from the digital data in order to proceed with conventional archaeological research. This proposed methodology allows archaeologists to skip time-consuming underwater measuring; what is more, it can provide more accurate data. This methodology can shorten ten years of excavation and recording to two years. This means that nautical archaeologists' field projects can be conducted much more quickly and

inexpensively. Consequently, with the same amount of budget and time, archaeologists can conduct more projects on underwater cultural heritage. Before closing this dissertation, the author would like to note a few more uses of this proposed methodology.

### *Digital in situ Preservation*

One of the great benefits of this proposed methodology is that it produces 1:1 scale constrained photogrammetric models of shipwreck sites, or real scale replication of underwater cultural heritage locations, in digital format. In 2001, the UNESCO Convention for Underwater Cultural Heritage was enacted. After this, underwater archaeology community recognized the importance of *in situ* preservation and became dedicated to promoting it. The UNESCO 2001 convention promotes protection for underwater cultural heritage sites; however, *in situ* preservation is not a perfect solution in terms of protection. Archaeologists and governments must anticipate unexpected factors of destruction. Taliban, ISIS, and other extreme activists have destroyed cultural heritage and museum displays in Syria and Iraq. Natural disasters, such as earthquakes, tsunamis, and volcanic activity have unexpectedly destroyed cultural heritage sites. For underwater cultural heritage sites, the activities of treasure hunters and net-dragging trawlers are always a major threat. Consequently, we must consider some type of safety net strategy along with *in situ* preservation. The author strongly believes that Computer Vision Photogrammetry is possibly the best solution. If archaeologists can succeed in creating 1:1 scale constrained photogrammetric models of cultural heritage sites, the

dimensions and textures of the cultural heritage sites can be recorded and remain as long as the data survives. Moreover, digital *in situ* preservation can preserve cultural heritage in its current condition; therefore, it can be used for monitoring purpose as the author discussed in Chapter IV. The idea of digital *in situ* preservation is not meant to replace the strategy of *in situ* preservation. Digital *in situ* preservation should be used as a safety net for when *in situ* preservation fails. As long as we have the data provided by 3D models and the textures of cultural heritage sites, we can create 1:1 real scale restoration or replication when destruction occurs in the future. Henceforth, the author strongly recommends that digital *in situ* preservation be used to protect our cultural heritage, including shipwreck sites.

#### *Computer Vision Photogrammetry as a Tool against Treasure Hunters*

One of the major threats to nautical archaeology is the activity of treasure hunters. In addition to selling artifacts for money, treasure hunters declare themselves to be archaeologists or explorers and proceed with excavation and salvaging activities without proper recording of shipwreck sites. This is a destruction of our common human heritage, and our history can be lost forever. Because treasure hunters declare their activities to be genuine archaeological research, they can receive permission from local governments to proceed with their activities.

For that reason, the author believes that Computer Vision Photogrammetry can be a strong tool to be used in the fight against their looting activities. Once nautical archaeologists produce 1:1 scale constrained photogrammetric models of shipwreck

sites, archaeologists can rightfully claim that most of the archaeological data can be acquired from the photogrammetric models. By publishing 3D models and submitting 3D data to local governments, archaeologists may be able to eliminate the justification given by treasure hunters that they must visit and destroy the shipwreck for their research. Moreover, if the proposed methodology becomes a new standard for underwater surveys and excavations, recording shipwreck sites before and after excavations could become the standard of underwater research. In that case, all activity on underwater cultural heritage becomes more transparent. Then, looting activities and destruction of shipwreck sites can be disclosed easily. In short, archaeological excavation using Computer Vision Photogrammetry, including the proposed methodology, can be a strong deterrent against treasure hunters. For that reason, the author strongly promotes the use of Computer Vision Photogrammetry and the proposed methodology as a new standard for nautical archaeology in order to protect underwater shipwreck sites from treasure hunters.

#### *Legacy Photogrammetry*

The author and his colleagues promote another aspect of Computer Vision Photogrammetry called Legacy Photogrammetry. Nautical archaeologists have been using photography for their underwater excavations since the 1960s. Many of the photos that were taken were used to create photomosaics of the shipwreck sites. Fortunately, some of these photos can be used for Computer Vision Photogrammetry. One of the author's colleagues, Thomas Van Damme, calls this application Legacy

Photogrammetry, using old data to create 3D models (Van Damme, 2015). Based on the author's experience, by choosing properly scanned photos and applying the proper masks and markers, Legacy Photogrammetry can be surprisingly successful (Fig. 6-1). In addition, many former excavations and research endeavors left good data regarding the dimensions and measurements of shipwrecks. Therefore, today's archaeologists can apply these measurements to constrain photogrammetric models to 1:1 scale. If 3D models are successfully created and constrained to a 1:1 scale, these models become diagnostic and can be used for further archaeological research (Fig. 6-2). There are many photos from former excavations and research endeavors being stored untouched. The author and his colleagues want to promote the possibility of using Legacy Photogrammetry to revisit and extract more data from previous studies.

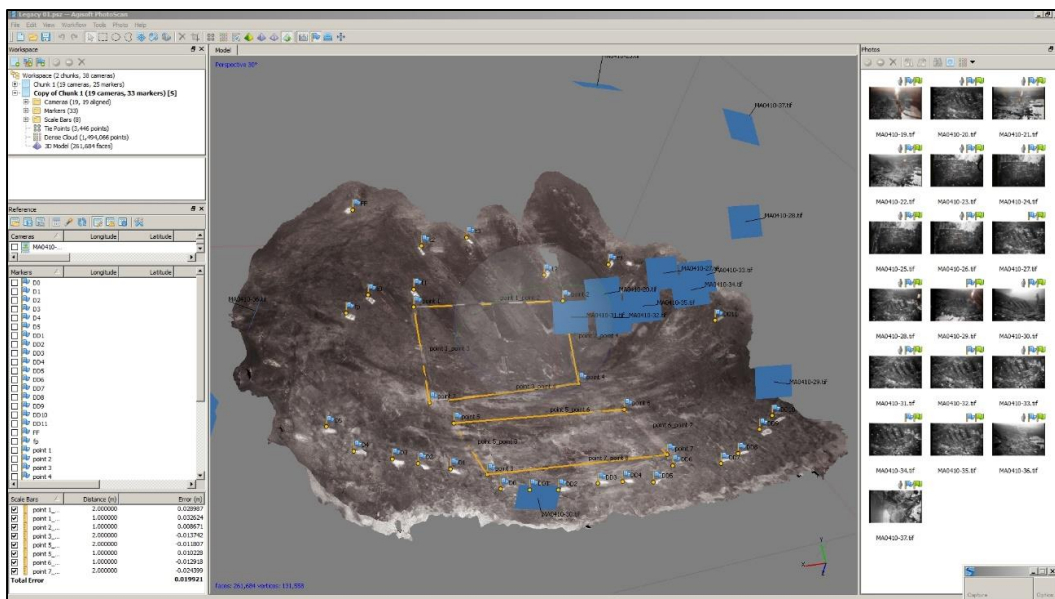


Figure 6-1. Legacy Photogrammetry of the *Batavia* shipwreck. The photogrammetric model was reconstructed based on 19 selected site photos. (Image: Yamafune)

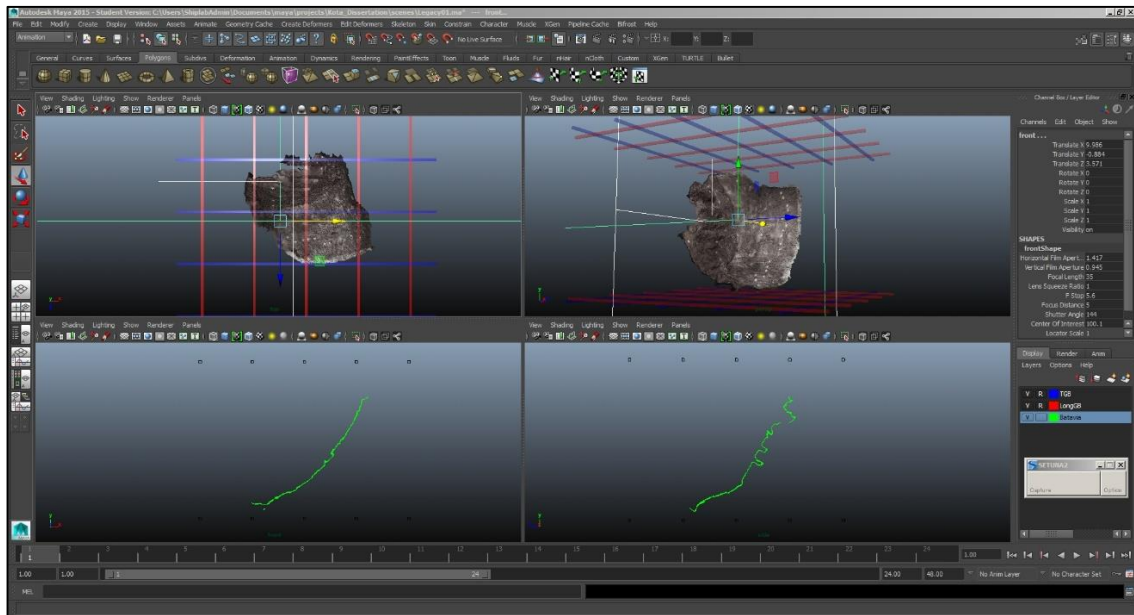


Figure 6-2. Section profile extraction of Batavia shipwreck. 1:1 scale constrained models can be diagnostic even though photos were taken decades ago. More scholarly researches and archaeological data of *Batavia* shipwreck can be seen in Van Duivenvoorde and Green's publication (2015). (Image: Yamafune)

### *To Conclude: Leaving Data for Future Generations*

The author believes that archaeology, the study of human history, has two main responsibilities: the first responsibility is to interpret the human past correctly, and the second responsibility is to protect the memories of humanity. The first responsibility is fulfilled by archaeological research. In this dissertation, the author has discussed a method to assist with this. Nevertheless, the author also wants to remark on the importance of the second responsibility of archaeology. Cultural heritage and all archaeological remains are the memories of humanity, like old pictures of a person. Without understanding and keeping the memory of the past, people cannot appreciate their life in the present or future. However, understanding the meaning of the past is a dynamic process: today's archaeologists can go as far as the data allows, but the future

archaeologists will inevitably have more data to refine our understanding of the past. Often we cannot fully comprehend the significance of an archaeological site or its artifacts at the time of its excavation and initial publication. As today's archaeologists, it is our important responsibility to protect and leave these memories intact for future generations. These memories can be in the form of cultural heritage. Fortunately, technologies are developing quickly; the cost of 3D printers is dropping and printing capacity is rising and engineers and scientists are developing applications of 3D holography and augmented reality. The application of 3D data is developing so rapidly that nobody can predict their capability in the future. Thus, the author believes that leaving 3D data to future generations is the one of our top priorities as archaeologists. As today's archaeologists can create 3D models from photos (which archaeologists in 1960s might not have imagined), future archaeologists will likely create something that we cannot even imagine today.

To conclude, the proposed methodology satisfies two major responsibilities of archaeologists: understanding the past correctly and leaving memories and data for future generations. This methodology can provide accurate archaeological data to archaeologists to help understand shipwreck sites; meanwhile, it produces 1:1 scale constrained photogrammetric models with high-resolution textures that provide detailed information. Additionally, the data acquisition depends primarily on photo-shooting that can be accomplished in a tremendously shorter time than conventional data acquisition methods, such as manual measuring. Once 1:1 scale constrained models are produced, archaeologists can extract accurate archaeological data from the model, and research can



proceed to data processing and data analysis methods that do not require revisiting underwater archaeological sites. If this methodology becomes a new standard and is taught to young students of nautical archaeology, the author believes that the standards of underwater surveys and excavations can be raised. And this possible new standard could eventually lead to protection of underwater cultural heritage. Yet, the author must note one more time, this proposed methodology is just a tool to assist in the conventional research tasks performed by nautical archaeologist; to use this methodology correctly, basic knowledge of the history of shipbuilding and an understanding of conventional reconstruction methods of shipwreck sites is a prerequisite.

The author hopes this dissertation will be used as a guideline for underwater excavations and research so that our grandchildren's generation can enjoy the history of shipwrecks being excavated today.

## REFERENCES

- Agisoft LLC, 2014, Agisoft PhotoScan User Manual: Professional Edition, Version 1.1, [http://www.agisoft.com/pdf/photoscan-pro\\_1\\_0\\_en.pdf](http://www.agisoft.com/pdf/photoscan-pro_1_0_en.pdf), (Accessed, 11/24/2015).
- Agisoft Online Forum, 2015, <http://www.agisoft.com/forum/index.php?PHPSESSID=e72c200ee49959b31e4d7f07ce926485&>, (Accessed 11/24/2015).
- Al-Ruzouq, Rami., 2012, Photogrammetry for Archaeological Documentation and Cultural Heritage Conservation. INTECH Open Access Publisher, Rijeka.
- Atkinson, K., Duncan, A., and Green, J., 1988, The Application of a Least Squares Adjustment Program to Underwater Survey. *International Journal of Nautical Archaeology* **17**, 119-131.
- Baker, P. E., and Green, J. N., 1976, Recording Techniques Used During the Excavation of the *Batavia*. *International Journal of Nautical Archaeology* **5**, 143-158.
- Bass, G. F., 1972, *A History of Seafaring; Based on Underwater Archaeology*, Walker, New York.
- Bass, G. F., and Rosencrantz, D. M., 1972, Submersibles in Underwater Search and Photogrammetric Mapping. *Underwater Archaeology. A Nascent Discipline*, UNESCO, 271-283.
- Bass, G. F., and Van Doorninck, F. H., 1971. A Fourth-Century Shipwreck at Yassi Ada. *American Journal of Archaeology*, **75.1**: 27–37.
- Bass, G. F., and Van Doorninck, F. H., 1982, *Yassi Ada. Vol. 1: A Seventh-century Byzantine Shipwreck*, Texas A&M University Press, College Station.
- Batur, K., 2014a, Department of Archaeology, University of Zadar, Zadar.
- Batur, K., 2014b, Department of Archaeology, University of Zadar, Zadar.
- Batur, K., 2014c, Department of Archaeology, University of Zadar, Zadar.
- Bowens, A., 2009, *Underwater Archaeology: the NAS Guide to Principles and Practice*, Malden, MA, Blackwell Publishing, Portsmouth.

Burtch, R., 2008. History of Photogrammetry, (based on lecture notes on the History of Photogrammetry at Ferris State University)  
<https://spatial.curtin.edu.au/local/docs/HistoryOfPhotogrammetry.pdf>, Last Updated 2008 (Accessed 11/24/2015).

Canciani, M., Gambogi, P., Romano, F. G., Cannata, G., and Drap, P., 2003, Low Cost Digital Photogrammetry for Underwater Archaeological Site Survey and Artifact Insertion. The Case Study of the Dolya Wreck in Secche della Meloria - Livorno – Italia. *International Archives of Photogrammetry Remote Sensing and Spatial Information Sciences* **34**, 95-100.

Capulli, M., and Castro, F., 2012, Navi Cucite di epoca romana: il caso del relitto Stella 1. *Atti dek II Convegno Nazionale di Archeologia, Storia, Etmologia Navale per la Salvezza del Patrimonio Maritimo Italiano*, Museo della Marineria di Cesenatico.

Castro, F., 2003, The Pepper Wreck. *International Journal of Nautical Archaeology* **32.1**: 6-23.

Castro, F., 2005a, *The Pepper Wreck: a Portuguese Indiaman at the Mouth of the Tagus River*, Texas A & M University Press, College Station.

Castro, F., 2005b, Rigging the Pepper Wreck. Part I: Masts and Yards. *International Journal of Nautical Archaeology* **34.1**:112-124.

Castro, F., 2007, Rising and Narrowing: 16th-Century Geometric Algorithms used to Design the Bottom of Ships in Portugal. *International Journal of Nautical Archaeology* **36.1**: 148-154.

Castro, F., 2008, The Concept of Iberian Ship. *Historical Archaeology* **42.2**: 63-87.

Castro, F., 2009, Rigging the Pepper Wreck. Part II: Sails. *International Journal of Nautical Archaeology* **38.1**: 105-115.

Castro, F., 2014a, Department of Anthropology, Texas A&M University, College Station.

Castro, F., 2014b, Department of Anthropology, Texas A&M University, College Station.

Castro, F., 2015, Department of Anthropology, Texas A&M University, College Station.

Castro, F., Fonseca, N. and Wells, A., 2010, Outfitting the Pepper Wreck. *Historical Archaeology* **44.2**: 14-34.

Castro, F. and Gomes-Dias, D., 2015, Moulds, Graminhos and Ribbands: A Pilot Study of the Construction of Saveiros in Valença and the Baía de Todos os Santos area, Brazil. *International Journal of Nautical Archaeology*, **44**: 410–422.

Castro, F., Yamafune, K., Eginton, C. and Derryberry, T., 2011, The Cais do Sodré Shipwreck, Lisbon, Portugal. *International Journal of Nautical Archaeology* **40**: 328–343.

Ch-Ch-Check It, 2011, Turn a Photograph into a Drawing | Photoshop CS5 Tutorial, <https://www.youtube.com/watch?v=HVUua9CzUiM>, date last updated 2011 (Accessed 11/24/2015).

Crisp, S., 2013, Camera Sensor size: Why Does it Matter and Exactly How Big Are They, <http://www.gizmag.com/camera-sensor-size-guide/26684/>, (Accessed 11/24/2015).

Deane, A., and Lavery, B., 1981, *Deane's Doctrine of Naval Architecture, 1670*, Conway Maritime Press, London

Diamanti, E., Georgopoulos, A., and Vlachaki, F., 2011, Geometric Documentation of Underwater Archaeological Sites, XIII CIPA International Symposium, Prague.

Doneus, M., Verhoeven, G., Fera, M., Briese, Ch., Kucera, M., and Neubauer, W., 2011, *From Deposit to Point Cloud: A Study of Low-cost Computer Vision Approaches for the Straightforward Documentation of Archaeological Excavations*, Geoinformatics (Faculty of Civil Engineering, Czech Technical University In Prague).

Drap, P., 2012, *Underwater Photogrammetry for Archaeology*, INTECH Open Access Publisher, Rijeka.

Gietler, S., 2009, Dome Ports and Macro Ports, *Underwater Photography Guide*, <http://www.uwphotographyguide.com/dome-ports-macro-ports>, (Accessed 11/24/2015).

Govorčin, S., 2014, Department of Archaeology, University of Zadar, Zadar.

Green, J., 2004, *Maritime archaeology: A Technical Handbook (2nd edition)*, Academic Press, London.

Green, J., and Gainsford, M., 2003, Evaluation of Underwater Surveying Techniques. *International Journal of Nautical Archaeology* **32**, 252-261.

Green, J., Matthews, S., and Turanli, T., 2002, Underwater Archaeological Surveying Using PhotoModeler, VirtualMapper: Different Applications for Different Problems. *International Journal of Nautical Archaeology* **31**, 283-292.

- Henderson, J., Pizarro, O., Johnson-Roberson, M., and Mahon, I., 2013, Mapping Submerged Archaeological Sites Using Stereo-vision Photogrammetry. *International Journal of Nautical Archaeology* **42**, 243-256.
- Holt, P., 2003, An Assessment of Quality in Underwater Archaeological Surveys Using Tape Measurements. *The International Journal of Nautical Archaeology* **31.2**, 246-251.
- Huang, T. S., 1996, Computer Vision: Evolution and Promise. *CERN Reports* **21**.
- Konecny, G., 2003. *Geoinformation Remote Sensing, Photogrammetry and Geographic Information Systems*, London, Taylor & Francis.
- Marcel, 2014, Dense Cloud Quality Setting, What Does It Control?, Agisoft PhotoScan Online Forum,  
<http://www.agisoft.com/forum/index.php?topic=1970.msg10498#msg10498>, date last updated 2014, (Accessed 11/24/2015).
- Marcel, 2015, Alignment Experiment, Agisoft PhotoScan Online Forum,  
<http://www.agisoft.com/forum/index.php?topic=3559.0>, date last updated 2015, (Accessed 11/24/2015).
- McCarthy J., and Benjamin J., 2014, Multi-image Photogrammetry for Underwater Archaeological Site Recording: An Accessible, Diver-based Approach. *Journal of Maritime Archaeology* **9**, 95-114.
- Oliveira, F. 1995, *Shang Chuan Zhi Zao Quan Shu*, Putaoya Hai Shi Xue Yuan, Macau.
- Pandozi, J. 2014, Bubble Media, Santa Eulària des Riu.
- Pasumansky, Alexey, 2015, Tie Points Once Again, Agisoft PhotoScan Online Forum,  
<http://www.agisoft.com/forum/index.php?topic=3517.msg18734#msg18734>, date last updated 2015, (Accessed 11/24/2015).
- Radić Rossi, I., Bondioli, M., Nicolardi, M., Brusić, Z., Čoralić, L., and Castro F., 2013. *The Shipwreck of Gnalić - Mirror of Renaissance Europe*, in Filep, A., Jurdana, E., and Pandžić, eds., *Gnalić - Blago potomulog broda iz 16. stoljeća*. Hrvatski Povijesni Muzej, Zagreb.
- Rosencrantz, D. M., 1975, Underwater Photography and Photogrammetry. *Photography in Archaeological Research*, School of American Research, University of New Mexico Press, Albuquerque, 265-310.
- Rule, N., 1989, The Direct Survey Method (DSM) of Underwater Survey, and Its Application Underwater. *International Journal of Nautical Archaeology* **18**, 157-162.

- Sarfield, J. P., 1984, Notes: Mediterranean Whole Moulding. *Mariner's Mirror* **70.1**, 86-8.
- Sarsfield, J. P., 1985a, Survival of Pre-Sixteenth Century Mediterranean Lofting Techniques in Bahia, in O. L. Filgueiras (ed.). *Fourth Meeting of the International Symposium on Boat and Ship Archaeology, Amsterdam 1988*, Oxford.
- Sarsfield, J. P., 1985b, From the Brink of Extinction. *Wooden Boat* **66**, 84-89.
- Sarsfield, J. P., 1991, Master Frame and Ribbands, in R. Reinder and P. Kees (eds), *Carvel Construction Technique: Skeleton-first, Shell-first: Fifth International Symposium on Boat and Ship Archaeology, Amsterdam 1988*, Oxford.
- Skarlatos, D., and Rova, M., 2010, Photogrammetric Approaches for the Archaeological Mapping of the Mazotos Shipwreck. *7th International Conference on Science and Technology in Archaeology and Conservation*, 7-12 December, Petra.
- Steffy, J. R., 1982, The Reconstruction of the 11th Century Serçe Liman Vessel: A Preliminary Report. *International Journal of Nautical Archaeology* **11.1**: 13-34.
- Steffy, J. R., 1994, *Wooden Ship Building and the Interpretation of Shipwrecks*, Texas A&M University Press, College Station.
- Szeliski, R., 2010, *Computer Vision Algorithms and Applications*. Springer, New York
- Torres, R., 2014a, Department of Anthropology, Universidade Federal da Bahia, Salvador.
- Torres, R., 2014b, Department of Anthropology, Universidade Federal da Bahia, Salvador.
- Torres, R., 2014c, Department of Anthropology, Universidade Federal da Bahia, Salvador.
- Torres, R., 2014d, Department of Anthropology, Universidade Federal da Bahia, Salvador.
- Van Damme, T., 2015, *Computer Vision Photogrammetry for Underwater Archaeological Site Recording: A Critical Assessment*, M.A. Thesis at University of Southern Denmark, Esbjerg.
- Van Doorninck, F. H., 1967. *The Seventh-century Byzantine Ship at Yassi Ada; Some Contributions to the History of Naval Architecture*, Dissertation at University of Pennsylvania, Philadelphia.

Van Duivenvoorde, W., and Green, J., 2015, *Dutch East India Company Shipbuilding: the Archaeological Study of Batavia and Other Seventeenth-century VOC Ships*, Texas A&M University Press, College Station.

Zhukovsky, M. O., Kuznetsov, V. D., and Olkhovsky, S. V., 2013, Photogrammetric techniques for 3-D underwater Record of the Antique Time Ship from Phanagoria, *ISPRS - International Archives of the Photogrammetry, Remote Sensing and Spatial Information Sciences* **XL-5/W2**, 717-721.